

106p.
CODE-2D*RQ+
6383*

**SURFACE-TO-AIR RETRIEVAL OF HEAVY SPACECRAFT
BY FIXED-WING AIRCRAFT**

VOLUME II - DEVELOPMENT OF ANALYTICAL TECHNIQUES

(NASA-CR-50514) SURFACE-TO-AIR RETRIEVAL OF
HEAVY SPACECRAFT BY FIXED-WING AIRCRAFT.
VOLUME 2: DEVELOPMENT OF ANALYTICAL
TECHNIQUES (Grumman Aerospace Corp.) 108 p

N90-70822

Unclas

00/18 0279429

Grumman

PROJECT 306

**SURFACE-TO-AIR RETRIEVAL
OF HEAVY SPACECRAFT
BY FIXED-WING AIRCRAFT**

VOLUME II - DEVELOPMENT OF ANALYTICAL TECHNIQUES

**PREPARED FOR THE
NATIONAL AERONAUTICS AND SPACE ADMINISTRATION
MANNED SPACECRAFT CENTER**

CONTRACT NAS9-195

PDR-306-II

2

JUNE 1962

[REDACTED]

CR-50,514

ABSTRACTVolume I

13958

Results are reported on an initial feasibility study of techniques which might permit fixed-wing aircraft in flight to pick up heavy spacecraft from the earth's surface. The effort was primarily analytical, but brief flight tests were conducted and found to substantiate a three-dimensional dynamic analysis of aircraft-line-payload behavior programmed on the IBM 7090. The analytical technique developed was then used to predict capsule pick-up accelerations and trajectories. Some attention was given to operational considerations such as adverse environments, landing a towed spacecraft, aircraft performance, separate space crew retrieval, line properties and special equipment required. On the basis of this study, it appears feasible to pick-up a 10,000 pound spacecraft from the earth's surface with a C-130 aircraft in flight. Recommendations are given for further study and flight test of the most promising techniques.

Volume II

Volume II contains three sections which cover 1) the analytical method developed to describe three dimensional aircraft-cable-payload dynamics, 2) a description of flight tests conducted to confirm the analysis and a comparison of theoretical and experimental results, and 3) calculations predicting the cable loads and capsule trajectories which would be encountered in effecting a retrieval of a heavy spacecraft. Recommendations are given for further analytical and experimental studies at the end of each section.

TABLE OF CONTENTS (VOLUME II)

	<u>Page</u>
Abstract -----	i
List of Tables -----	iii
List of Figures -----	iv
Introduction -----	vi
Summary -----	vii
 SECTION I - ANALYSIS -----	 1
A. Introduction -----	1
B. The General Equations of Motion -----	1
C. Boundary Conditions -----	20
D. Inextensible Cable -----	22
E. Conclusions and Recommendations -----	23
 SECTION II - EXPERIMENT -----	 25
A. Purpose -----	25
B. Experimental Technique -----	25
C. Experimental Results and Comparison with Theory - Circling Line -----	 36
D. Experimental Results and Comparison with Theory - Snatch Type Pickup -----	 55
 SECTION III - CALCULATIONS -----	 69
A. Introduction -----	69
B. Circling Line in Air -----	69
C. Capsule Pickups -----	81
D. Conclusions and Recommendations -----	90
 BIBLIOGRAPHY -----	 92

LIST OF TABLES

<u>Table No.</u>	<u>Title</u>	<u>Page No.</u>
1	Summary of Flight Test Program	26
2	Summary of Circling Line Test Results	46
3	Snatch Type Pickup - Summary of Test Results	55
4	Line Configurations used for Calculations	70
5	Effects of Line Taper on End Point Circle and Vertical Separation for Full Scale Apollo	72
6	Lift-off Maneuvers Originating from the Circling Line Configuration	82
7	Variations in Circling Line Configuration Necessary to Reduce End Point Circle and Vertical Separation	90

LIST OF FIGURES

<u>Figure No.</u>	<u>Title</u>	<u>Page No.</u>
1	Idealized Cable	3
2	Ag-Cat Test Aircraft with Scale Capsule Model	30
3	Ag-Cat Line Release Attachment in Open Position	31
4	Ag-Cat Line Release Attachment in Closed Position	32
5	Ag-Cat Cowl Instrument Panel	33
6	Cockpit Instrument Panel of Ag-Cat	34
7	Oscillograph Installation in Ag-Cat Hopper	35
8	Circling Line - Ag-Cat Model (Experimental Results) Time Histories of Azimuth and Elevation Angles	38
9 to 13	Circling Line - Ag-Cat Model (Experimental Results) Horizontal Payload Trajectory	
9	Nylon Cable - Payload = $45\frac{1}{2}$ lbs.	39
10	Nylon Cable - Payload = $112\frac{1}{2}$ lbs.	40
11	Polypropylene Cable - Payload = $46\frac{1}{2}$ lbs.	41
12	Polypropylene Cable - Payload = $104\frac{1}{2}$ lbs.	42
13	Steel Cable - Payload = $104\frac{1}{2}$ lbs.	43
14	Circling Line - Ag-Cat Model (Experimental Results) Time History of Payload Horizontal and Vertical Motion	44
15	Circling Line - Ag-Cat Model (Experimental Results) Tension Time History - Test Run #10	45
16	Circling Line - Ag-Cat Model Cable Shape in Still Air	48
17	Circling Line - Ag-Cat Model Comparison of Theoretical and Experimental Results	49
18	Circling Line - Ag-Cat Model Vertical Separation and End Point Radius vs. Normal Force Coefficient	51
19	Circling Line - Ag-Cat Model Effect of Wind Shear	53
20	Circling Line - Apollo Configuration Effect of 5 knot/2500 ft. Wind Shear (Time History)	54
21	Snatch Type Pickup - Ag-Cat Model (Experimental Results) - Time History of Cable Tension Measured at Airplane During Snatch Pickup #2	56
22	Snatch Type Pickup - Ag-Cat Model (Experimental Results) 57 Time History of Cable Tension at Airplane During Snatch Pickup #3	
23	Snatch Type Pickup - Ag-Cat Model Payload Trajectory for Pickup #3	58
24	Snatch Type Pickup - Ag-Cat Model Effect of Balloon Drag	60
25	Snatch Type Pickup - Ag-Cat Model Comparison of Experimental and Theoretical Results - Payload Trajectory	61
26	Snatch Type Pickup - Ag-Cat Model Comparison of Experimental and Theoretical Results - Tension Time History	62
27	Short-Time Load-Deflection Tests 3/16 Diameter 3 Strand Nylon Rope	64

LIST OF FIGURES (CONT.)

<u>Figure No.</u>	<u>Title</u>	<u>Page No.</u>
28	Short-Time Load-Delection Tests Fulton Hollow Braid	65
29	Snatch Type Pickup - Ag-Cat Model Analytical Approximation to Experimental Elasticity Curve	66
30	Snatch Type Pickup - Ag-Cat Model Effects of Damping on Payload Trajectory	67
31	Snatch Type Pickup - Ag-Cat Model Effect of Damping on Tension Time History	68
32	Circling Line - Ag-Cat Model Vertical Separation, End Point Radius and Velocity vs. A/C Velocity	73
33	Circling Line - Ag-Cat Model Vertical Separation and End Point Radius vs. A/C Radius	74
34	Circling Line - Ag-Cat Model Vertical Separation and End Point Radius vs. Line Length	75
35	Circling Line - Ag-Cat Model Vertical Separation and End Point Radius vs. Cable Diameter	76
36	Circling Line - Ag-Cat Model Vertical Separation and End Point Radius vs. Payload Weight	77
37	Circling Line - Apollo Configuration Effect of a 12 ft. Diameter Parachute	78
38	Circling Line - Apollo Configuration Effects of a 5 knot/2500 ft. Wind Shear	79
39	Circling Line - Apollo Configuration Effects of Wind	80
40	Snatch Type Pickup - Apollo Configuration Variations in Airplane and Capsule Cable Lengths	83
41	Circling Line - Apollo Configuration Horizontal Force Required to Move Bottom of Cable in Specified Path on the Ground	84
42	Circling Line - Apollo Configuration Pickup Using Maneuver #1	85
43	Circling Line - Apollo Configuration Pickup Using Maneuver #1, Capsule Tied Down	86
44	Circling Line - Apollo Configuration Pickup Using Maneuver #2	87
45	Circling Line - Apollo Configuration Pickup Using Maneuver #3	88
46	Circling Line - Apollo Configuration Pickup Using Maneuver #4	89

INTRODUCTION

An extensive literature search on the subject of cable motion has revealed that analytic work done has been of limited scope. Much of this work consists of investigation of the steady state motion of some particular configuration, and almost all of it considers two-dimensional motion only.

In order to investigate the merits of the various retrieval schemes discussed in Volume I, a more versatile analysis was needed. Therefore, a new approach was taken to develop an analysis which gives a description of elastic cable motion and loads, both transient and steady state, in three dimensions. It felt that this analysis is a more complete treatment of the problem than has existed previously.

In particular, two types of retrieval techniques were investigated, the circling line and the snatch type pickup. The circling line maneuver is, as its name implies, one where the aircraft flies a circular pattern while towing a cable. Attachment to the capsule to be retrieved is made at the bottom end of the cable. The snatch-type pickup is one where the cable is attached to the capsule and is vertically supported by some device such as a balloon. Attachment is made at the upper end of this cable by the aircraft, which usually flies a straight line pattern.

SUMMARY

Theory

The analysis derived in Volume II of this report represents a description of cable motion, both transient and steady state, in three dimensions. The idealized model for the analysis was obtained by choosing discrete points along the cable, and concentrating at these points the mass and area of the cable segments between them. The result is a series of lumped masses joined by straight lines which have the extensional elasticity properties of the cable under consideration.

The dynamics of this model were derived by means of the energy method of J. L. Lagrange, using spherical coordinates to describe the three degrees of freedom of each mass point. Motion of the top of the cable (the airplane) is specified, while the bottom may either be free or constrained to move in a horizontal plane (the ground). Motion in this plane may either be specified or free and subject to applied frictional forces. The aerodynamic forces were assumed to consist of a force normal to the cable segment which follows the usual " $\sin^2 \alpha$ " law for infinitely long cylinders, and a parasitic drag component opposite to the direction of local velocity.

Since the complexity of this analysis is such as to make application to any but the simplest cases prohibitively laborious, use of a high-speed electronic digital computer is required. A program was written for the IBM 7090 computer which is capable of obtaining solutions for a given configuration in a matter of minutes.

It is believed that the assumptions and restrictions made in developing this analysis are such as will not impose any serious limitations on its usefulness as an engineering tool. With the use of the IBM 7090 computer, it can calculate tension, position, velocity and acceleration at any point in the cable as a function of time, for variations in any of the following parameters:

1. Line Description

- a) diameter at each point
- b) mass at each point
- c) aerodynamic force coefficients at each point
- d) initial length of each segment
- e) elastic characteristics of each segment

2. Attachments to the line

- a) mass at any point, in particular the payload
- b) drag at any point, as the drag of the payload or a parachute
- c) buoyancy at any point

3. Initial configuration of the line
 - a) shape
 - b) orientation
 - c) proportion of line attached to airplane vs. that attached to payload
4. Wind effects
 - a) wind velocity constant (or zero)
 - b) wind varying with altitude
5. Lower end conditions
 - a) end point fixed on the ground
 - b) end point motion on the ground arbitrarily specified
 - c) end point motion free on the ground with specified static and dynamic friction coefficients
 - d) end point free in the air

However, it is felt that the analysis could be made even more useful by increasing its scope somewhat, and it is recommended that the following subjects be incorporated in future studies:

1. Variation of unstretched line length with time
2. The possibility of specifying applied forces rather than motion at the top of the cable
3. The possibility of specifying arbitrary applied force time histories at any point in the cable.

The first of these will allow computation of the effects of paying line out and reeling it into the airplane towing the cable. Such a requirement might come up both in landing a hook for attachment to the payload and drawing the payload up to the airplane.

The second will permit calculation of the feedback between airplane and cable, that is, how the cable forces applied to the airplane affect its performance, and how the resultant airplane motion affects the cable motion. The latter is expected to be of less importance, but effect on airplane performance might be significant in the case of heavy payloads.

The third suggested addition makes provision for computing the effect on cable motion of attached aerodynamic devices (e.g. paravanes), as well as various kinds of impact forces which might be encountered.

Experiment

A series of flight tests were performed to obtain in-flight data of payload performance for circling line and snatch type pickup retrieval methods. The purpose of the tests was to determine the accuracy and possible limitations of the theory previously discussed, under actual field conditions.

The Grumman "Ag-Cat", which has high maneuverability at low speeds, was used as the towing vehicle for the tests. Nylon cable was used for the snatch-type pickup whereas three types of cable (nylon, polypropylene and steel) were used for the circling line tests. A small scale model (30" high, 25" dia.) of the Gemini capsule was used as the test payload.

Circling Line - For the circling line, the test program was designed so that trends in unrestrained payload motion could be determined as a function of air-plane bank angle, payload weight and cable drag/weight ratio. In an attempt to minimize wind effects, the aircraft was allowed to drift with the wind while performing the circling maneuver.

The average values of side to side traverse as measured experimentally were compared to analytically predicted values. Predicted and experimental values show that the area in which the payload moves reduces sharply as aircraft bank angle, which is inversely related to aircraft circle size, increases. Increasing the payload weight from 50 to 100 lbs. causes a definite increase in payload circle size. An increase in drag/weight ratio (nylon = 16.7, polypropylene = 10.5, and steel = 2.3), causes a decrease in payload circle size for small aircraft circles (bank angle = 50°). However, for the larger circles the trend appears less significant or more difficult to determine because of the poor agreement between experimental and theoretical results for the polypropylene line.

During the experiment a previously reported phenomenon was observed. The payload did not maintain a constant altitude but, rather, displayed a cyclical altitude variation. Since only direct wind and not wind shear is eliminated by allowing the aircraft to drift, an investigation of the effects of wind shear was made. Simplified wind profiles were used since no experimental data had been taken. The vertical motion (or yo-yo) obtained was found to be of the same magnitude (50-200 ft.) as those obtained experimentally and it is believed that this motion is primarily due to this cause.

Snatch-Type Pickup - For the snatch type pickup, a 10 ft. dia. hydrogen filled balloon attached to the test payload by means of a 150 ft. nylon line was erected at the test site. The test aircraft, flying at constant altitude and velocity, made connection by trailing a hook into the capsule cable loops, which were draped over the supporting balloon. Unfortunately, large segments of the balloon remained on the cable throughout the pickup even though it was punctured on impact.

Because no measured data was available describing the impact forces on the hook and balloon and the subsequent balloon mass and inertial properties, a straightforward comparison between experimental and theoretical results was difficult. It was found, however, that average values of balloon drag could be assumed to approximate these complicated conditions, which give a fairly good first approximation to the payload motion and cable load. It is recommended that an analytical investigation of these conditions be performed so that they may adequately be predicted beforehand, in order to eliminate the need for extensive flight testing to obtain average working values. Snatch type pickups from the circling line maneuver and using a scheme such as Fulton's "Skyhook" should also be made to study other phenomena of this pickup uncomplicated by the effects of a large supporting balloon.

Calculations

Analytical calculations were performed in order to obtain data with which to study the feasibility of fixed-wing aircraft retrieval techniques for heavy space capsules.

It was found that certain controls (e.g. line length, aircraft velocity, line diameter, etcetera) are available which can be used to facilitate delivery of the end of a circling cable to the object being retrieved.

In general, it was found that increasing drag forces decreases end point circle while increasing mass increases the circle size. Hard and fast rules are difficult to make, however, since position of mass and drag forces along the cable is of considerable importance, and since interaction of all these effects is extremely complex.

Atmospheric wind is another factor which must be taken into consideration in the overall design of circling line retrieval systems because of the vertical end point motion it produces. It is felt that further study should be undertaken to alleviate this effect, since it appears to be a difficulty which must be overcome, particularly when trying to land the retrieved capsule. One possibility is to investigate aircraft maneuvers which might reduce the yo-yo, another is the attachment of devices to the line such as parachutes or balloons, which would damp this motion out.

It was found that heavy capsules attached to the cable result in large end point circles for the circling line. In returning the capsule to the ground, this leads to the problems of a) placement, and b) impact loads due to high horizontal velocity. Because of these phenomena, alternate schemes for landing are discussed in Volume I of this report.

A variety of promising techniques for effecting capsule lift off were studied. Snatch-type pickups of heavy capsules can be used, with relatively low accelerations, if long cables are used. This has the disadvantage, however, of excessive drop-kit weights. Part of the line could initially be trailed from the airplane, but this leads to less satisfactory end point trajectories.

Pickup techniques based on the circling line maneuver show considerable potential. Landing and attachment of the hook from this maneuver appears straightforward, and it is felt that satisfactory lift-off trajectories can be obtained by means of slight variations on the maneuvers studied. This type of pickup does not involve the difficulties of dropping large equipment packages or of making high speed contact with a balloon-supported line.

Only relatively simple examples of pickup maneuvers were tried due to the press of time. Much could be gained by an optimization study of these techniques, in which the effects of accelerating the airplane, climbing, reeling in line, using different maneuvers and different kinds of cable, to mention a few possibilities, would be studied.

SECTION I - ANALYSIS

A. Introduction

The analysis which follows is a description of cable motion in three dimensions, both transient and steady-state. Since the immediate purpose for writing this analysis was to describe airplane-towed cables, the boundary conditions initially assumed were that the motion of one end of the cable be arbitrarily specified while the other end be free. Expressions are later introduced to restrain the free end, either by specifying external forces or the motion itself.

The energy method of J. L. Lagrange was used to develop this analysis, and the assumptions made were such as to maintain the greatest possible degree of generality.

B. The General Equations of Motion

1) The Coordinate System:

In order to take this analysis out of the realm of the academic and make an engineering tool of it, it is written with the requirement in mind of programming it for a high-speed, large capacity digital computer. To this end a numerical approach is taken immediately, which makes the use of generalized (independent) coordinates mandatory.

The most convenient sets of such coordinates are the Cartesian and spherical. The prescribed motion of the top of the cable is related to a right-handed orthogonal Cartesian coordinate system, while the motion of the cable itself is related to the top by means of local spherical coordinates describing the motion of each point with respect to the point immediately above. Thus, at any point a distance s measured along the unstretched cable from the top, at time t ,

$$\begin{aligned} \chi(s, t) &= \chi_T(t) + \int_0^{s(s,t)} \sin \theta(s, t) \cos \phi(s, t) d\xi(s, t) \\ &= \chi_T(t) + \int_0^s \sin \theta(s, t) \cos \phi(s, t) \frac{\partial \xi(s, t)}{\partial s} ds \quad (1a) \end{aligned}$$

and similarly

$$y(s, t) = y_T(t) + \int_0^s \sin \theta(s, t) \sin \phi(s, t) \frac{\partial \xi(s, t)}{\partial s} ds \quad (1b)$$

$$z(s, t) = z_T(t) + \int_0^s \cos \theta(s, t) \frac{\partial \xi(s, t)}{\partial s} ds \quad (1c)$$

in which

χ_T , y_T and Z_T locate the top of the cable,
 θ and ϕ are the local angular coordinates,
 σ is the local radial coordinate, corresponding to length along the stretched cable, and
 S and Σ are the dummy variables of integration corresponding to σ and σ .

Rewriting in terms of first differences and applying block integration gives, if the top of the cable is point 1,

$$\chi_i(t) = \chi_1(t) + \sum_{j=2}^i h_j(t) \sin \theta_j(t) \cos \phi_j(t) \quad (2a)$$

$$y_i(t) = y_1(t) + \sum_{j=2}^i h_j(t) \sin \theta_j(t) \sin \phi_j(t) \quad (2b)$$

$$Z_i(t) = Z_1(t) + \sum_{j=2}^i h_j(t) \cos \theta_j(t) \quad (2c)$$

in which h_j is the distance between the j th and $j-1$ th point on the cable. This coordinate system is demonstrated in Figure 1.

2) Assumptions:

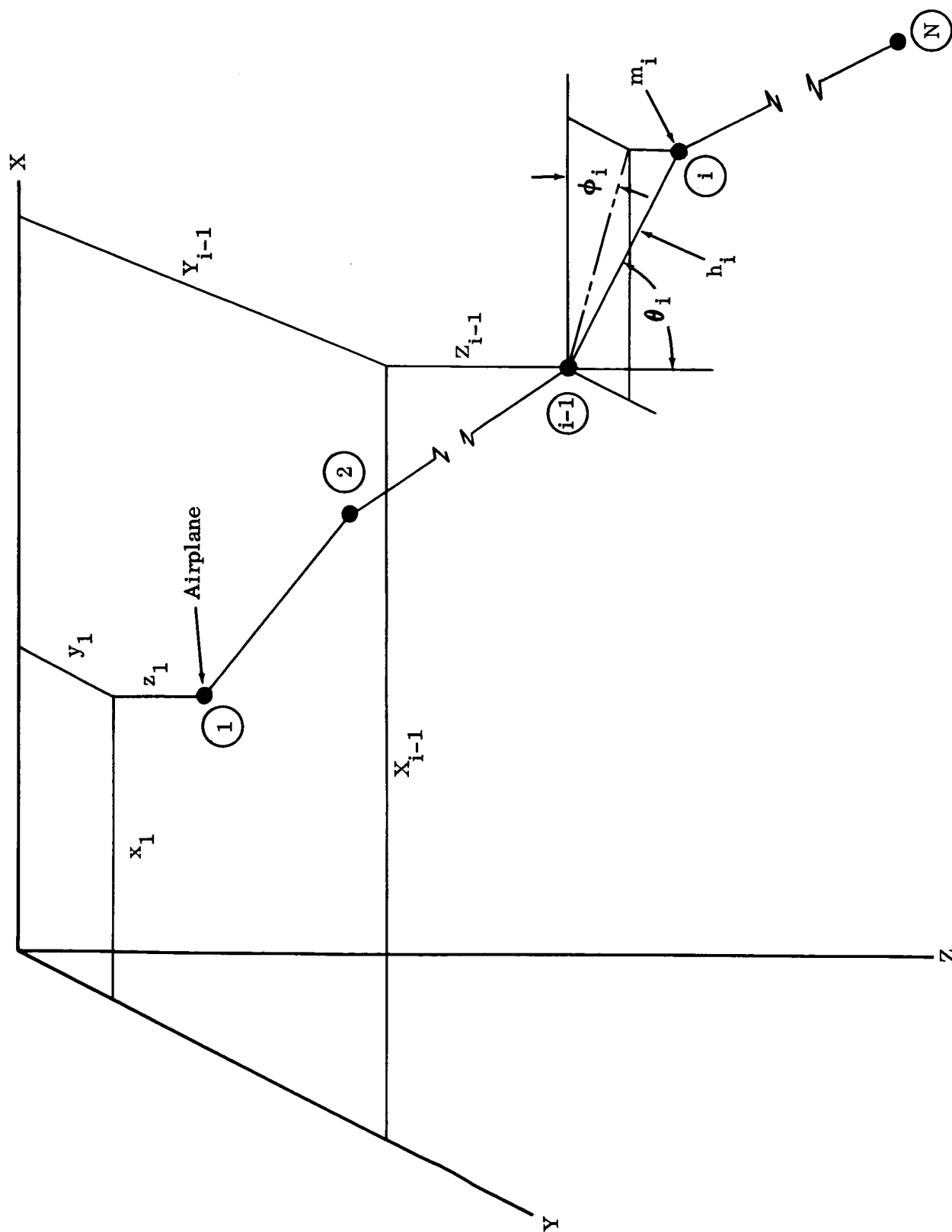
Equations (2) comprise a formulation in which discrete points on a cable are considered rather than the entire cable as a continuum. Thus the infinite-degree-of-freedom system is replaced by one with a finite number of degrees of freedom for which solutions can be obtained. The coordinates in this system now give the length and orientation of the straight line between adjacent points of the cable. If the mass of the cable is then concentrated at these discrete points, the result is a lumped-mass system with straight lines between, which have the property of being able to sustain tension but not compression. This is the mathematical model used for the analysis which follows.

It should be noted that the order of approximation represented by this model is consistent with that of the block integration technique used above, in that applying the same technique to the energy integral of the continuous cable results in the energy expressions obtainable from the model directly.

For the purposes of this analysis the cable is divided into N points ($N-1$ segments) with three degrees of freedom each, subject to the following assumptions:

1. The mass and projected area of each segment is concentrated at its lower point.

Fig. 1 Idealized Cable



2. Bending resistance of the cable is not considered.
3. The aerodynamic normal force on the cable follows the $\sin^2 \alpha$ law for infinitely long cylinders. (See section I-B-6-a).

3) Lagrange's Equations:

The Lagrange formulation for the equations of motion of a system with M degrees of freedom is

$$\frac{\partial}{\partial t} \left(\frac{\partial T}{\partial \dot{q}_i} \right) - \frac{\partial T}{\partial q_i} + \frac{\partial U}{\partial q_i} = Q_i, \quad i = 1, 2, 3, \dots, M \quad (3)$$

in which the q_i are the generalized coordinates (θ_i , ϕ_i and h_i in this case), T is the kinetic energy of the system, U is the potential energy, and the Q_i are the generalized forces applied.

4) Kinetic Energy

The kinetic energy of the system

$$T = \frac{1}{2} M V^2 = \frac{1}{2} \sum_{i=2}^N m_i (\dot{x}_i + \dot{y}_i + \dot{z}_i)^2 \quad (4)$$

where m_i is the mass associated with the i th segment. The velocity components \dot{x}_i , \dot{y}_i and \dot{z}_i are obtained by differentiating Equations(2) with respect to time, which gives

$$\dot{x}_i = \dot{x}_1 + \sum_{j=2}^i \left[\dot{h}_j \sin \theta_j \cos \phi_j + \dot{\theta}_j h_j \cos \theta_j \cos \phi_j + \dot{\phi}_j h_j \sin \theta_j \sin \phi_j \right] \quad (5a)$$

$$\dot{y}_i = \dot{y}_1 + \sum_{j=2}^i \left[\dot{h}_j \sin \theta_j \sin \phi_j + \dot{\theta}_j h_j \cos \theta_j \sin \phi_j + \dot{\phi}_j h_j \sin \theta_j \cos \phi_j \right] \quad (5b)$$

$$\dot{z}_i = \dot{z}_1 + \sum_{j=2}^i \left[\dot{h}_j \theta_j \cos \theta_j - \dot{\theta}_j h_j \sin \theta_j \right] \quad (5c)$$

Substituting Equations(5) into Equation (4) gives the kinetic energy in terms of the generalized coordinates, as follows:

$$\begin{aligned}
T = & \sum_{i=2}^N \frac{1}{2} m_i \left\{ \dot{\chi}_i^2 + \dot{y}_i^2 + \dot{z}_i^2 + \right. \\
& + 2 \dot{\chi}_i \sum_{j=2}^i (\dot{h}_j \sin \theta_j \cos \phi_j + \dot{\theta}_j h_j \cos \theta_j \cos \phi_j - \dot{\phi}_j h_j \sin \theta_j \sin \phi_j) + \\
& + 2 \dot{y}_i \sum_{j=2}^i (\dot{h}_j \sin \theta_j \sin \phi_j + \dot{\theta}_j h_j \cos \theta_j \sin \phi_j + \dot{\phi}_j h_j \sin \theta_j \cos \phi_j) + \\
& + 2 \dot{z}_i \sum_{j=2}^i (\dot{h}_j \cos \theta_j - \dot{\theta}_j h_j \sin \theta_j) + \\
& + \sum_{j=2}^i \sum_{k=2}^i (\dot{h}_j \sin \theta_j \cos \phi_j + \dot{\theta}_j h_j \cos \theta_j \cos \phi_j + \\
& - \dot{\phi}_j h_j \sin \theta_j \sin \phi_j) (\dot{h}_k \sin \theta_k \cos \phi_k + \\
& + \dot{\theta}_k h_k \cos \theta_k \cos \phi_k - \dot{\phi}_k h_k \sin \theta_k \sin \phi_k) + \quad (6) \\
& + \sum_{j=2}^i \sum_{k=2}^i (\dot{h}_j \sin \theta_j \sin \phi_j + \dot{\theta}_j h_j \cos \theta_j \sin \phi_j + \\
& + \dot{\phi}_j h_j \sin \theta_j \cos \phi_j) (\dot{h}_k \sin \theta_k \sin \phi_k + \\
& + \dot{\theta}_k h_k \cos \theta_k \sin \phi_k + \dot{\phi}_k h_k \sin \theta_k \cos \phi_k) + \\
& \left. + \sum_{j=2}^i \sum_{k=2}^i (\dot{h}_j \cos \theta_j - \dot{\theta}_j h_j \sin \theta_j) (\dot{h}_k \cos \theta_k - \dot{\theta}_k h_k \sin \theta_k) \right\}
\end{aligned}$$

The change in kinetic energy due to an incremental change in velocity of the j th mass is

$$\begin{aligned}
\frac{\partial T}{\partial \dot{\theta}_j} = & \sum_{i=j}^N m_i h_j \left\{ \cos \theta_j \cos \phi_j \left[\dot{\chi}_i + \sum_{k=2}^i (\dot{h}_k \sin \theta_k \cos \phi_k + \right. \right. \\
& + \dot{\theta}_k h_k \cos \theta_k \cos \phi_k - \dot{\phi}_k h_k \sin \theta_k \sin \phi_k) \left. \right] + \\
& + \cos \theta_j \sin \phi_j \left[\dot{y}_i + \sum_{k=2}^i (\dot{h}_k \sin \theta_k \sin \phi_k + \right. \\
& + \dot{\theta}_k h_k \cos \theta_k \sin \phi_k + \dot{\phi}_k h_k \sin \theta_k \cos \phi_k) \left. \right] + \quad (7a) \\
& - \sin \theta_j \left[\dot{z}_i + \sum_{k=2}^i (\dot{h}_k \cos \theta_k - \dot{\theta}_k h_k \sin \theta_k) \right] \left. \right\}
\end{aligned}$$

$$\begin{aligned} \frac{\partial T}{\partial \dot{\phi}_j} = \sum_{i=j}^N m_i h_j \left\{ -\sin \theta_j \sin \phi_j \left[\dot{x}_1 + \sum_{k=2}^i (\dot{h}_k \sin \theta_k \cos \phi_k + \right. \right. \\ \left. \left. + \dot{\theta}_k h_k \cos \theta_k \cos \phi_k - \dot{\phi}_k h_k \sin \theta_k \sin \phi_k) \right] + \right. \\ \left. + \sin \theta_j \cos \phi_j \left[\dot{y}_1 + \sum_{k=2}^i (\dot{h}_k \sin \theta_k \sin \phi_k + \right. \right. \\ \left. \left. + \dot{\theta}_k h_k \cos \theta_k \sin \phi_k + \dot{\phi}_k h_k \sin \theta_k \cos \phi_k) \right] \right\} \end{aligned} \quad (7b)$$

$$\begin{aligned} \frac{\partial T}{\partial \dot{h}_j} = \sum_{i=j}^N m_i \left\{ \sin \theta_j \cos \phi_j \left[\dot{x}_1 + \sum_{k=2}^i (\dot{h}_k \sin \theta_k \cos \phi_k + \right. \right. \\ \left. \left. + \dot{\theta}_k h_k \cos \theta_k \cos \phi_k - \dot{\phi}_k h_k \sin \theta_k \sin \phi_k) \right] + \right. \\ \left. + \sin \theta_j \sin \phi_j \left[\dot{y}_1 + \sum_{k=2}^i (\dot{h}_k \sin \theta_k \sin \phi_k + \right. \right. \\ \left. \left. + \dot{\theta}_k h_k \cos \theta_k \sin \phi_k + \dot{\phi}_k h_k \sin \theta_k \cos \phi_k) \right] + \right. \\ \left. + \cos \theta_j \left[\dot{z}_1 + \sum_{k=2}^i (\dot{h}_k \cos \theta_k - \dot{\theta}_k h_k \sin \theta_k) \right] \right\} \end{aligned} \quad (7c)$$

The change in kinetic energy due to an incremental change in position is

$$\begin{aligned} \frac{\partial T}{\partial \theta_j} = \sum_{i=j}^N m_i \left\{ \left[\dot{h}_j \cos \theta_j \cos \phi_j - \dot{\theta}_j h_j \sin \theta_j \cos \phi_j - \dot{\phi}_j h_j \cos \theta_j \sin \phi_j \right] \times \right. \\ \times \left[\dot{x}_1 + \sum_{k=2}^N (\dot{h}_k \sin \theta_k \cos \phi_k + \dot{\theta}_k h_k \cos \theta_k \cos \phi_k + \right. \\ \left. - \dot{\phi}_k h_k \sin \theta_k \sin \phi_k) \right] + \\ \left. + \left[\dot{h}_j \cos \theta_j \sin \phi_j - \dot{\theta}_j h_j \sin \theta_j \sin \phi_j + \dot{\phi}_j h_j \cos \theta_j \cos \phi_j \right] \times \right. \\ \times \left[\dot{y}_1 + \sum_{k=2}^N (\dot{h}_k \sin \theta_k \sin \phi_k + \dot{\theta}_k h_k \cos \theta_k \sin \phi_k + \right. \\ \left. + \dot{\phi}_k h_k \sin \theta_k \cos \phi_k) \right] + \\ \left. + \left[-\dot{h}_j \sin \theta_j - \dot{\theta}_j h_j \cos \theta_j \right] \left[\dot{z}_1 + \sum_{k=2}^i \dot{h}_k \cos \theta_k - \dot{\theta}_k h_k \sin \theta_k \right] \right\} \end{aligned} \quad (8a)$$

$$\begin{aligned}
\frac{\partial T}{\partial \phi_j} = & \sum_{i=j}^N m_i \left\{ \left[-\dot{h}_j \sin \theta_j \sin \phi_j - \dot{\theta}_j h_j \cos \theta_j \sin \phi_j - \dot{\phi}_j h_j \sin \theta_j \cos \phi_j \right] \times \right. \\
& \times \left[\ddot{\chi}_1 + \sum_{k=2}^i (\dot{h}_k \sin \theta_k \cos \phi_k + \dot{\theta}_k h_k \cos \theta_k \cos \phi_k + \right. \\
& \quad \left. \left. - \dot{\phi}_k h_k \sin \theta_k \sin \phi_k) \right] + \right. \\
& + \left[-\dot{h}_j \sin \theta_j \cos \phi_j + \dot{\theta}_j h_j \cos \theta_j \cos \phi_j - \dot{\phi}_j h_j \sin \theta_j \sin \phi_j \right] \times \\
& \times \left[\ddot{y}_1 + \sum_{k=2}^i (\dot{h}_k \sin \theta_k \sin \phi_k + \dot{\theta}_k h_k \cos \theta_k \sin \phi_k + \right. \\
& \quad \left. \left. + \dot{\phi}_k h_k \sin \theta_k \cos \phi_k) \right] \right\} \quad (8b)
\end{aligned}$$

$$\begin{aligned}
\frac{\partial T}{\partial h_j} = & \sum_{i=j}^N m_i \left\{ \left[\dot{\theta}_j \cos \theta_j \cos \phi_j - \dot{\phi}_j \sin \theta_j \sin \phi_j \right] \left[\ddot{\chi}_1 + \sum_{k=2}^i (\dot{h}_k \sin \theta_k \cos \phi_k + \right. \right. \\
& \quad \left. \left. + \dot{\theta}_k h_k \cos \theta_k \cos \phi_k - \dot{\phi}_k h_k \sin \theta_k \sin \phi_k) \right] + \right. \\
& + \left[\dot{\theta}_j \cos \theta_j \sin \phi_j + \dot{\phi}_j \sin \theta_j \cos \phi_j \right] \left[\ddot{y}_1 + \sum_{k=2}^i (\dot{h}_k \sin \theta_k \sin \phi_k + \right. \\
& \quad \left. \left. + \dot{\theta}_k h_k \cos \theta_k \sin \phi_k + \dot{\phi}_k h_k \sin \theta_k \cos \phi_k) \right] + \right. \\
& \left. + \left[-\dot{\theta}_j \sin \theta_j \right] \left[\ddot{z}_1 + \sum_{k=2}^i (\dot{h}_k \cos \theta_k - \dot{\theta}_k h_k \sin \theta_k) \right] \right\} \quad (8c)
\end{aligned}$$

Differentiating Equations (7) with respect to time and subtracting Equations (8) then yields

$$\begin{aligned}
\frac{d}{dt} \left(\frac{\partial T}{\partial \dot{\theta}_j} \right) - \frac{\partial T}{\partial \theta_j} = & \sum_{i=j}^N m_i h_j \left\{ \cos \theta_j \cos \phi_j \left[\ddot{\chi}_1 + \sum_{k=2}^i (\ddot{\theta}_k h_k \cos \theta_k \cos \phi_k + \right. \right. \\
& \quad \left. \left. - \ddot{\phi}_k h_k \sin \theta_k \sin \phi_k - h_k [\ddot{\theta}_k^2 + \ddot{\phi}_k^2] \sin \theta_k \cos \phi_k + \right. \right. \\
& \quad \left. \left. - 2 \ddot{\theta}_k \dot{\phi}_k h_k \cos \theta_k \sin \phi_k + \ddot{h}_k \sin \theta_k \cos \phi_k + \right. \right. \\
& \quad \left. \left. + 2 \ddot{\theta}_k h_k \cos \theta_k \cos \phi_k - 2 \ddot{\phi}_k h_k \sin \theta_k \sin \phi_k \right] + \right. \\
& \quad \left. + \sin \theta_j \cos \phi_j \left[\ddot{y}_1 + \sum_{k=2}^i (\ddot{\theta}_k h_k \cos \theta_k \sin \phi_k + \right. \right. \\
& \quad \left. \left. + 2 \ddot{\phi}_k h_k \sin \theta_k \cos \phi_k + \ddot{h}_k \sin \theta_k \sin \phi_k + \right. \right. \\
& \quad \left. \left. + 2 \ddot{\theta}_k h_k \cos \theta_k \sin \phi_k - 2 \ddot{\phi}_k h_k \sin \theta_k \cos \phi_k \right] + \right. \\
& \quad \left. + \left[-\ddot{\theta}_j \sin \theta_j \right] \left[\ddot{z}_1 + \sum_{k=2}^i (\ddot{h}_k \cos \theta_k - \ddot{\theta}_k h_k \sin \theta_k) \right] \right\} \quad (9a)
\end{aligned}$$

(Cont.)

(Equation 9a continued from previous page)

$$\begin{aligned}
& + \cos \theta_j \sin \phi_j \left[\ddot{y}_1 + \sum_{k=2}^i (\ddot{\theta}_k h_k \cos \theta_k \sin \phi_k + \right. \\
& + \ddot{\phi}_k h_k \sin \theta_k \cos \phi_k - h_k [\dot{\theta}_k^2 + \dot{\phi}_k^2] \sin \theta_k \sin \phi_k + \\
& + 2 \dot{\theta}_k \dot{\phi}_k h_k \cos \theta_k \cos \phi_k + \ddot{h}_k \sin \theta_k \sin \phi_k + \\
& + 2 \dot{\theta}_k \dot{h}_k \cos \theta_k \sin \phi_k + 2 \dot{\phi}_k \dot{h}_k \sin \theta_k \cos \phi_k) \left. \right] + \\
& - \sin \theta_j \left[\ddot{z}_1 - \sum_{k=2}^i (\ddot{\theta}_k h_k \sin \theta_k + \dot{\theta}_k^2 h_k \cos \theta_k + \right. \\
& - \ddot{h}_k \cos \theta_k + 2 \dot{\theta}_k \dot{h}_k \sin \theta_k) \left. \right] \left. \right\}
\end{aligned}$$

$$\begin{aligned}
\frac{d}{dt} \left(\frac{\partial T}{\partial \dot{\phi}_j} \right) - \frac{\partial T}{\partial \phi_j} &= \sum_{i=j}^N m_i h_j \left\{ -\sin \theta_j \sin \phi_j \left[\ddot{y}_1 + \sum_{k=2}^i (\ddot{\theta}_k h_k \cos \theta_k \cos \phi_k + \right. \right. \\
& - \ddot{\phi}_k h_k \sin \theta_k \sin \phi_k - h_k [\dot{\theta}_k^2 + \dot{\phi}_k^2] \sin \theta_k \cos \phi_k + \\
& - 2 \dot{\theta}_k \dot{\phi}_k h_k \cos \theta_k \sin \phi_k + \\
& + \ddot{h}_k \sin \theta_k \cos \phi_k + 2 \dot{\theta}_k \dot{h}_k \cos \theta_k \cos \phi_k + \\
& \left. \left. - 2 \dot{\phi}_k \dot{h}_k \sin \theta_k \sin \phi_k \right) \right] + \quad (9b) \\
& + \sin \theta_j \cos \phi_j \left[\ddot{y}_1 + \sum_{k=2}^i (\ddot{\theta}_k h_k \cos \theta_k \sin \phi_k + \right. \\
& + \ddot{\phi}_k h_k \sin \theta_k \cos \phi_k - h_k [\dot{\theta}_k^2 + \dot{\phi}_k^2] \sin \theta_k \sin \phi_k + \\
& + 2 \dot{\theta}_k \dot{\phi}_k h_k \cos \theta_k \cos \phi_k + \\
& + \ddot{h}_k \sin \theta_k \sin \phi_k + 2 \dot{\theta}_k \dot{h}_k \cos \theta_k \sin \phi_k + \\
& \left. \left. + 2 \dot{\phi}_k \dot{h}_k \sin \theta_k \cos \phi_k \right) \right] \left. \right\}
\end{aligned}$$

$$\begin{aligned}
\frac{d}{dt} \left(\frac{\partial T}{\partial \dot{h}_j} \right) - \frac{\partial T}{\partial h_j} = & \sum_{i=j}^N m_i \left\{ \sin \theta_j \cos \phi_j \left[\ddot{\chi}_i + \sum_{k=2}^i (\ddot{\theta}_k h_k \cos \theta_k \cos \phi_k + \right. \right. \\
& - \ddot{\phi}_k h_k \sin \theta_k \sin \phi_k - h_k [\ddot{\theta}_k^2 + \ddot{\phi}_k^2] \sin \theta_k \cos \phi_k + \\
& - 2 \dot{\theta}_k \dot{\phi}_k h_k \cos \theta_k \sin \phi_k + \ddot{h}_k \sin \theta_k \cos \phi_k + \\
& + 2 \dot{\theta}_k \dot{h}_k \cos \theta_k \cos \phi_k - 2 \dot{\phi}_k \dot{h}_k \sin \theta_k \sin \phi_k) \left. \right] + \\
& + \sin \theta_j \sin \phi_j \left[\ddot{\chi}_i + \sum_{k=2}^i (\ddot{\theta}_k h_k \cos \theta_k \sin \phi_k + \right. \\
& + \ddot{\phi}_k h_k \sin \theta_k \cos \phi_k - h_k [\ddot{\theta}_k^2 + \ddot{\phi}_k^2] \sin \theta_k \sin \phi_k + \\
& + 2 \dot{\theta}_k \dot{\phi}_k h_k \cos \theta_k \cos \phi_k + \\
& + \ddot{h}_k \sin \theta_k \sin \phi_k + 2 \dot{\theta}_k \dot{h}_k \cos \theta_k \sin \phi_k + \\
& + 2 \dot{\phi}_k \dot{h}_k \sin \theta_k \cos \phi_k) \left. \right] + \\
& + \cos \theta_j \left[\ddot{z}_i - \sum_{k=2}^i (\ddot{\theta}_k h_k \sin \theta_k + \ddot{\theta}_k^2 h_k \cos \theta_k + \right. \\
& - \ddot{h}_k \cos \theta_k + 2 \dot{\theta}_k \dot{h}_k \sin \theta_k) \left. \right] \left. \right\} \quad (9c)
\end{aligned}$$

Equations (9) may also be written in terms of Cartesian accelerations as

$$\begin{aligned}
\frac{d}{dt} \left(\frac{\partial T}{\partial \dot{\theta}_j} \right) - \frac{\partial T}{\partial \theta_j} = & \sum_{i=j}^N m_i h_j \left\{ \ddot{\chi}_i \cos \theta_j \cos \phi_j + \ddot{y}_i \cos \theta_j \sin \phi_j + \right. \\
& \left. - \ddot{z}_i \sin \theta_j \right\} \quad (10a)
\end{aligned}$$

$$\frac{d}{dt} \left(\frac{\partial T}{\partial \dot{\phi}_j} \right) - \frac{\partial T}{\partial \phi_j} = \sum_{i=j}^N m_i h_j \left\{ -\ddot{\chi}_i \sin \theta_j \sin \phi_j + \ddot{y}_i \sin \theta_j \cos \phi_j \right\} \quad (10b)$$

$$\frac{d}{dt} \left(\frac{\partial T}{\partial \dot{h}_j} \right) - \frac{\partial T}{\partial h_j} = \sum_{i=1}^N m_i \left\{ \ddot{x}_i \sin \theta_j \cos \phi_j + \ddot{y}_i \sin \theta_j \sin \phi_j + \ddot{z}_i \cos \theta_j \right\} \quad (10c)$$

5) Potential Energy:

The potential energy of the system is simply weight times height, or

$$U = -g \sum_{i=2}^N m_i z_i = -g \sum_{i=2}^N m_i \sum_{j=2}^i h_j \cos \theta_j \quad (11)$$

The change in potential energy due to change in position is

$$\frac{\partial U}{\partial \theta_j} = g \sum_{i=j}^N m_i h_i \sin \theta_j \quad (12a)$$

$$\frac{\partial U}{\partial \phi_j} = 0 \quad (12b)$$

$$\frac{\partial U}{\partial h_j} = -g \sum_{i=j}^N m_i \cos \theta_j \quad (12c)$$

6) Generalized Forces:

a. Aerodynamic

The aerodynamic forces on the cable are considered to be in two parts. These are a normal force component following the $\sin^2 \alpha$ law (Ref. Volume I) and a parasitic drag component which is colinear with and of opposite sense to the cable velocity vector.

The coefficients by which these forces are determined are of the following form:

The normal force coefficient

$$C_N = C_{DC} \sin^2 \alpha \quad (13)$$

where C_{DC} is an empirical factor and α is the angle between the velocity vector and the cable tangent at a point. This is decomposed into lift and drag components, and the parasitic drag is added to the drag due to normal force, whence the lift and drag coefficients are, respectively,

$$C_L = C_{DC} \sin^2 \alpha \cos \alpha \quad (14)$$

$$C_D = C_{DC} \sin^3 \alpha + C_{AD} \quad (15)$$

where C_{AD} is the coefficient of parasitic drag.

The aerodynamic forces are then

$$L_i = C_{L_i} q_i A_i \quad (16)$$

$$D_i = C_{D_i} q_i A_i \quad (17)$$

in which the dynamic pressure

$$q_i = \frac{1}{2} \rho V_i^2 \quad (18)$$

ρ being the air density, and the area associated with the i th point is diameter times length; $A_i = d_i h_i$.

The direction of the drag force is taken to be along the velocity vector and of opposite sense. The lift force is normal to it and in the plane defined by the velocity vector and the cable segment. These directions are analytically defined as follows:

Let \hat{i} , \hat{j} and \hat{k} be unit vectors along the x , y and z directions respectively. Then at any point the velocity vector is

$$V_i = \dot{x}_i \hat{i} + \dot{y}_i \hat{j} + \dot{z}_i \hat{k} \quad (19)$$

The unit vector in the direction of the local cable tangent is

$$\mathbf{R}_i = \sin \theta_i \cos \phi_i \mathbf{i} + \sin \theta_i \sin \phi_i \mathbf{j} + \cos \theta_i \mathbf{k} \quad (20)$$

The angle α may be defined as

$$\sin \alpha_i = \frac{|\mathbf{R}_i \times \mathbf{V}_i|}{|\mathbf{R}_i| |\mathbf{V}_i|} \quad (21a)$$

$$\cos \alpha_i = \frac{\mathbf{R}_i \cdot \mathbf{V}_i}{|\mathbf{R}_i| |\mathbf{V}_i|} \quad (21b)$$

The lift force vector is then given by

$$\begin{aligned} \mathbf{L}_i &= -\frac{1}{2} \left[\rho C_{Dc} d h \frac{(\mathbf{R} \times \mathbf{V}) \times \mathbf{V}}{(|\mathbf{R} \times \mathbf{V}| |\mathbf{V}|)} \frac{\mathbf{R} \cdot \mathbf{V}}{|\mathbf{R}| |\mathbf{V}|} \left(\frac{|\mathbf{R} \times \mathbf{V}|}{|\mathbf{R}| |\mathbf{V}|} \right)^2 |\mathbf{V}|^2 \right]_i \\ &= -\frac{1}{2} \left[\rho C_{Dc} d h \frac{[(\mathbf{R} \times \mathbf{V}) \times \mathbf{V}](\mathbf{R} \cdot \mathbf{V}) |\mathbf{R} \times \mathbf{V}|}{|\mathbf{V}|^2} \right]_i \end{aligned} \quad (22)$$

The drag force vector is

$$\begin{aligned} \mathbf{D}_i &= -\frac{1}{2} \left[\rho C_{Dc} d h |\mathbf{V}| \mathbf{V} \left\{ \left(\frac{|\mathbf{R} \times \mathbf{V}|}{|\mathbf{R}| |\mathbf{V}|} \right)^3 + C_{AD} \right\} \right]_i \\ &= -\frac{1}{2} \left[\rho C_{Dc} d h \frac{\mathbf{V}}{|\mathbf{V}|^2} (|\mathbf{R} \times \mathbf{V}|^3 + C_{AD}) \right]_i \end{aligned} \quad (23)$$

This formulation of lift and drag is especially amenable to the inclusion of crosswind effects on the system. This is most readily accomplished by modifying the local velocity vector \mathbf{V}_i used in Equations (22) and (23). Thus, instead of Equation (19), the velocity is given by

$$\mathbf{V}_i = (\dot{x}_i + w_{x_i}) \mathbf{i} + (\dot{y}_i + w_{y_i}) \mathbf{j} + (\dot{z}_i + w_{z_i}) \mathbf{k} \quad (19a)$$

in which the wind velocity components w_x , w_y , w_z are defined in any manner desired.

Obtaining the generalized forces due to lift and drag, which are derived above in the Cartesian coordinate system, is accomplished simply by transforming them into the generalized (spherical) coordinate system. Thus, if the components of the vectors \mathbf{L}_i and \mathbf{D}_i are called L_{xi} , L_{yi} , L_{zi} and D_{xi} , D_{yi} , D_{zi} respectively, the generalized force on the system in the θ_j direction is

$$Q_{\theta_j} = \sum_{i=1}^N \left[(L_x + D_x)_i \frac{\partial x_i}{\partial \theta_j} + (L_y + D_y)_i \frac{\partial y_i}{\partial \theta_j} + (L_z + D_z)_i \frac{\partial z_i}{\partial \theta_j} \right] \quad (24a)$$

and similarly

$$Q_{\phi_j} = \sum_{i=1}^N \left[(L_x + D_x)_i \frac{\partial x_i}{\partial \phi_j} + (L_y + D_y)_i \frac{\partial y_i}{\partial \phi_j} + (L_z + D_z)_i \frac{\partial z_i}{\partial \phi_j} \right] \quad (24b)$$

$$Q_{h_j} = \sum_{i=1}^N \left[(L_x + D_x)_i \frac{\partial x_i}{\partial h_j} + (L_y + D_y)_i \frac{\partial y_i}{\partial h_j} + (L_z + D_z)_i \frac{\partial z_i}{\partial h_j} \right] \quad (24c)$$

b. Due to axial deformation

It is readily apparent that the force applied to the i th point due to cable elongation will always be along the h_i coordinate and that it will be exactly the tension corresponding to that elongation. The generalized force on the system is then simply,

$$Q_{\theta_j} = 0 \quad (25a)$$

$$Q_{\phi_j} = 0 \quad (25b)$$

$$Q_{h_j} = P_j, P_j \text{ being the tension.} \quad (25c)$$

The difficulty here arises in relating tension and deformation analytically, since the variety of tensile properties available makes the formulation of a single analytic statement unthinkable. It is for this reason that tension is included as a generalized force rather than a potential function. In this way any method of describing the relation between tension and deformation may be used, including tables of experimental data, although these are likely to be unwieldy except in the simplest of cases.

For the purpose of obtaining a solution, a first approximation is made to the load-deflection curve shown in Figure (27) for braided nylon cable. The loading curve is represented by a table of strain vs. the ratio of load to strain, upon which linear interpolation is performed. (This gives exact results if the curve being approximated is a quadratic; if the curve is given by $y = Ax^2 + Bx$, with the intercept at the origin, then $y/x = Ax + B$, which is a linear function.) The unloading curve is then considered to be of the same shape as the loading curve but rotated about the maximum load point an appropriate amount. Elongation damping is incorporated as a function of mass, stiffness and elongation rate, where the stiffness is merely taken as the ratio of current load to current strain.

Given a value of strain ϵ_i , length h_i and elongation rate \dot{h}_i for a segment, the following steps yield the tension P_i :

$h_i \geq$ any previous value:

The table is entered and a value of P_i/ϵ_i obtained.

$h_i <$ some previous value:

$$\epsilon_T = \frac{\epsilon_i - \epsilon_m(1-C)}{C} \quad (26)$$

where C is the rotation factor for the unloading curve,

ϵ_m is the previous maximum strain, and

ϵ_T replaces ϵ_i for the table and further computation.

Then the tension

$$P_i = \epsilon_i \left(\frac{P_i}{\epsilon_i} \right) + k \left(2 \sqrt{m_i P_i / \epsilon_i} \dot{h}_i \right) \quad (27)$$

c. Total forces

The generalized forces on the cable are now the sum of aerodynamic and elongation forces, giving

$$Q_{\theta_j} = \sum_{i=j}^N \left[(L_x + D_x)_i \frac{\partial x_i}{\partial \theta_j} + (L_y + D_y)_i \frac{\partial y_i}{\partial \theta_j} + (L_z + D_z)_i \frac{\partial z_i}{\partial \theta_j} \right] \quad (28a)$$

$$Q_{\phi_j} = \sum_{i=j}^N \left[(L_x + D_x)_i \frac{\partial x_i}{\partial \phi_j} + (L_y + D_y)_i \frac{\partial y_i}{\partial \phi_j} + (L_z + D_z)_i \frac{\partial z_i}{\partial \phi_j} \right] \quad (28b)$$

$$Q_{h_j} = \sum_{i=1}^N \left[(L_x + D_x)_i \frac{\partial x_i}{\partial h_j} + (L_y + D_y)_i \frac{\partial y_i}{\partial h_j} + (L_z + D_z)_i \frac{\partial z_i}{\partial h_j} \right] - P_j \quad (28c)$$

The elements of the matrix used for transforming from Cartesian to spherical coordinates are obtained by differentiating Equations(2) with respect to the appropriate spherical coordinate, giving terms of the form

$$\frac{\partial x_i}{\partial \theta_j} = h_j \cos \theta_j \cos \phi_j$$

$$\frac{\partial x_i}{\partial \phi_j} = -h_j \sin \theta_j \sin \phi_j$$

$$\frac{\partial x_i}{\partial h_j} = \sin \theta_j \cos \phi_j$$

and so forth.

7) The Final Equations:

All the terms required by the Lagrange formulation are now defined, and the final equations of motion of the cable model postulated may be obtained by substituting Equations (9), (12) and (28) into Equations(3). If

$$M_j = \sum_{i=1}^N m_i$$

and it is noted that

$$\sum_{i=1}^N \sum_{k=2}^i m_i f_R = \sum_{k=2}^{j-1} \sum_{i=j}^N m_i f_R + \sum_{k=j}^N \sum_{i=k}^N m_i f_R = \sum_{k=2}^{j-1} M_j f_R + \sum_{k=j}^N M_k f_R$$

then the necessary algebra and trigonometric substitutions which yield the final equations are readily performed. These are

$$\begin{aligned}
& \sum_{k=2}^{j-1} M_j \left\{ \ddot{\Theta}_k h_k [\cos \Theta_j \cos \Theta_k \cos(\phi_k - \phi_j) + \sin \Theta_j \sin \Theta_k] + \right. \\
& \quad - \ddot{\Phi}_k h_k [\cos \Theta_j \sin \Theta_k \sin(\phi_k - \phi_j)] + \\
& \quad \left. + \ddot{h}_k [\cos \Theta_j \sin \Theta_k \cos(\phi_k - \phi_j) + \sin \Theta_j \cos \Theta_k] \right\} + \\
& + \sum_{k=j}^N M_k \left\{ \ddot{\Theta}_k h_k [\cos \Theta_j \cos \Theta_k \cos(\phi_k - \phi_j) + \sin \Theta_j \sin \Theta_k] + \right. \\
& \quad - \ddot{\Phi}_k h_k [\cos \Theta_j \sin \Theta_k \sin(\phi_k - \phi_j)] + \\
& \quad \left. + \ddot{h}_k [\cos \Theta_j \sin \Theta_k \cos(\phi_k - \phi_j) + \sin \Theta_j \cos \Theta_k] \right\} = \\
& + \sum_{i=j}^N \left\{ m_i \sum_{k=2}^i \left[h_k (\ddot{\Theta}_k^2 + \dot{\Phi}_k^2) \cos \Theta_j \sin \Theta_k \cos(\phi_k - \phi_j) + (29a) \right. \right. \\
& \quad + 2 h_k \dot{\Theta}_k \dot{\Phi}_k \cos \Theta_j \cos \Theta_k \sin(\phi_k - \phi_j) + \\
& \quad - 2 \dot{\Theta}_k \dot{h}_k [\cos \Theta_j \cos \Theta_k \cos(\phi_k - \phi_j) + \sin \Theta_j \sin \Theta_k] + \\
& \quad + 2 \dot{\Phi}_k \dot{h}_k \cos \Theta_j \sin \Theta_k \sin(\phi_k - \phi_j) + \\
& \quad \left. - h_k \dot{\Theta}_k^2 \sin \Theta_j \cos \Theta_k \right] + \\
& \quad - \left[(m_i \ddot{x}_i - [D_{x_i} + L_{x_i}]) \cos \Theta_j \cos \phi_j + \right. \\
& \quad + (m_i \ddot{y}_i - [D_{y_i} + L_{y_i}]) \cos \Theta_j \sin \phi_j + \\
& \quad \left. - (m_i [\ddot{z}_i - g] - [D_{z_i} + L_{z_i}]) \sin \Theta_j \right] \left. \right\}
\end{aligned}$$

$$\begin{aligned}
& \sum_{k=2}^{j-1} M_i \left\{ \ddot{\theta}_k h_k [\sin \theta_j \cos \theta_k \sin (\phi_k - \phi_j)] + \right. \\
& \quad + \ddot{\phi}_k h_k [\sin \theta_j \sin \theta_k \cos (\phi_k - \phi_j)] + \\
& \quad \left. + \ddot{h}_k [\sin \theta_j \sin \theta_k \sin (\phi_k - \phi_j)] \right\} + \\
& + \sum_{k=j}^N M_k \left\{ \ddot{\theta}_k h_k [\sin \theta_j \cos \theta_k \sin (\phi_k - \phi_j)] + \right. \\
& \quad + \ddot{\phi}_k h_k [\sin \theta_j \sin \theta_k \cos (\phi_k - \phi_j)] + \\
& \quad \left. + \ddot{h}_k [\sin \theta_j \sin \theta_k \sin (\phi_k - \phi_j)] \right\} = (29b) \\
& + \sum_{i=j}^N \left\{ -m_i \sum_{k=2}^i \left[h_k (\ddot{\theta}_k^2 + \dot{\phi}_k^2) \sin \theta_j \sin \theta_k \sin (\phi_k - \phi_j) + \right. \right. \\
& \quad + 2 h_k \dot{\theta}_k \dot{\phi}_k \sin \theta_j \cos \theta_k \cos (\phi_k - \phi_j) + \\
& \quad + 2 \dot{\theta}_k \dot{h}_k \sin \theta_j \cos \theta_k \sin (\phi_k - \phi_j) + \\
& \quad \left. + 2 \dot{\phi}_k \dot{h}_k \sin \theta_j \sin \theta_k \cos (\phi_k - \phi_j) \right] + \\
& \quad + \left[(m_i \ddot{x}_i - [D_{x_i} + L_{x_i}]) \sin \theta_j \sin \phi_j + \right. \\
& \quad \left. - (m_i \ddot{y}_i - [D_{y_i} + L_{y_i}]) \sin \theta_j \cos \phi_j \right] \left. \right\}
\end{aligned}$$

$$\begin{aligned}
& \sum_{k=2}^{j-1} M_j \left\{ \ddot{\theta}_k h_k \left[\sin \theta_j \cos \theta_k \cos (\phi_k - \phi_j) - \cos \theta_j \sin \theta_k \right] + \right. \\
& \quad - \ddot{\phi}_k h_k \left[\sin \theta_j \sin \theta_k \sin (\phi_k - \phi_j) \right] + \\
& \quad \left. + \ddot{h}_k \left[\sin \theta_j \sin \theta_k \cos (\phi_k - \phi_j) + \cos \theta_j \cos \theta_k \right] \right\} + \\
& + \sum_{k=j}^N M_k \left\{ \ddot{\theta}_k h_k \left[\sin \theta_k \cos \theta_k \cos (\phi_k - \phi_j) - \cos \theta_j \sin \theta_k \right] + \right. \\
& \quad - \ddot{\phi}_k h_k \left[\sin \theta_j \sin \theta_k \sin (\phi_k - \phi_j) \right] + \\
& \quad \left. + \ddot{h}_k \left[\sin \theta_j \sin \theta_k \cos (\phi_k - \phi_j) + \cos \theta_j \cos \theta_k \right] \right\} = \\
& + \sum_{i=j}^N \left\{ m_i \sum_{k=2}^i \left[h_k (\ddot{\theta}_k^2 + \dot{\phi}_k^2) \sin \theta_j \sin \theta_k \cos (\phi_k - \phi_j) \right] + (29c) \right. \\
& \quad + 2 h_k \dot{\theta}_k \dot{\phi}_k \sin \theta_j \cos \theta_k \sin (\phi_k - \phi_j) + \\
& \quad - 2 \dot{\theta}_k \dot{h}_k \left[\sin \theta_j \cos \theta_k \cos (\phi_k - \phi_j) - \cos \theta_j \sin \theta_k \right] + \\
& \quad + 2 \dot{\phi}_k \dot{h}_k \sin \theta_j \sin \theta_k \sin (\phi_k - \phi_j) + \\
& \quad + h_k \dot{\theta}_k^2 \cos \theta_j \cos \theta_k + \\
& \quad - \left[(m_i \ddot{x}_i - [D_{x_i} + L_{x_i}]) \sin \theta_j \cos \phi_j + \right. \\
& \quad + (m_i \ddot{y}_i - [D_{y_i} + L_{y_i}]) \sin \theta_j \sin \phi_j + \\
& \quad \left. + (m_i [\ddot{z}_i - g] - [D_{z_i} + L_{z_i}]) \cos \theta_j \right] \Big\} - P_j
\end{aligned}$$

Let the right-hand sides of Equations(29) be called Σ_{1j} , Σ_{2j} and Σ_{3j} respectively, and let the following substitutions be made for the trigonometric functions:

$$\alpha_{jk} = -h_k \cos \theta_j \sin \theta_k \sin(\phi_k - \phi_j) \quad (30a)$$

$$\beta_{jk} = h_k [\cos \theta_j \cos \theta_k \cos(\phi_k - \phi_j) + \sin \theta_j \sin \theta_k] \quad (30b)$$

$$C_{jk} = [\cos \theta_j \sin \theta_k \cos(\phi_k - \phi_j) + \sin \theta_j \cos \theta_k] \quad (30c)$$

$$\gamma_{jk} = h_k \sin \theta_j \cos \theta_k \sin(\phi_k - \phi_j) \quad (30d)$$

$$\mathcal{T}_{jk} = h_k \sin \theta_j \sin \theta_k \cos(\phi_k - \phi_j) \quad (30e)$$

$$D_{jk} = \sin \theta_j \sin \theta_k \sin(\phi_k - \phi_j) \quad (30f)$$

$$E_{jk} = h_k [\sin \theta_j \cos \theta_k \cos(\phi_k - \phi_j) - \cos \theta_j \sin \theta_k] \quad (30g)$$

$$F_{jk} = -h_k \sin \theta_j \sin \theta_k \sin(\phi_k - \phi_j) \quad (30h)$$

$$G_{jk} = \sin \theta_j \sin \theta_k \cos(\phi_k - \phi_j) + \cos \theta_j \cos \theta_k \quad (30i)$$

Equations(29) may now be written succinctly in matrix form for solution:

$$\begin{bmatrix} M_i \alpha_{jk} & M_i \beta_{jk} & M_i C_{jk} \\ M_i \mathcal{T}_{jk} & M_i \gamma_{jk} & M_i D_{jk} \\ M_i F_{jk} & M_i E_{jk} & M_i G_{jk} \end{bmatrix} \begin{bmatrix} \ddot{\phi}_j \\ \ddot{\theta}_j \\ \ddot{h}_j \end{bmatrix} = \begin{bmatrix} \Sigma_{1j} \\ \Sigma_{2j} \\ \Sigma_{3j} \end{bmatrix} \quad (31)$$

where $i = j$ for $2 \leq k \leq j$
 $i = k$ for $j \leq k \leq N$

Given the initial position and velocity of each of the N points on the cable, this set of simultaneous equations is solved for the unknown accelerations. These are then integrated twice numerically using Adams Method, giving the new positions and velocities, which are in turn used to obtain the new accelerations from Equations(31). This cycle is repeated for as long a period as may be of interest. A program has been written for the IBM 7090 digital computer which performs the sequence of operations outlined above, using any integration interval desired. An interval on the order of .001 sec. has been found generally applicable.

31

C. Boundary Conditions

Expressions are developed here by which the bottom of the cable is constrained to move in a horizontal plane. This is done to simulate the various effects which might result from having the lower end of the cable on the ground. Specifically, two types of action are considered: that in which the end point of the cable is free to move in the horizontal plane but is subjected to static and dynamic friction forces, and that in which the motion of the bottom point in the horizontal plane is specified, regardless of any applied loads. In either case, the constraint is removed and the bottom becomes free when the vertical component of tension in the last cable segment exceeds a predetermined value.

1) Forces applied:

It is apparent from Section I-B above that each point mass has three degrees of freedom, namely θ , ϕ and h . If the bottom point is now constrained to move in a horizontal plane it is left with only two degrees of freedom. In this case, it is necessary to revert to the Cartesian coordinate system, in which the missing degree of freedom can be simply described as Z_N , the vertical displacement. It is equally convenient to describe the remaining degrees of freedom as X_N and Y_N .

The number of Equations (31) to be solved simultaneously is then reduced by three, and the tension in the last cable segment is applied to the $(N-1)$ th point as a generalized force. The tension, aerodynamic forces and ground friction forces on the N th point are used to set up two separate equations on X_N and Y_N . These equations are obtained as follows:

The upward component of force on the last mass point is

$$F_z = (P \cos \theta - L_z)_N \quad (32)$$

The friction forces then depend on the net downward force, or

$$F_f = C_f (m_N g - F_z) \quad (33a)$$

$$F_s = C_s (m_N g - F_z) \quad (33b)$$

where C_f is the coefficient of sliding friction and C_s is the coefficient of static friction. The applied forces in the horizontal plane are

$$F_x = (L_x + D_x - P \sin \theta \cos \phi)_N \quad (34a)$$

$$F_y = (L_y + D_y - P \sin \theta \sin \phi)_N \quad (34b)$$

If the total applied force is less than the static friction force, that is,

$$\sqrt{F_x^2 + F_y^2} < F_s$$

then \ddot{X}_N and \ddot{Y}_N are set to zero and the point is assumed stationary. If the reverse is true, the components of the sliding friction force in the x and y directions become applied forces in their respective directions, and the accelerations are defined as

$$\ddot{X}_N = \left[F_x - F_f \left(\frac{\dot{X}_N}{\sqrt{\dot{X}_N^2 + \dot{Y}_N^2}} \right) \right] \frac{1}{m_N} \quad (35a)$$

$$\ddot{Y}_N = \left[F_y - F_f \left(\frac{\dot{Y}_N}{\sqrt{\dot{X}_N^2 + \dot{Y}_N^2}} \right) \right] \frac{1}{m_N} \quad (35b)$$

which are integrated along with the spherical accelerations obtained by solution of Equations (31). This is continued until the net downward force becomes negative, that is,

$$F_z > m_N g$$

after which the bottom point is considered free to move upward, and the entire system is solved by means of Equations (31).

2) Motion specified:

If it is found necessary to move the end of the cable from one point on the ground to another (e.g., from the point of impact to the payload) the three degrees of freedom of the N^{th} mass point may be constrained such that Z_N is a constant (ground level), \dot{Z}_N is zero, and X_N , \dot{X}_N , Y_N and \dot{Y}_N are specified to produce the desired motion. The dynamics of the rest of the system are again solved for by means of Equations (31), reduced in number by three. Tension in the last cable segment is still applied as a generalized force to the $(N-1)^{\text{th}}$ point, although it does not now affect motion of the N^{th} point. If at any time the vertical component of force F_z on the last point exceeds some predetermined multiple of the end point weight, the end point is considered to have lifted off, and it then regains its three degrees of freedom.

D. Inextensible Cable

It was pointed out at the end of Part B of this section that the computer program of the analysis typically uses integration time increments on the order of .001 second. Obviously, then, a 100-second run takes 100,000 cycles which, with the amount of algebra involved, takes a considerable amount of computer time even on the IBM 7090. Such small time increments are required because the extensional degrees of freedom contain high frequency components. The frequency components in the angular degrees of freedom are much lower, however, so that if extensibility is eliminated larger time increments may be used, resulting in a considerable saving of computer time. A further saving arises from the fact that removing the extensional degrees of freedom reduces the number of simultaneous equations to solve and integrate from $3(N-1)$ to $2(N-1)$, as well as eliminating certain computations altogether (e.g. elasticity).

Of course, this is done at the cost of a certain amount of generality. An analysis which considered the mass points to be a fixed distance apart would not be suitable for certain types of cable motion in which longitudinal transients were of considerable significance (e.g. Snatch-Type pickups, described in Section II). On the other hand, if the steady state were of primary interest (as in some Circling Line maneuvers, also described in Section II) the main effect is that nominal rather than calculated cable lengths are used, resulting in somewhat different (conservative) tensions. Since this situation arises frequently enough to make the time saving worthwhile, a computer program has been written along these lines.

The analysis developed in Part B of this section is relatively easily modified by setting each h_j equal to a constant, so that its derivatives are all zero. By the same token, all derivatives taken with respect to h_j or its time derivatives disappear as well. Thus, Equations (10), for example, now consist of Θ_j (10a) and Φ_j (10b) expressions only.

If these substitutions are made throughout the analysis in a consistent fashion, and if the remaining dependent equations on h_j (e.g. Equation 10c) are discarded, the result is the following simplified set of simultaneous equations:

$$\begin{bmatrix} M_i \alpha_{jk} & M_i \beta_{jk} \\ M_i \gamma_{jk} & M_i \delta_{jk} \end{bmatrix} \begin{bmatrix} \ddot{\Phi}_j \\ \ddot{\Theta}_j \end{bmatrix} = \begin{bmatrix} \Sigma_{1j} \\ \Sigma_{2j} \end{bmatrix} \quad (31a)$$

$$\begin{array}{lll} \text{where} & k = j & \text{for } 2 \leq k \leq j \\ & i = k & \text{for } j \leq k \leq N \end{array}$$

These equations are processed in the same manner as outlined for Equations (31). A time increment of the order of .05 second has been found typical for the computer program of this simplified analysis.

It should be noted that it is in this simplified analysis that the merits of the spherical coordinates used appear most strongly. The generalized coordinate of this model are now Θ_j and Φ_j , the h_j having merely been deleted. Cartesian coordinates are in this case quite unsuitable, since all three are still needed to describe motion.

E. Conclusions and Recommendations

The analytical techniques developed in this section represent a general description of cable response due to arbitrary prescribed motion of one end. It is felt that the assumptions and restrictions made are such as will not impose any serious limitations on the usefulness of these techniques as an engineering tool. Having been programmed for the IBM 7090 computer, the analysis is presently capable of calculating tension, position, velocity and acceleration at any predetermined point in the cable as a function of time. Variations in any of the following parameters are readily handled:

1. Line Description

- a) diameter at each point
- b) mass at each point
- c) aerodynamic force coefficient at each point
- d) initial length of each segment
- e) elastic characteristics of each segment

2. Attachments to the line

- a) mass at any point, in particular the payload
- b) drag at any point, as the drag of the payload or a parachute
- c) buoyancy at any point

3. Initial configuration of the line

- a) shape
- b) orientation
- c) proportion of line attached to airplane vs. that attached to payload

4. Wind effects

- a) wind velocity constant (or zero)
- b) wind velocity varying with altitude

5. Lower end conditions

- a) end point fixed on the ground
- b) end point motion on the ground arbitrarily specified
- c) end point motion free on the ground with specified static and dynamic friction coefficients
- d) end point free in the air

It is felt that this analysis could be made more useful by increasing its scope somewhat. Specifically, three things could be added to facilitate solution of the problems in designing an aircraft-cable-payload system. These are:

- 1. Variation of unstretched line length with time.
- 2. The possibility of specifying applied forces rather than motion at the top of the cable.
- 3. The possibility of specifying arbitrary applied force time histories at any point in the cable.

35

Grumman PROJECT 306

The first of these will allow computation of the effects of paying line out from and reeling it into the airplane towing the cable. Such a requirement might come up both in landing a hook for attachment to the payload and in drawing the payload up to the airplane.

The second will permit calculation of the feedback between airplane and cable; that is, how the cable forces applied to the airplane affect its performance, and how changes in airplane motion affect cable motion. The latter is expected to be of less importance, but effect on airplane performance might be significant in the case of heavy payloads.

The third suggested addition makes provision for computing the effect on cable motion of attached aerodynamic devices (e.g. paravanes), as well as various kinds of impact forces which might be encountered.

SECTION II - EXPERIMENT

A. Purpose

A series of flight tests were performed to obtain in-flight data of payload performance for circling line and snatch type pick-up retrieval methods. An outline of the test program is given in Table 1. The purpose of the tests was to determine the accuracy and possible limitations of the theory previously discussed, under actual field conditions. For the circling line, the program was designed to determine trends in unrestrained payload motion as a function of certain governing parameters. For example, trends were established for variations in airplane bank angle, payload weight and cable drag/weight ratio. To determine characteristics of ground-to-air payload motion, the snatch type technique was used.

B. Experimental Technique

1) Test Apparatus:

a. Test Vehicle

The test vehicle used was the Grumman "Ag-Cat" (an agricultural crop-duster aircraft) shown in Figure 2. This aircraft is a bi-plane with an overall length of 24' 4", a gross weight of approximately 2600 lbs., a maximum speed of 110 mph in level flight and a stall speed of approximately 48 mph. A glider tow release mechanism was installed in the aircraft for these tests. It was located on the fuselage near the trailing edge of the left lower wing root with the release mechanism inside the cockpit. This release fitting is shown in Figures 3 and 4. Cockpit and cowl instrumentation are shown in Figures 5 and 6.

High maneuverability at low speeds and relatively low cost, maintenance free operation made the Ag-Cat a well suited vehicle for this program.

b. Test Payload

The test payload, in the shape of a small scale Gemini capsule, was fabricated at the Contractor's facilities. The capsule was approximately 30" in height and the diameter varied from 10" at the top to 25" at the base. The outer covering was a heavy canvas fabric painted bright orange for maximum visibility. The interior of the capsule was filled with layers of ensolite to provide rigidity and to absorb forces due to landing. The basic capsule weighed approximately 20 lbs. but the weight was increased during the test by adding bags of lead shot internally. The capsule is shown in Figure 2. This payload was used for circling line tests conducted in flights 1 thru 5. At the conclusion of flight 5, the line and payload was released from the aircraft at an abnormally high altitude and the capsule was severely damaged. A canvas bag of approximately the same dimensions was used for the remaining flights.

Table 1
Summary of Flight Test Program

<u>A. Circling Line Tests</u>						
Test #	Flight Conditions			Type of Line	Approx. Length of Line Ft.	Approx. Payload Wt.
	Velocity MPH (Approx.)	Altitude Ft. (Approx.)	Bank Angle			
1 a b c	75	2500	30° 40° 50°	$\frac{1}{4}$ " Nylon Line	1800	50#
2 a b c	75	2500	30° 40° 50°	$\frac{1}{4}$ " Nylon Line	1800	100#
3 a b c	75	2500	30° 40° 50°	$\frac{1}{2}$ " Poly Pro	1800	50#
4 a b c	75	2500	30° 40° 50°	$\frac{1}{2}$ " Poly Pro	1800	100#
5 a b c	75	2500	30° 40° 50°	$\frac{1}{4}$ " Steel Cable	1800	50#

<u>B. Snatch Type Pick-up Tests</u>						
#1	75	175'	0°	3/16" Nylon Line	150'	50#
#2	75	225'	0°	3/16" Nylon Line	200'	50#
#3	75	160'	0°	3/16" Nylon Line	150'	50#

c. Balloons

Ten foot diameter hydrogen-filled balloons were used in the snatch-type pick-up tests to support the line attached to the test payload. The balloons were made of 3-mil polyethelene and weighed 4.9 pounds each.

d. Test Lines

Circling Line Tests

Test lines procured from commercial vendors were used to conduct the circling line tests. Three specific lines of varying drag/weight ratio were used to determine the effect of this ratio on the motion of the payload under otherwise similiar conditions. These lines were:

- 1) 1/4" diameter - 3 strand nylon rope (1.5#/100 ft.)
- 2) 1/2" diameter - 3 strand polypropylene rope (4.75#/100 ft.)
- 3) 1/4" diameter - 6 x 7 plough steel cable (11#/100 ft.)

Snatch Type Pick-up Tests

All snatch type pick-up tests were conducted using 3/16" diameter - 3 strand nylon rope attached to the payload and 1/8" x 3/8" braided nylon rope trailed from the aircraft, holding the bob-weight.

2) Instrumentation,

a. Strain Link and Oscillograph

A 500 lb. maximum load calibrated strain link was installed at the line attachment to the aircraft to measure line tension. The link is a bending member which by means of strain gages converts loads into electrical signals. To record the tension time history a 6-channel 409 Century Oscillograph was installed in the hopper section of the test aircraft. The paper speed of the oscillograph was set at approximately 2 inches per second to provide continuous recording for approximately 15 minutes. Controls for operating this system were installed in the cockpit. (See Figure 7.)

b. Ground Cameras

Ground motion picture cameras were set up at the test site to photograph the motion of the payload during circling line and snatch pick-up tests. For circling line tests, the cameras were operated at 24 frames per second. After several attempts, it was found that the payload was not visible on film when the camera was positioned far enough away from the payload to record its entire path of travel. Thereafter, the cameras were used only to record payload lift-off.

During snatch type pick-up tests, three ground cameras operating at 64 frames/second were used. One camera was located approximately 800 ft. from the line of flight to record simultaneously the aircraft

and payload trajectories. The second camera was positioned to record the hook impact with the supporting balloon, while the third camera recorded initial payload motion. The results obtained with these cameras are available for viewing.

c. Transits

Since adequate data could not be obtained using photographic means for the circling line tests, manually operated transits were used to track the payload. Two transits were stationed approximately 1000 ft. apart, each with a crew of five persons. As the operator tracked the payload, one crew member read elevation angles, another azimuth angles, while the remaining two recorded the readings and called out time. A prearranged signal between the two stations insured that both began tracking simultaneously, and thereafter each took readings at five second intervals.

d. Fairchild Flight Analyzer

Along with the motion picture cameras, a Fairchild Flight Analyzer was used to record payload trajectory during snatch type pickups. This instrument displays pictorially on a single negative the space traverse of a moving object. To accomplish this, an operator tracks the object manually using binoculars attached to the camera. The camera exposed a photographic plate in 58 vertical strips during a full sweep (70°) of its field. This results in a series of images of the capsule appearing at equally spaced positions along its trajectory. While the position of the object is being recorded, the time at exposure is recorded at the base of each strip by a timing mechanism capable of being read accurately to a thousandth of a second. Since the camera was set back from the flight path a predetermined amount (700 ft.), a proper scale factor could be determined to correlate distances measured from the data plate with the full scale dimensions of the trajectory.

3) Test Area:

The flight test program for the Surface-to-Air Retrieval Study was conducted in its entirety at the Contractor's flight test facility at Calverton, New York, which includes 78,400 sq. ft. of hangar space, a 10,000 ft. runway and a 7500 ft. runway on 3500 acres of land. The snatch type pick-up tests were conducted along the shorter runway, with numbered cards placed at 100 ft. intervals to provide recorded reference dimensions for film data reduction. The circling line tests were conducted over the runways since large open areas were required to allow drifting due to winds.

4) Procedure:

a. Circling Line Tests

The 1800 ft. test line was laid out in a straight line along the runway in front of the aircraft. One end was attached to the aircraft through the strain link at the glider tow release mechanism and the

opposite end was attached to the test payload. As the aircraft took off and climbed, approaching the payload, the line was gently lifted off the runway. The aircraft climbed to approximately 1800 feet while orbiting the test payload. At this altitude, all the cable was in the air and the test line began to tighten. The climb was continued until the payload was lifted off and brought up to a sufficient altitude. During this maneuver, the payload was dragged a considerable distance along the ground before becoming airborne. The pilot then flew the aircraft and payload to the area of operation. When the ground crew, manning cameras and transits, were ready to record, a radio signal was transmitted to the test aircraft via the Operations Tower and the test was initiated. After starting the oscillograph to record line tension, the pilot turned the aircraft into a constant velocity, constant bank angle maneuver holding altitude constant. In an attempt to minimize wind effects, the entire system was permitted to drift with the wind. When sufficient data were obtained from the transits, the run was ended and a new run commenced at a different bank angle. When all runs were completed for the flight, the test line and payload were dropped by releasing the glider tow mechanism, and the airplane landed.

b. Snatch Pick-up Tests

A hydrogen filled balloon attached to the test payload by means of a nylon line of approximately 150 ft. was erected at the test site, along the 7500 ft. runway. Additional nylon line was draped over the balloon in two loops at right angles to one another and connected to the vertical nylon line below. The Fairchild Flight Analyzer and movie cameras were set up at the test site and placed at pre-determined positions to record the first 1000 feet of horizontal travel. The test aircraft, trailing the bob-weight-hook, then flew at constant airspeed and altitude such that the hook punctured the balloon and engaged the line looped around it. An attempt was made to keep the trajectory in one plane by directing the flight path of the test vehicle along the direction of wind. The pilot started the oscillograph during the approach and a record of tension in the line through-out the trajectory was obtained.

Fig. 2 . Ag-Cat Test Aircraft with Scale Capsule Model

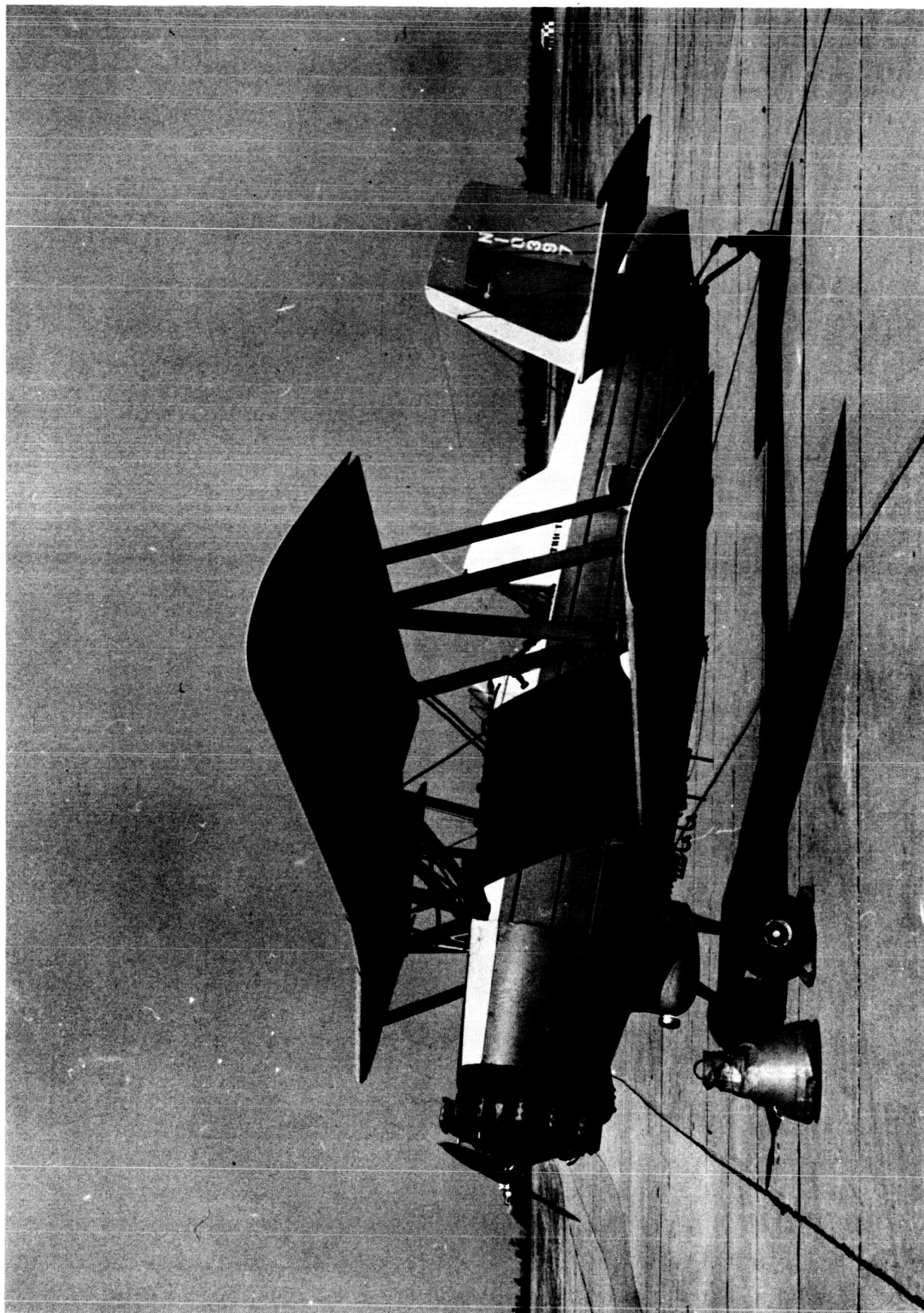


Fig. 3 . Ag-Cat Line Release Attachment in *Closed* Position

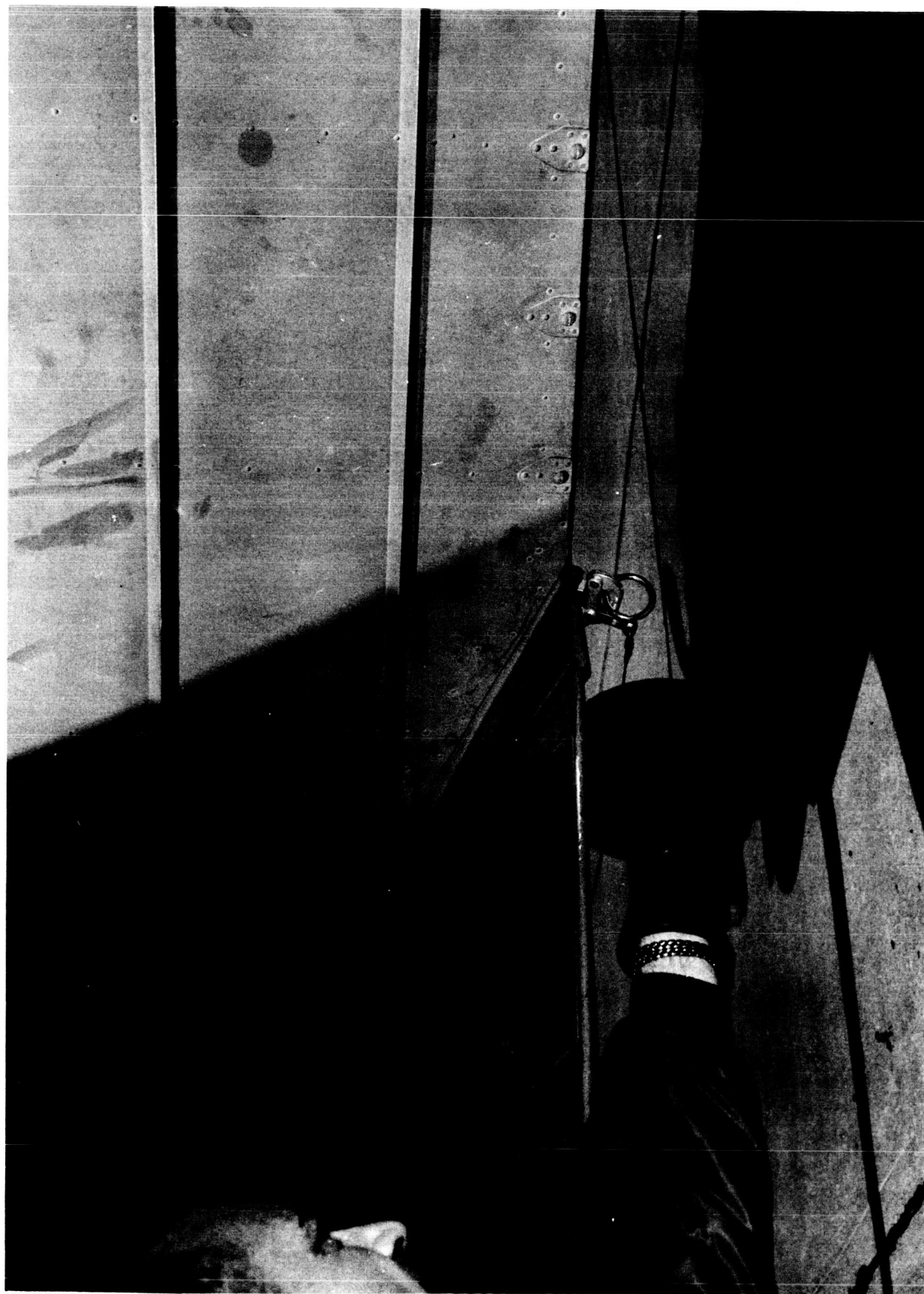
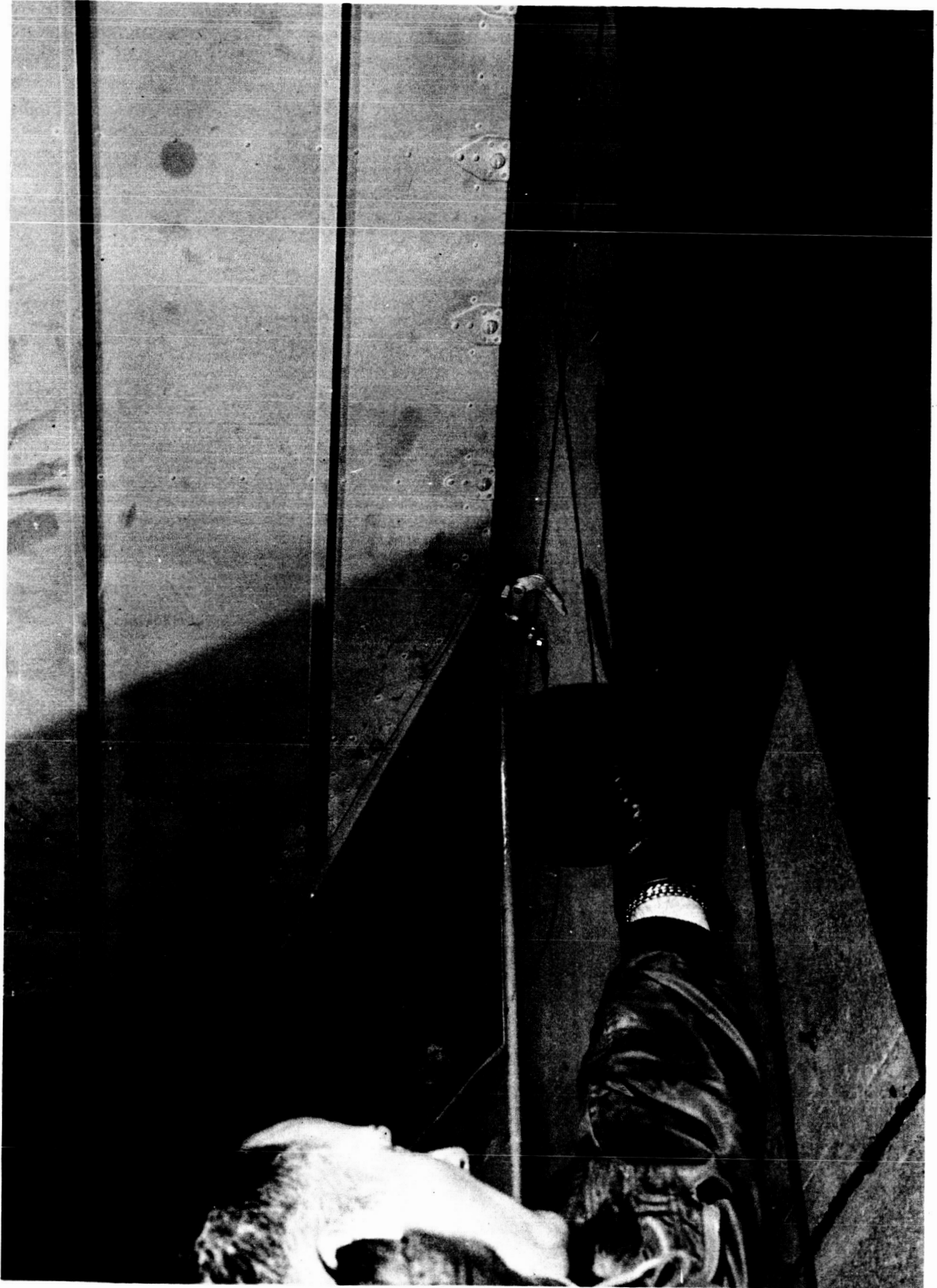


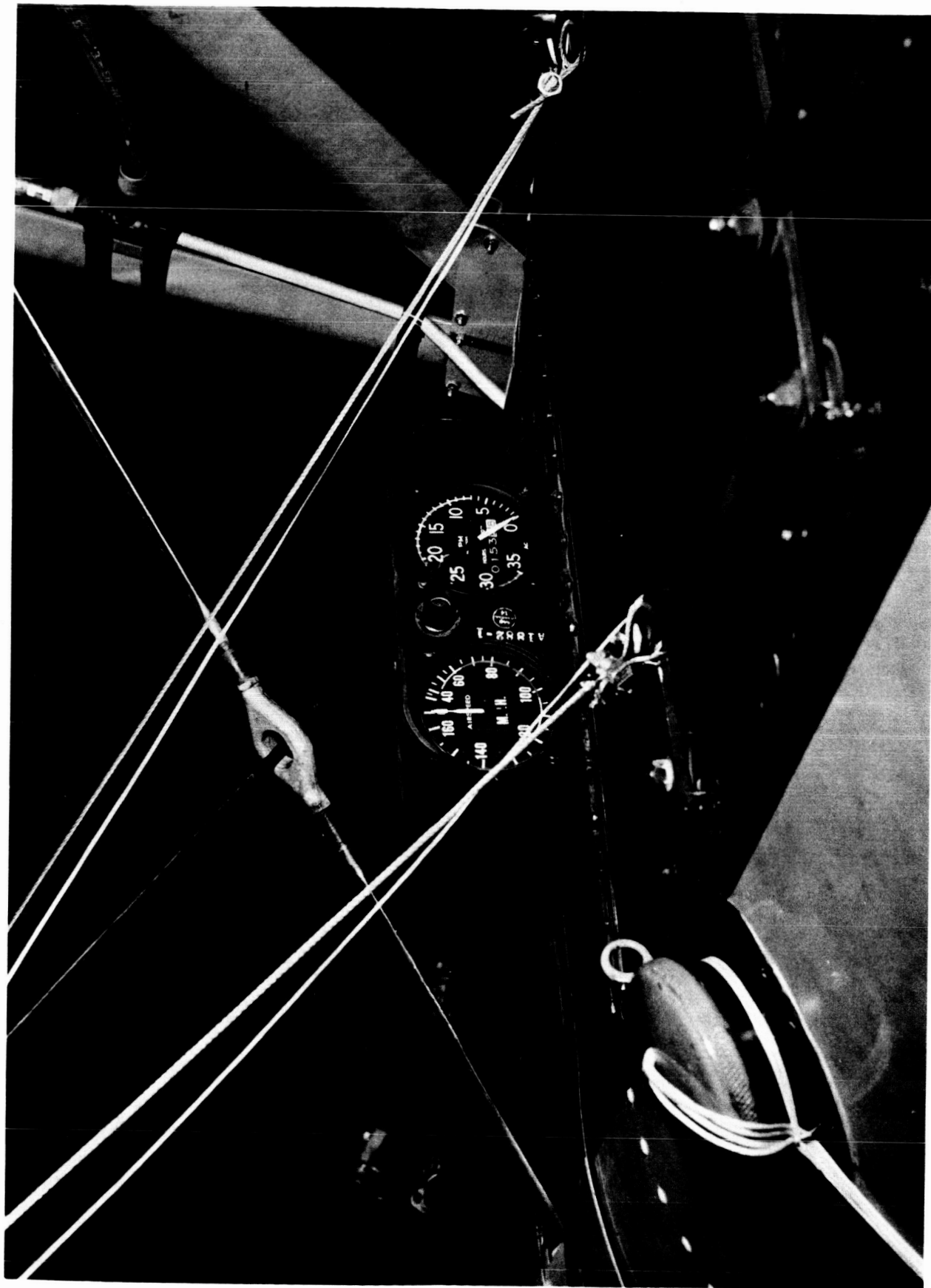
Fig. 4 . Ag-Cat Line Release Attachment in OPEN Position



4.4

Grumman PROJECT 306

Fig. 5 . Ag-Cat Cowl Instrument Panel



45

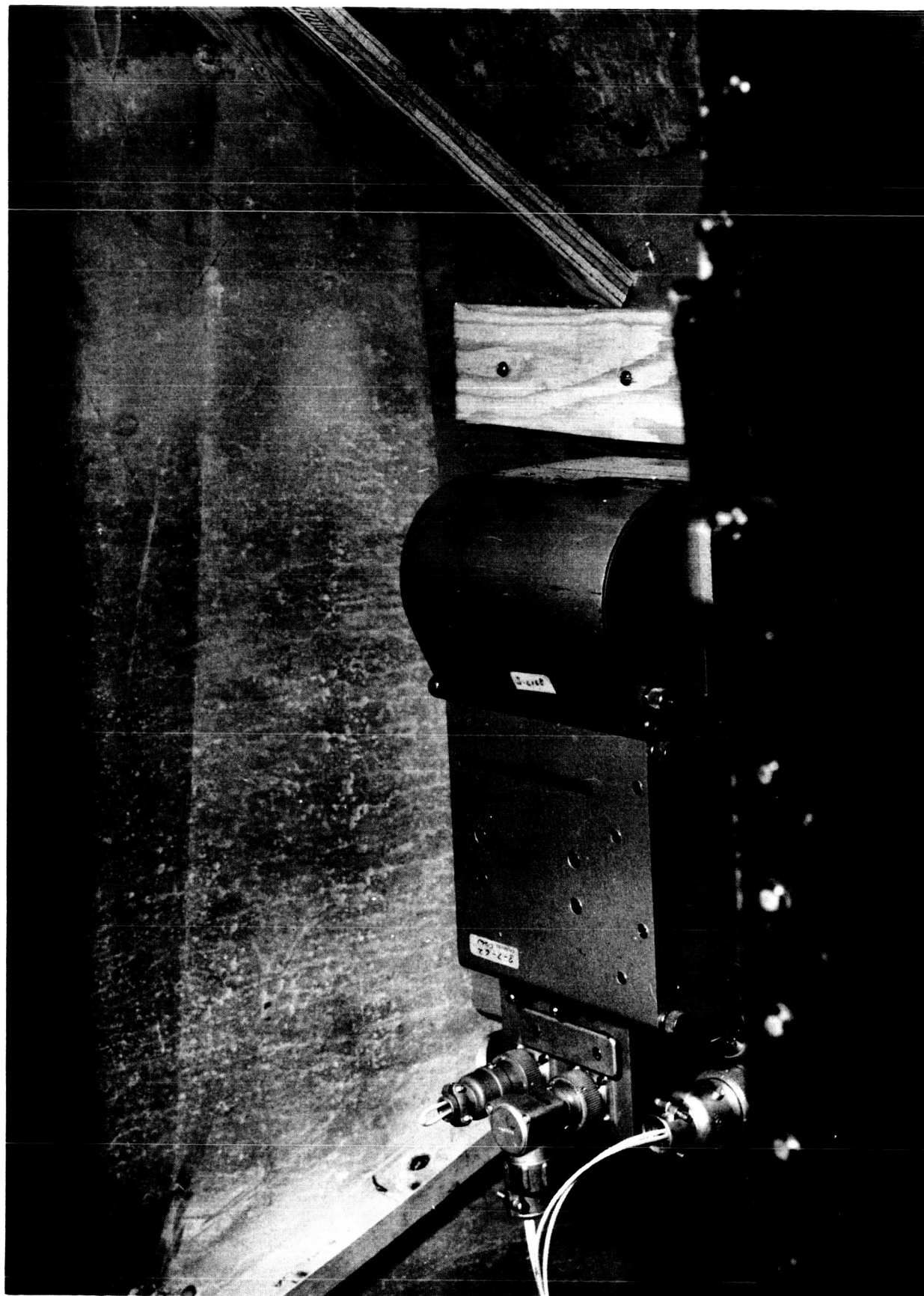
Grumman PROJECT 306

Fig. 6 . Cockpit Instrument Panel of Ag-Cat



46

Fig. 7 . Oscillograph Installation in Ag-Cat Hopper



C. Experimental Results and Comparison With Theory - Circling Line

1) Introduction:

Using the techniques and equipment previously described, a series of tests were performed to determine the effects on payload motion of variations in certain governing conditions. The conditions which were systematically varied were airplane bank angle, cable drag/weight ratio, and payload weight. The results obtained from these tests are herein compared to results predicted for these cases using the equations of motion developed in Section I.

2) Data Reduction:

a. Transit Data

For each test case, elevation and azimuth angles, obtained using the transit tracking system, were plotted against time, as shown in Figure 8. In all cases, the elevation and azimuth angles display a definite periodic variation with time. Therefore, these plots were used to correct any data obviously in error by graphic interpolation.

Using this data, the payload position in space as a function of time was calculated in a rectangular coordinate system using elementary trigonometry and plotted as shown in Figures 9 through 13. As was previously mentioned, the aircraft was allowed to drift with the wind in order to minimize wind effects. This procedure was followed in an attempt to eliminate complicated wind profile measurements, simplify aircraft maneuvers, and, also, to simplify theoretical calculations. Since under no wind, for the circling line, the payload trajectory is a circle concentric with and parallel to the circle described by the aircraft, the payload, under constant drift conditions, would be expected to describe a cycloidal trajectory. At first glance, the trajectories plotted appear to describe the expected trajectories, and, if so, the size of the envelope of the side to side traverse along the axis of drift should compare with the diameter of payload circle under no drift conditions. However, a previously reported phenomenon was observed and measured during the tests. The vertical motion of the payload was not negligible, but instead, displayed a periodic variation with time. Therefore, a check was made to determine if the horizontal motion was also near to that which was assumed. This was done by plotting horizontal and vertical components of displacement versus time as shown in Figure 14. The horizontal components were plotted for those portions of the time histories where the vertical displacements were steadiest. Notice that the projection along the displacement axis of the displacement variation is different in the two different directions. If the payload motion was that of a translating circle these projections would be equal. Therefore, limits of the side to side motion in two directions obtained in this fashion were used to describe the payload horizontal path. These values are summarized in Table 2.

b. Strain Link Data

The oscillograph recordings of line tension during the circling line tests show that the tension varied over a wide range of values during each run. A typical time history of the tension is shown in Figure 15. Due to various technical difficulties data was not obtained for many of the test runs. The results obtained are also summarized in Table 2.

Fig. 8 Circling Line - Ag Cat Model (Experimental Results)
Time History of Azimuth and Elevation Angles
Test Run No. 12 - Transit Sta. No. 2

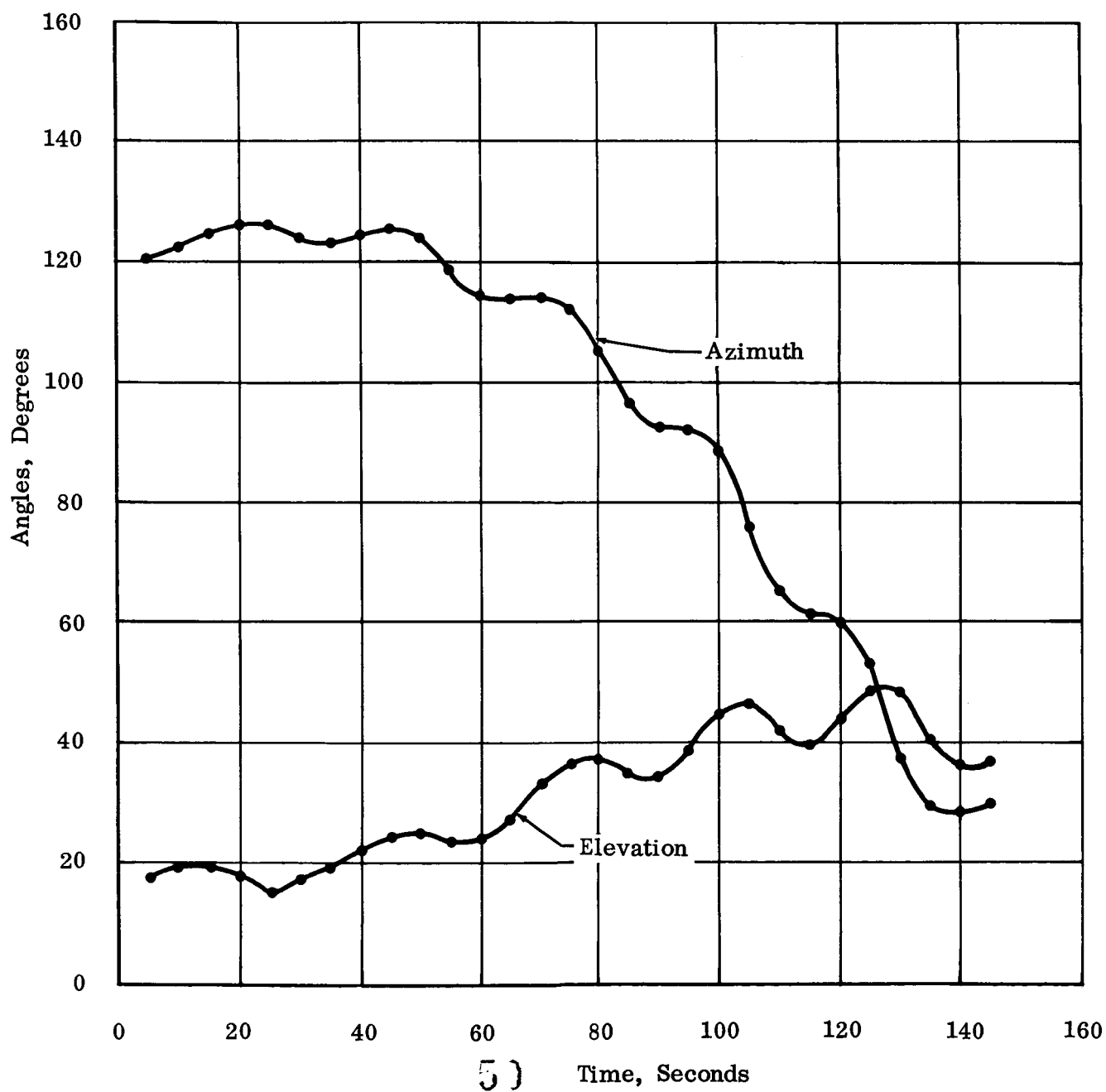


Fig. 9 Circling Line - Ag Cat Model (Experimental Results)
Payload Horizontal Trajectory (Nylon Cable - Payload = 45-1/2 lb)

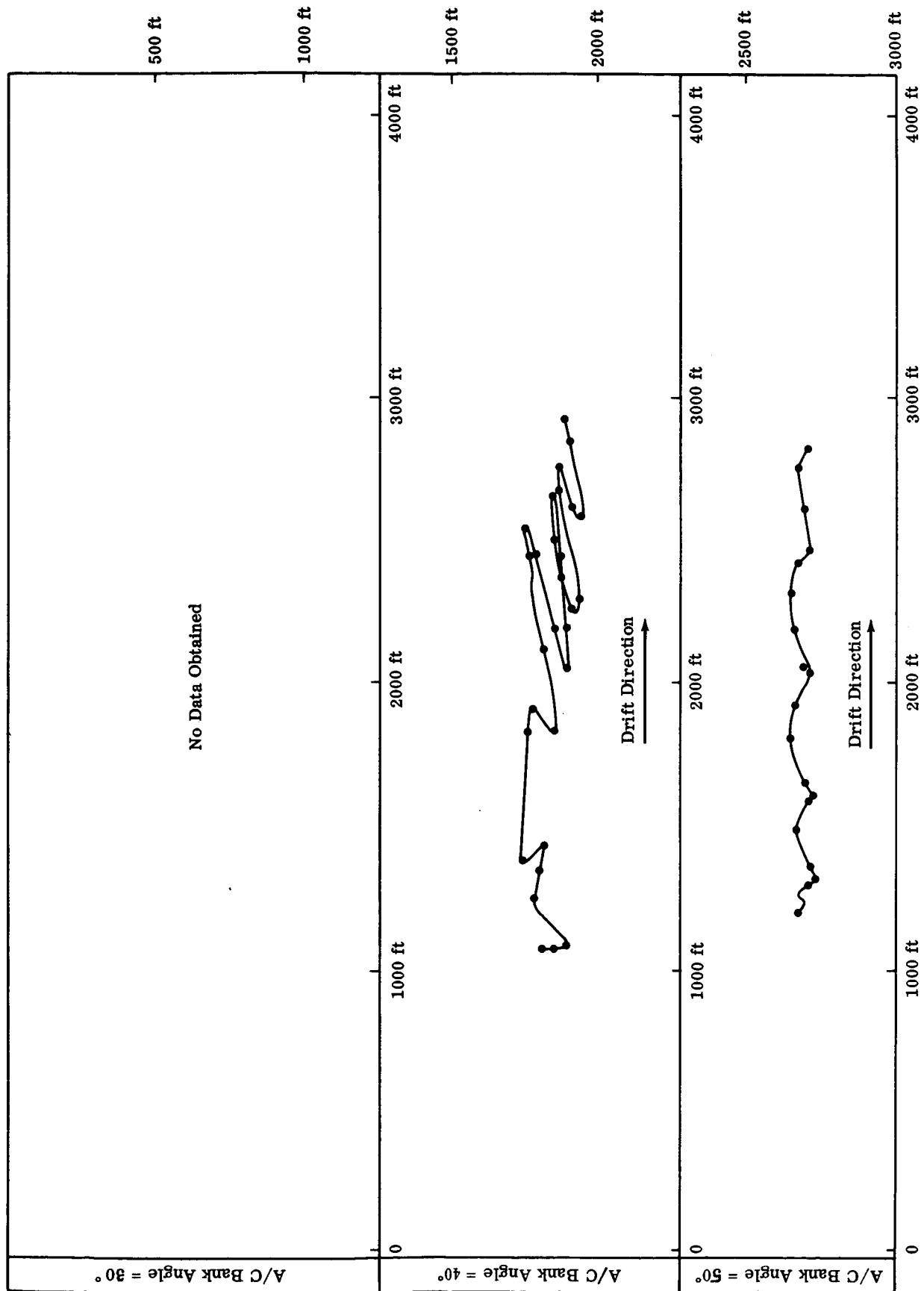


Fig. 10 Circling Line - Ag Cat Model (Experimental Results)
 Payload Horizontal Trajectory (Nylon Cable = 112 1/2 lb)

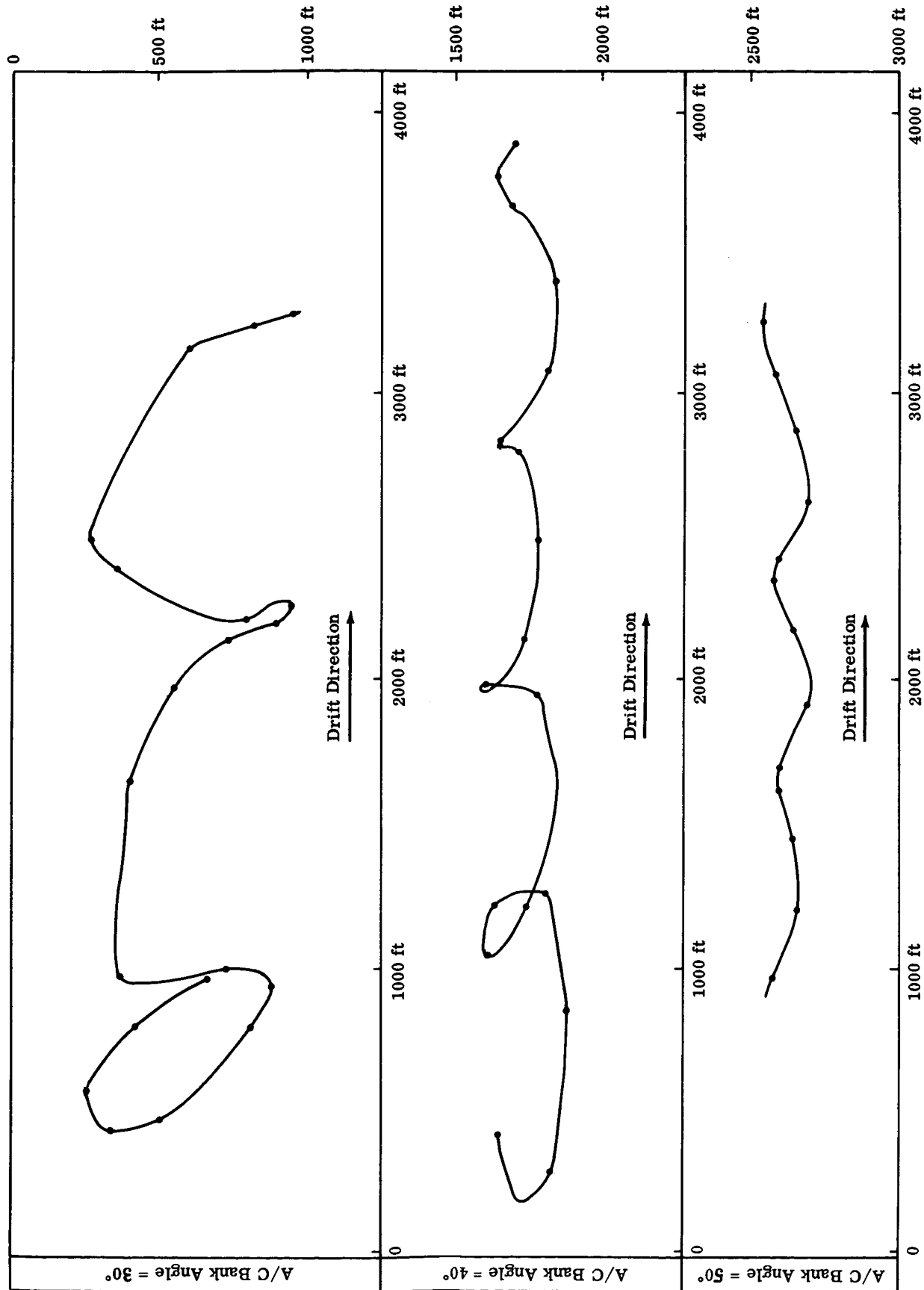
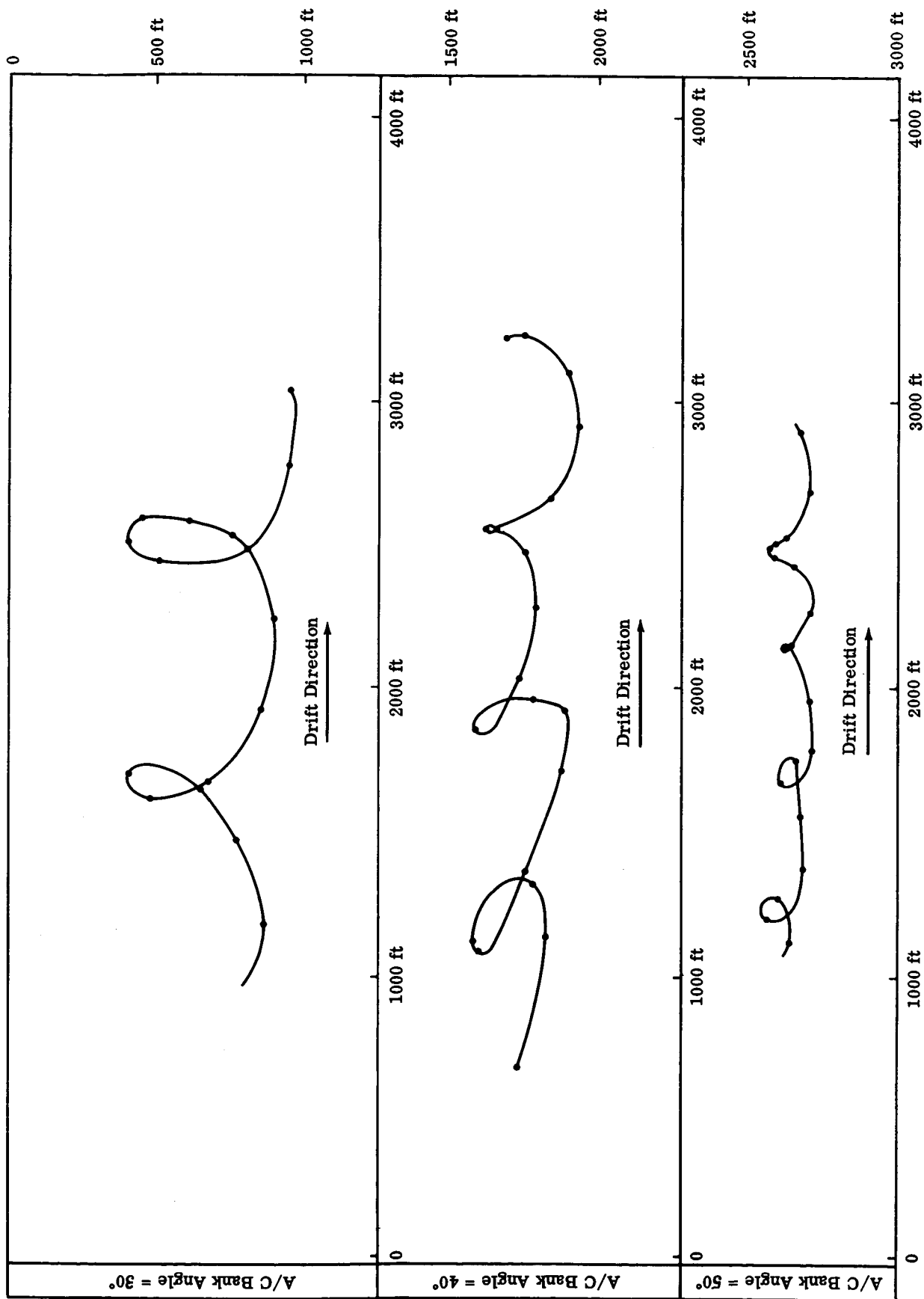


Fig. 11 Circling Line - Ag Cat Model (Experimental Results)
 Payload Horizontal Trajectory (Polypropylene Cable - 46 1/2 lb)



53

Fig. 12 Circling Line - Ag Cat Model (Experimental Results)
 Payload Horizontal Trajectory (Polypropylene Cable -
 Payload = 104-1/2 lbs)

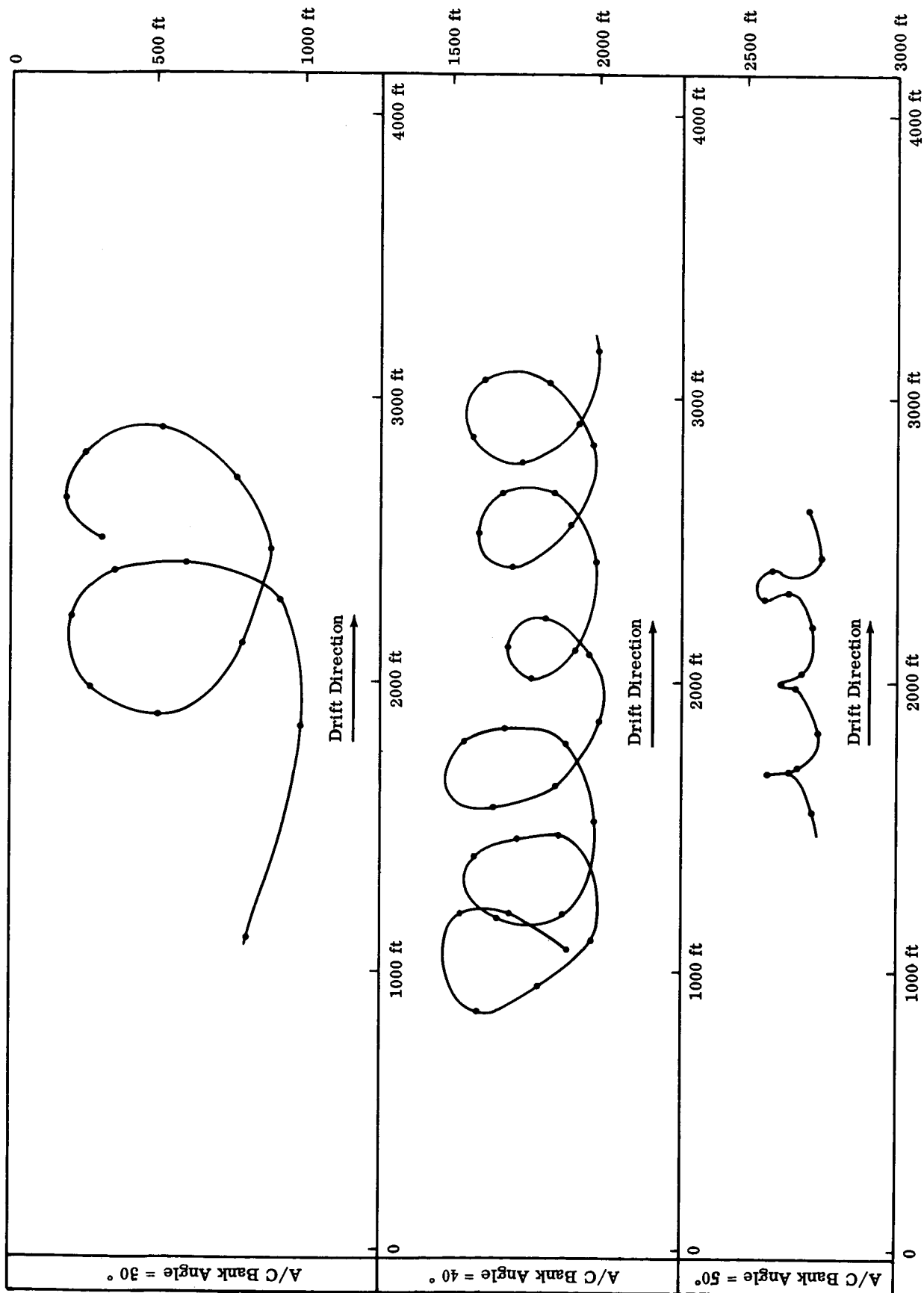
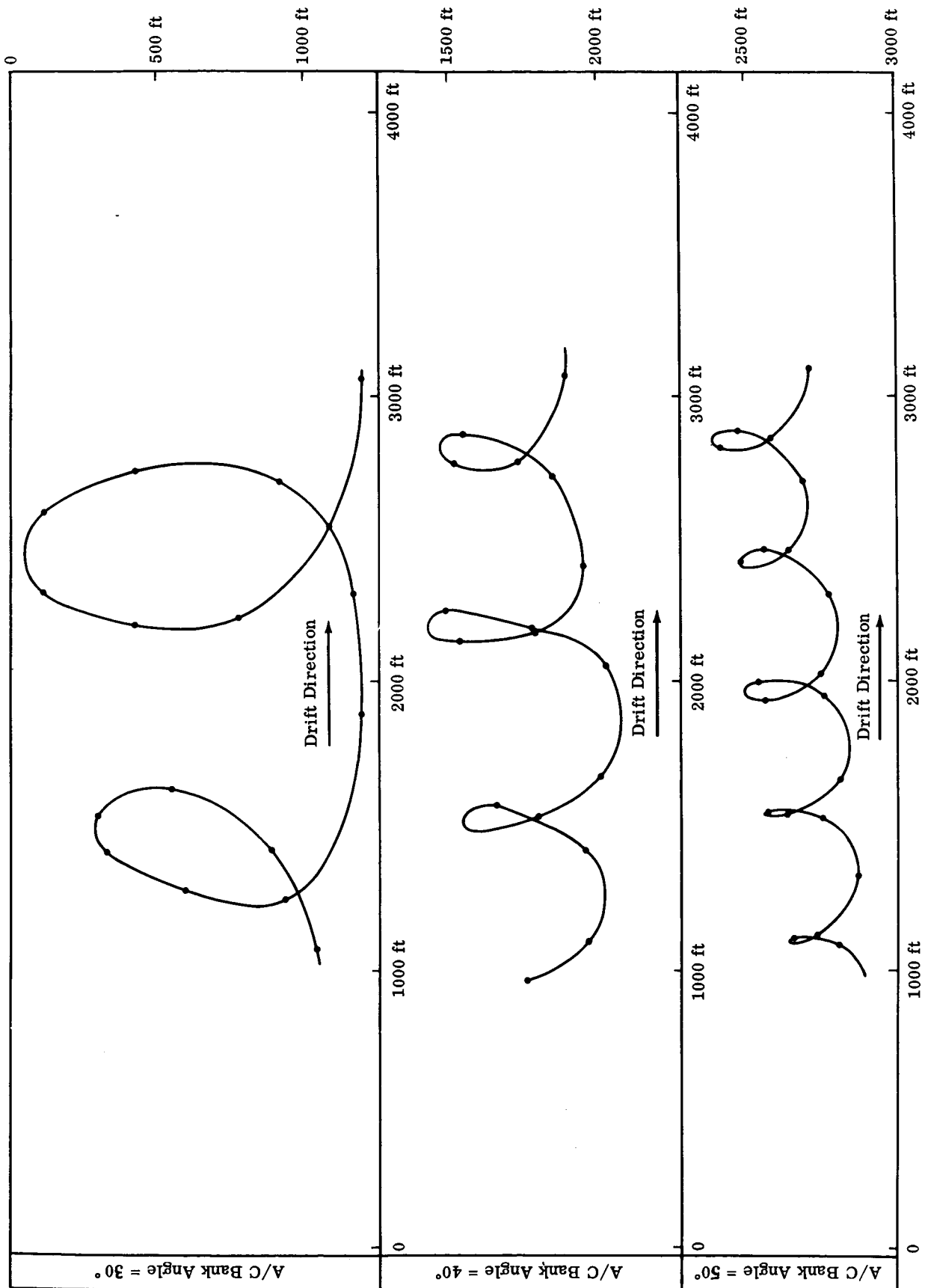


Fig. 13 Circling Line - Ag Cat Model (Experimental Results)
 Payload Horizontal Trajectory (Steel Cable - Payload = 104 1/2 lb)



55

Fig. 14 Circling Line - Ag Cat Model (Experimental Results)
Time History of Payload Horizontal and Vertical Motion Test
Run No. 12

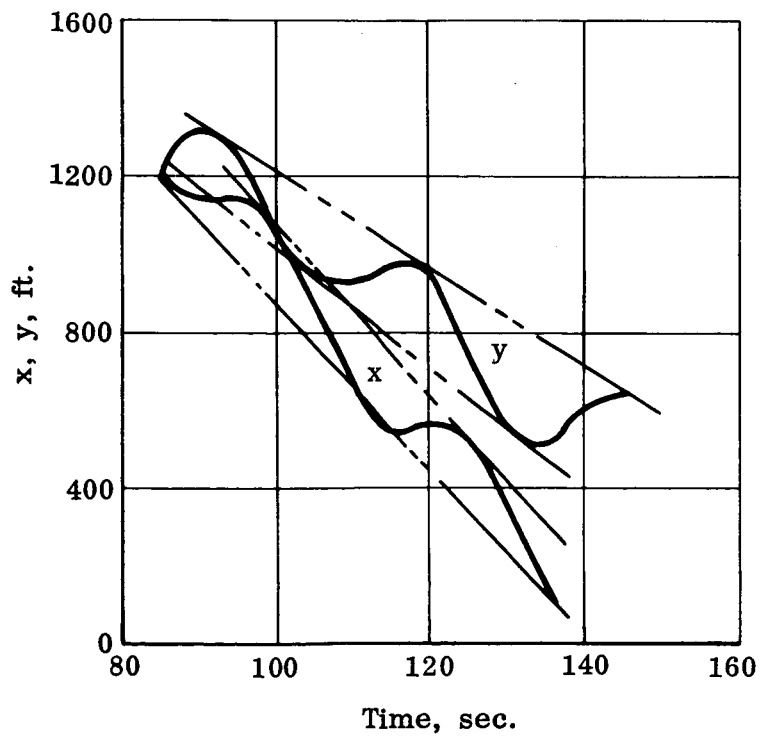
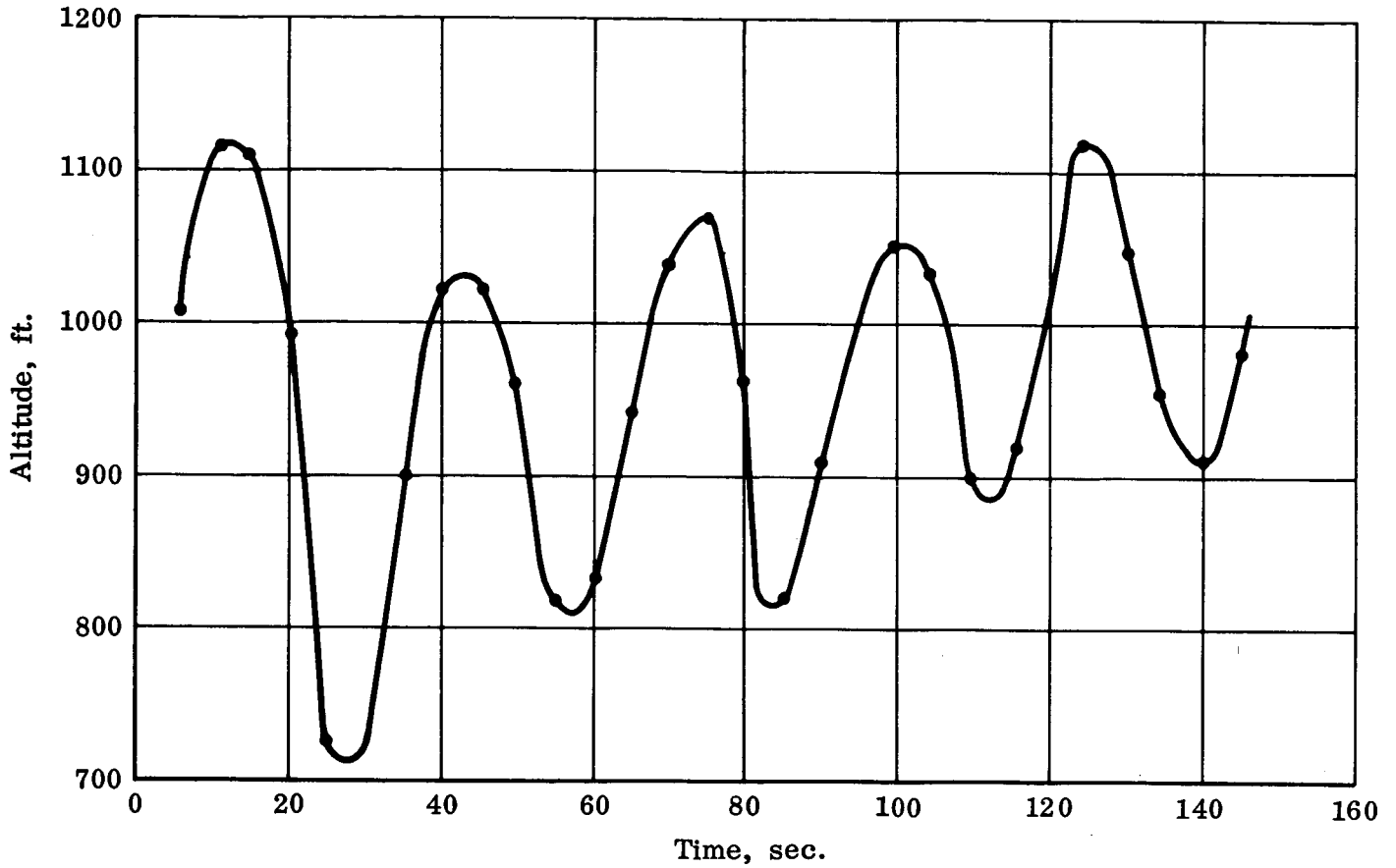
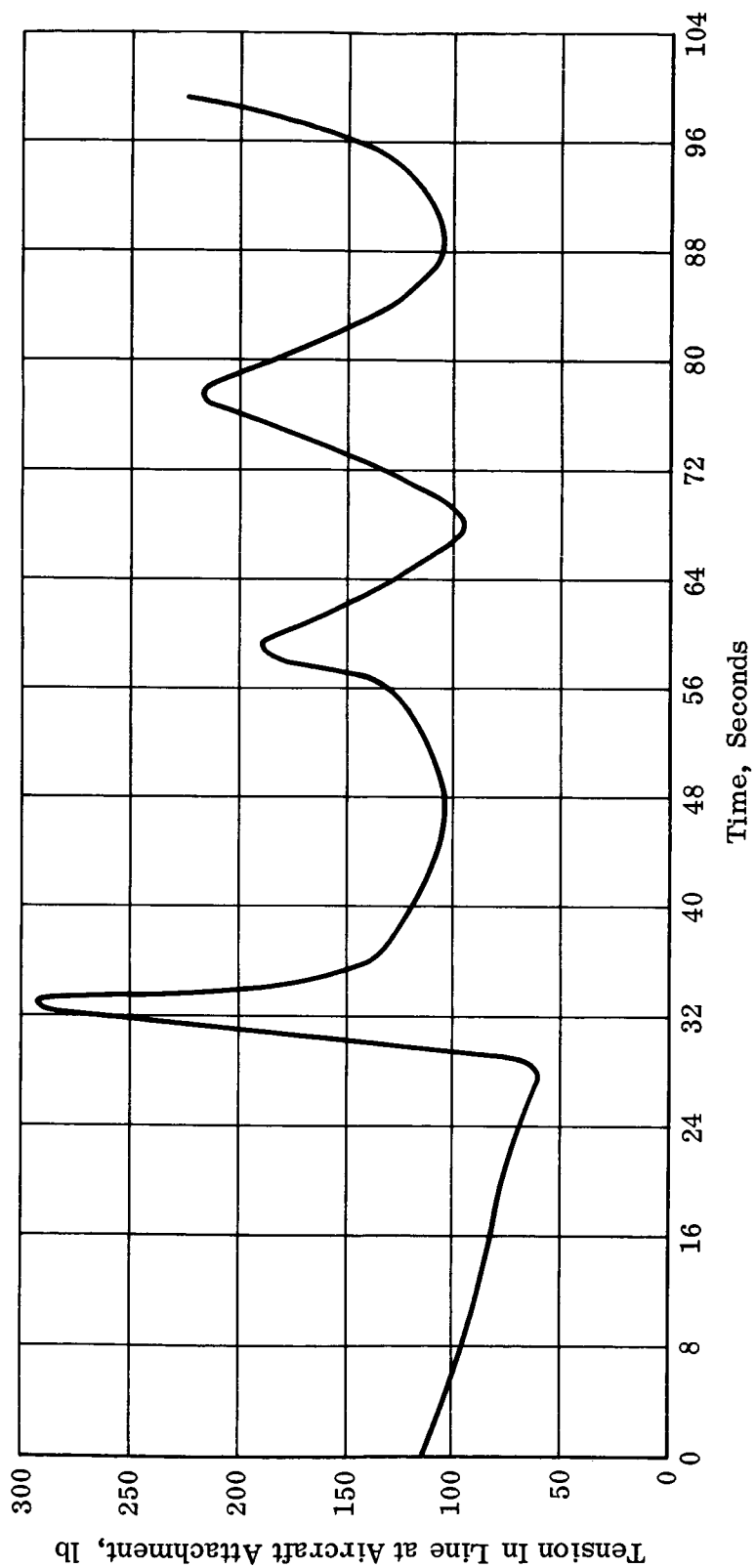


Fig. 15 Circling Line - Ag Cat Model (Experimental Results)

Tension Time History

Test Run No. 10



3) Summary of Test Results:

Flight	Run	Airplane Conditions		Wind Mag. & Dir.	Line Length	Type of Line	Payload Wgt.	Payload Trajectory Variation (ft.)			Tension Variation (lbs)	
		Vel. (MPH)	Alt. (ft)					Z	X	Y	Max	Min
4*	1	75	2500	15-20 Knots @ 30°	1855 ft	1" Nylon	45½#	-	-	-	-	-
	2			40°				125-255	95	350-450	-	-
	3			50°				100-170	50-120	120-180	-	-
	4							205-220	560	520	-	-
5	5			25 Knots @ 40°	1855 ft	1" Nylon	112½#	90-140	210-260	350	-	-
	6			0 to 30°				50-120	100-120	120-130	-	-
	7*			30				-	-	-	-	-
	8			12 Knots @ 45°	1835 ft	1" Poly-Pro	46½#	No data taken; repeated these conditions in runs #11, 12, & 13				
7	11			12 Knots @ 45°	1835 ft	1" Poly-Pro	46½#	160-270	400-440	510-540	224	78
	12							200-260	190-210	200-280	215	78
	13							75-80	70-150	90-120	293	60
8	14			15 Knots @ 320°	1835 ft	1" Poly-Pro	104½#	40-160	640-740	710-780	225	154
	15							135-215	400-450	430-450	182	140
	16							40-130	100-120	130-240	366	183
9	17			15 Knots @ 320°	2000 ft	1" Steel	104½#	120-150	770-850	600-740	-	-
	18							50-105	420-560	350-370	-	-
	19							110-150	220-300	220-280	-	-

* No Data taken for flights 1 thru 3

* Run 7 identical to run 4

4) Theoretical Calculations:

Using the inextensible cable analysis as developed in Section I-D, calculations were made to determine payload trajectory and vertical separation for each of the circling line test cases. Since circling line produces relatively steady motion, eliminating the need for the inclusion of elastic effects, this form of the analysis was used because of the large savings in problem running time on the IBM 7090 computer. Since the calculations were made for zero wind conditions, the predicted payload trajectories were circles of various sizes, concentric with and parallel to the airplane circle. (See Figure 16.)

5) Comparison of Experimental and Theoretical Results:

The average values of side to side traverse as measured experimentally for various airplane bank angles, cable drag/weight ratios, and payload weight are compared to the payload circle size calculated analytically (see Figure 17). Because of the variations in payload altitude observed during testing and the uncertainty as to exact aircraft altitude, values of vertical separation were not compared. Later calculations showed that tensions calculated using inextensible cable theory are higher than those for which elastic deformations are allowed. Because of this and since very little tension data was obtained no comparison is presented here.

Since the test aircraft was flown at constant airspeed (75 mph) variations in bank angle cause variations in airplane circle size. The airplane circle radii were calculated to be 650 ft., 448 ft., and 315 ft. for 30°, 40°, and 50° bank respectively. Predicted and experimental values show that the area in which the payload moves reduces sharply as airplane circle size decreases, for the cases where this is the only condition varied. See the columns of Figure 17.

The drag/weight ratio was varied by using cables of different diameter and linear density. The diameter/linear density ratios were 16.7, 10.5 and 2.3 for the nylon, polypropylene, and steel cables. For the smaller payload circles (airplane circle = 315 ft.), figure 17 shows that these circles decrease as drag/weight ratio is increased. For the larger circles, the experimental results appear to follow the same rule. The theoretical results predict a smaller payload circle for the polypropylene cable than for the higher drag/weight nylon cable. However, it is difficult to compare theory and experiment for these cases because of the generally poor agreement between the two for the polypropylene cable.

For the nylon and polypropylene cables the weight of the payload was varied from approximately 50 lbs. to 100 lbs. This increase in payload weight produces a definite increase in payload circle size as is shown in Figure 17.

6) Check of Theoretical Assumptions:

It was the primary purpose of the experiment to determine the trends just discussed, as a check on the analysis. Fairly close agreement in the magnitude of the circle sizes was obtained. The predicted circles, however,

Fig. 16 Ag Cat Model

Cable Shape in Still Air
A/C Vel. 75 mph - Turn Rad 650 ft.
Length of Cable 3600 ft.
No Payload

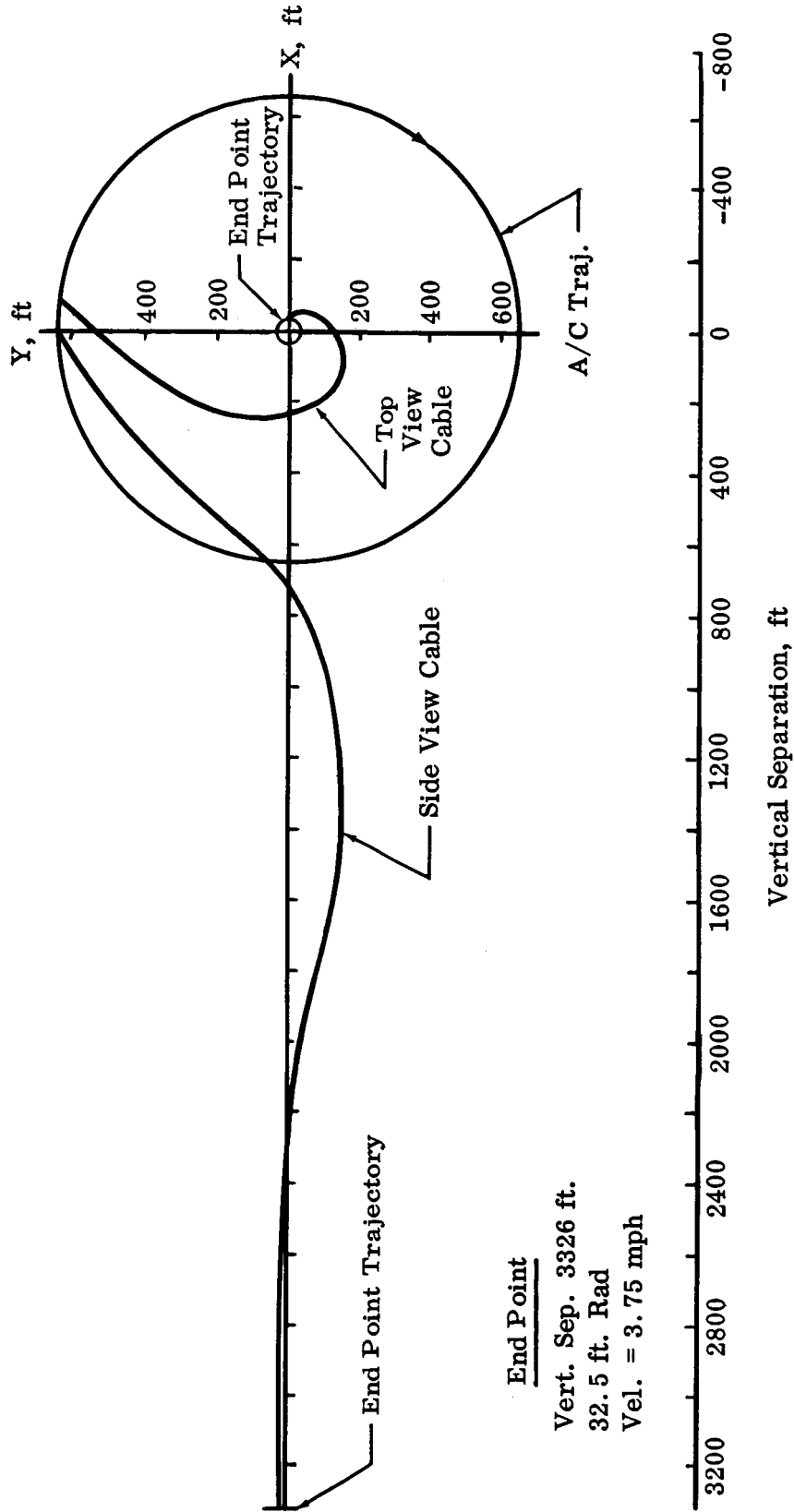
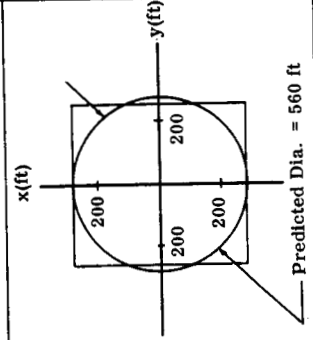
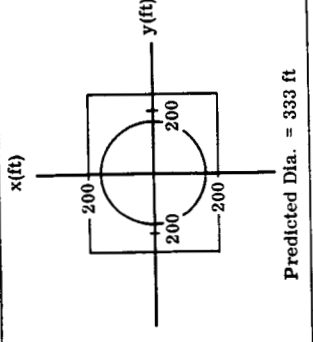
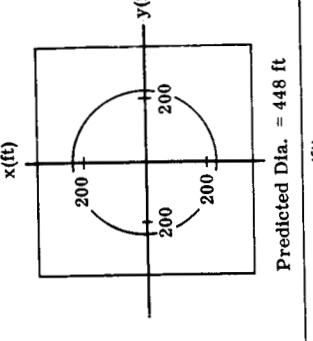
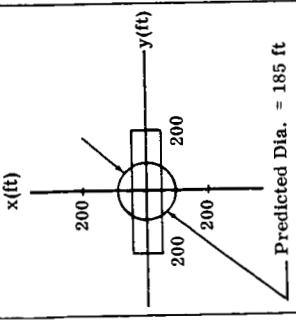
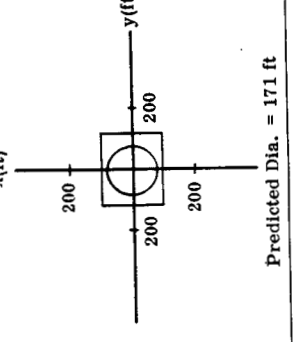
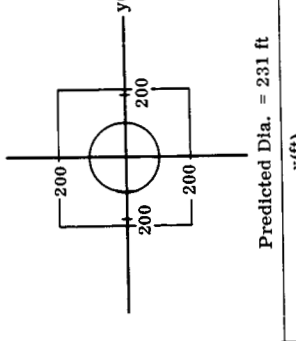
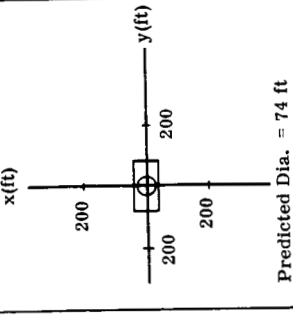
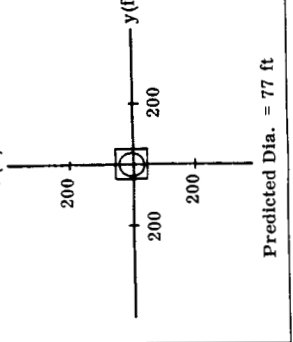
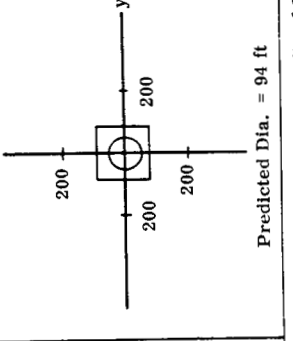


Fig. 17. Circling Line - Ag Cat Model
Comparison of Theoretical and Experimental

Results A/C Vel = 75 mph

	Nylon Cable (Length - 1855 ft. Dia - 1/4 in. Density - .015 lbs/ft)	Polypropylene Cable (Length - 1835 ft. Dia - 1/2 in. Density - .0475 lbs/ft)	Steel Cable (Length - 2000 ft. Dia - 1/4 in. Density - .11 lbs/ft)
	Payload = 45 1/2 lbs	Payload = 46 1/2 lbs	Payload = 104 1/2 lbs
Airplane Bank Angle = 30°	 Predicted Dia. = 560 ft	 Predicted Dia. = 333 ft	 Predicted Dia. = 764 ft
Airplane Bank Angle = 40°	 Predicted Dia. = 185 ft	 Predicted Dia. = 171 ft	 Predicted Dia. = 414 ft
Airplane Bank Angle = 50°	 Predicted Dia. = 74 ft	 Predicted Dia. = 77 ft	 Predicted Dia. = 193 ft

Note - Rectangles Denote Average Limits of Experimentally Observed Horizontal Motion

Summary PROJECT 308

were generally smaller than those obtained experimentally by an average value of approximately 20%, with the largest part of the error due to the polypropylene line cases. In an effort to find an explanation for this, and to explain the cyclical variation in altitude observed during the test, a check of certain theoretical assumptions was made.

a. Normal Force Coefficient

For the three types of line used, the normal force coefficient was assumed to be 1.19 (Reference Vol. I). Calculations were made to determine the effect on circle size of a variation of the normal force coefficient (see Figure 18). A decrease in normal force coefficient causes an increase payload circle size. However, this coefficient must be decreased to .7 to produce a 28% increase in circle size. This large a decrease cannot be reconciled with available data. Since the payload circle is not extremely sensitive to variations in normal force coefficient, for reasonable values of the same, the original value used appears adequate for calculating purposes. The discrepancy can not be explained by this factor alone.

b. Air Density

It was assumed that variation of air density with altitude was negligible. This assumption was checked by including air density variation into the calculations for the AgCat model. The payload circle and vertical separation were within $2\frac{1}{2}\%$ of the values calculated for constant air density.

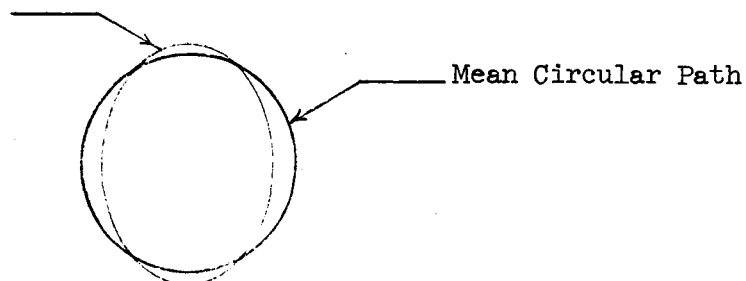
c. Payload Drag Coefficient

To obtain an indication of the sensitivity of the circling line configuration to the magnitude of the payload drag coefficients, this coefficient was reduced by 30%. This drastic change produces only a 1.4% increase in the payload circle size for the examples checked.

d. Airplane Flight Path

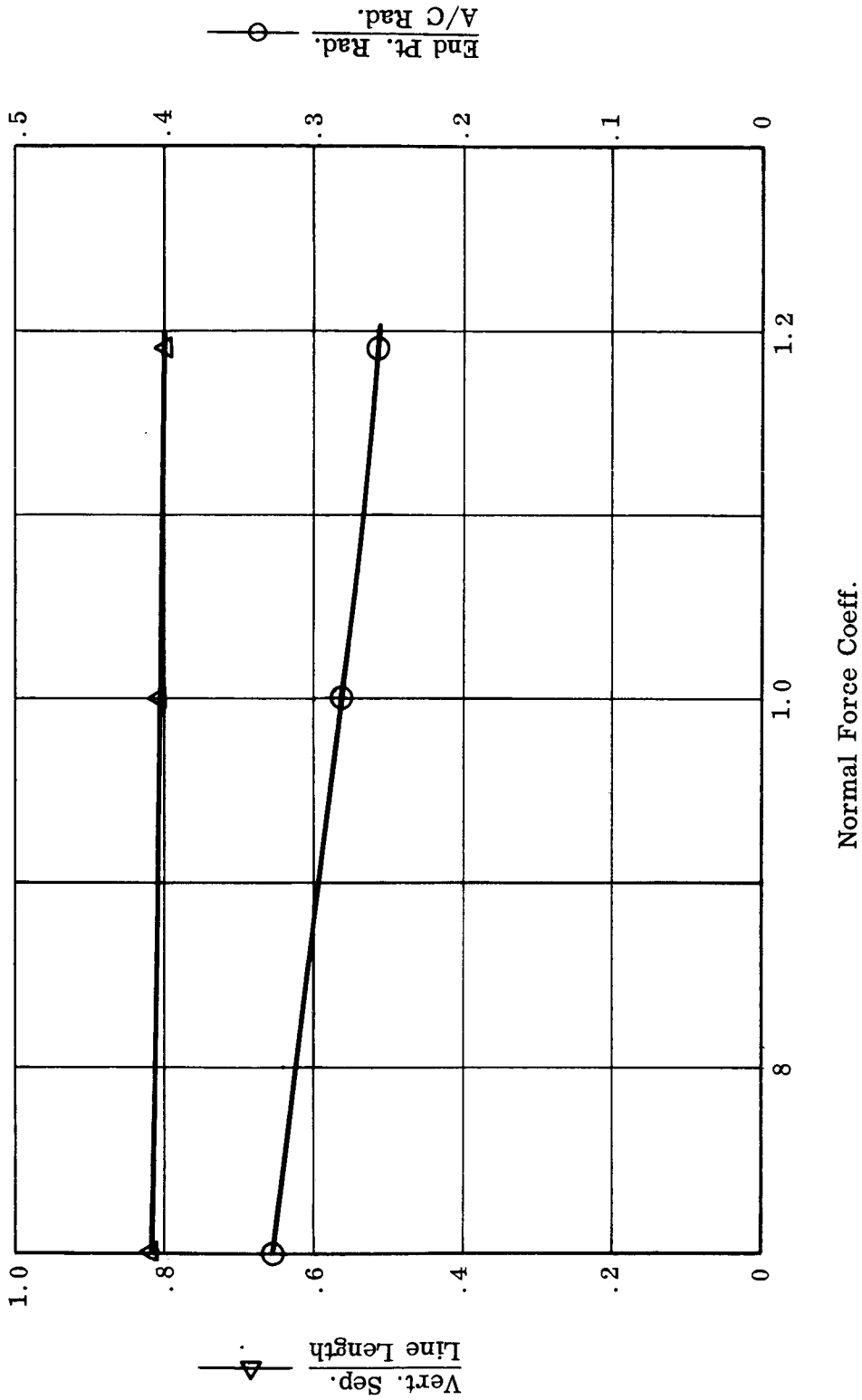
In the analysis it was assumed that the aircraft path was a perfect circle. A check was made by giving a slight variation from a circle to the airplane trajectory as shown below.

A/C Flight Path



**Fig. 18 Circling Line - Ag Cat Model
Vert. Sep. & End Pt. Rad.
Vs. Normal Force Coeff.**

1835 Ft Cable Length-1/2" Dia Polypro Cable
A/C Vel - 75 Mph - Payload - 46 1/2 lb



A 3.5% variation only produces a 2.5% maximum deviation from the circular end point circle, and a 10 to 20 ft. vertical motion results. Again, this factor alone cannot account for the full discrepancy.

e. Wind Shear

Since wind profiles were not measured experimentally and since reliable low altitude wind shear data is virtually non-existent (Reference 11) simplified wind profiles were chosen for this investigation. Wind shear loadings of 2 knots/2500 ft., 5 knots/2500 ft. and 10 knots/2500 ft. were applied to the circling line configurations. The wind shear was assumed constant in direction and varied linearly with altitude. Under this wind shear loading, the lower end of the cable no longer orbits about the center of the airplane circle, and no longer maintains a constant altitude, but shows instead a cyclical altitude variation (yo-yo) as is shown in Figure 19. As the magnitude of the wind shear is increased the end point trajectory moves further away from the center line of the airplane circle and its projection in the horizontal plane becomes less circular. The magnitude of the yo-yo is also increased as the wind shear is increased. Keeping the same wind profile and increasing the airplane circle size and therefore the end point circle size causes an increase in yo-yo.

A plot was made of the time history of the end point trajectory upon application of a full force wind shear loading to a circling line configuration (see Figure 20). Early in the time history, during the transient state, the yo-yo is considerably less than when a repetitive trajectory is finally attained. Also, early in the time history the end point trajectory has a larger variation side to side (Reference X & Y vs. time, Figure 20).

The magnitude of the yo-yo obtained for these wind shear profiles (100-200 ft.) compares with the yo-yo measured experimentally and it appears likely that most of the vertical motion is due to this type of loading. Since the payload swings out from the windless position upon application of gust type load and since most of the flights were made in moderate to severe turbulence, this affords a possible explanation for the underestimate of payload circle size calculated previously.

7) Conclusions and Recommendations:

The analysis predicts, satisfactorily trends in horizontal payload motion due to variations in certain governing conditions. The trends determined were:

1. Decreasing airplane circle causes decreasing payload circle.
2. Increasing cable drag/weight ratio causes decreasing payload circle.*
3. Decreasing payload weight causes decreasing payload circle.

* This was only true for small bank angles (see Discussion, Part 5.)

Fig. 19 Circling Line - Ag-Cat Model

Effect of $\dot{\theta}_{Shear}$

A/C Alt = 2500 ft - A/C Vel = 75 Mph - Cable Dia = 1/2"

Cable Length = 1835 ft - Cable Density = .0475 lb/ft -

Payload Wgt = 46-1/2#

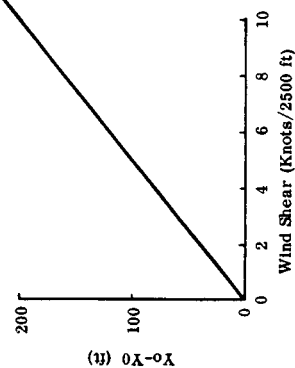
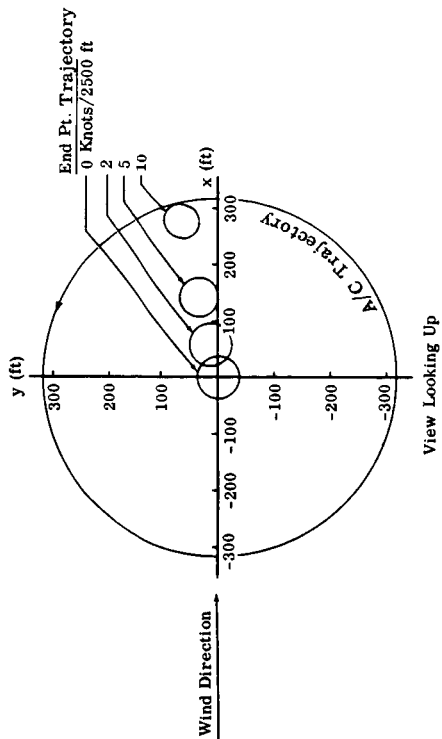
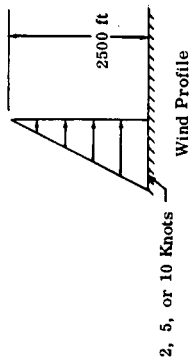
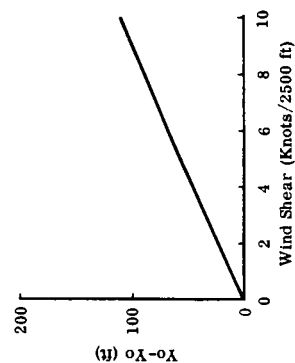
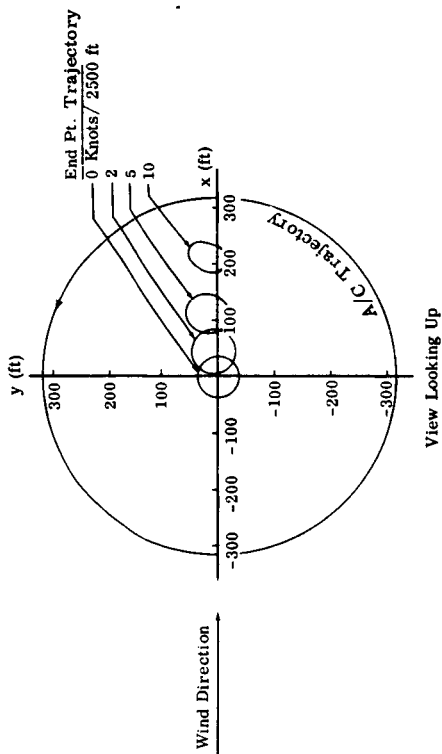
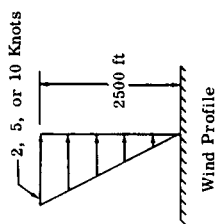


Fig. 19 Circling Line - Ag-Cat Model

Effect of ω Shear

A/C Alt = 2500 ft - A/C Vel = 75 Mph - Cable Dia = 1/2"

Cable Length = 1835 ft - Cable Density = .0475 lb/ft -

Payload Wgt = 46-1/2#

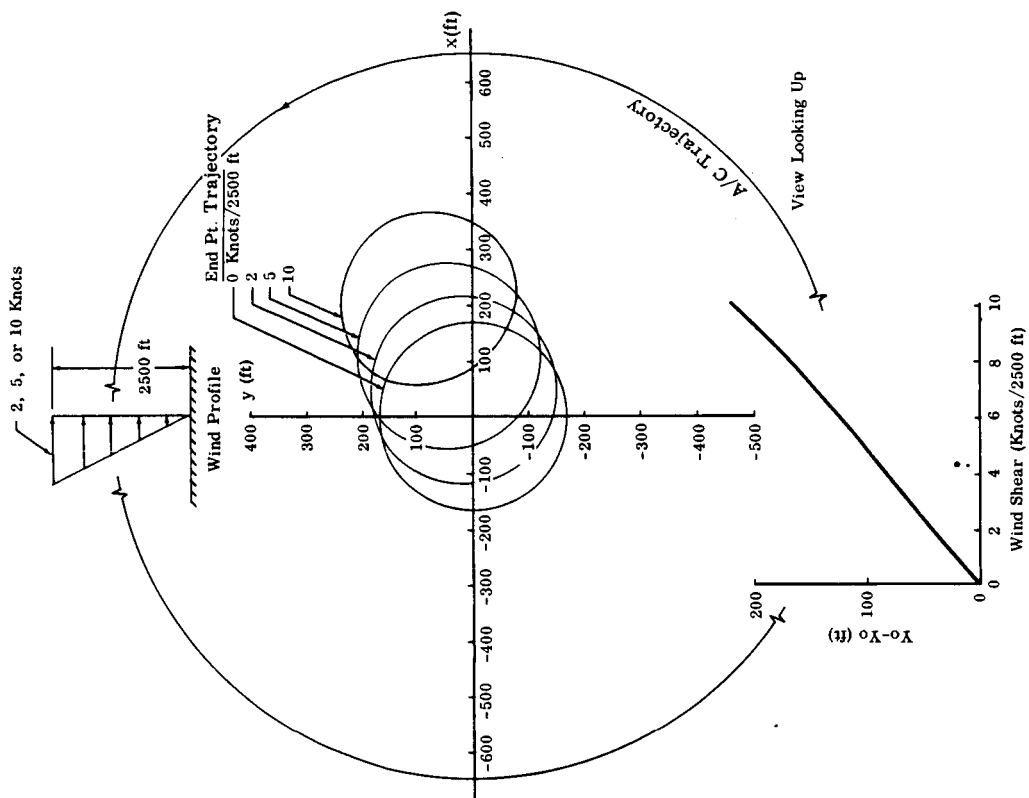
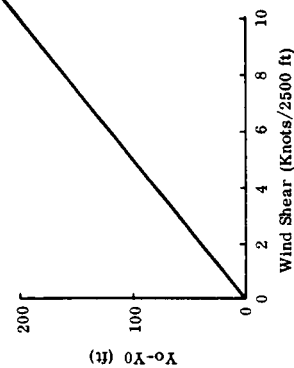
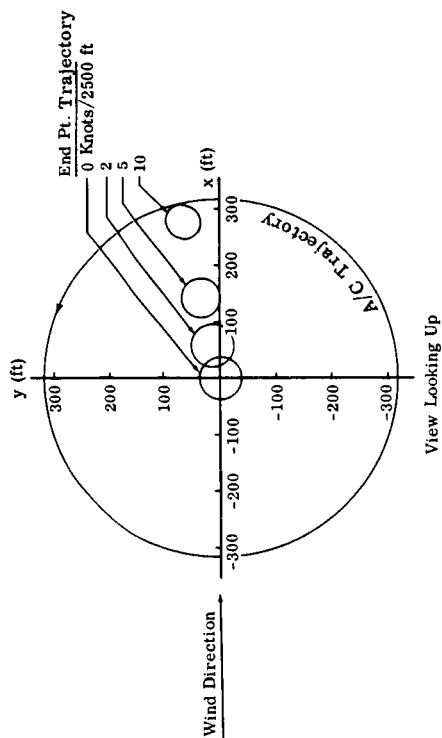
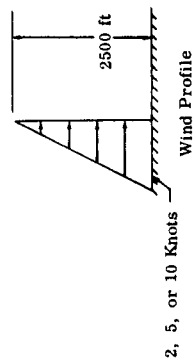
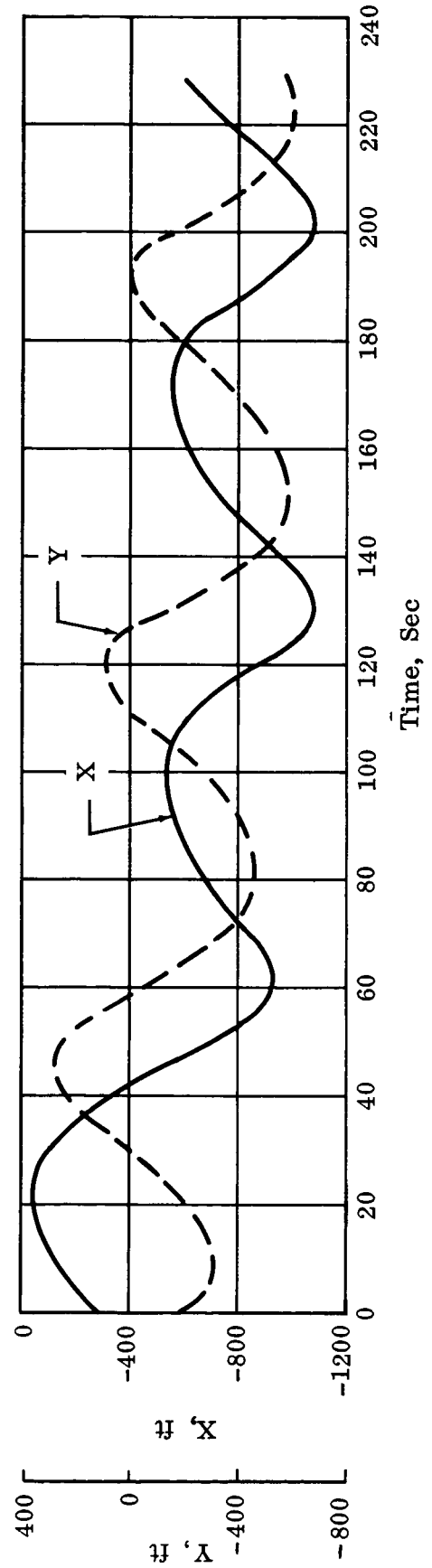
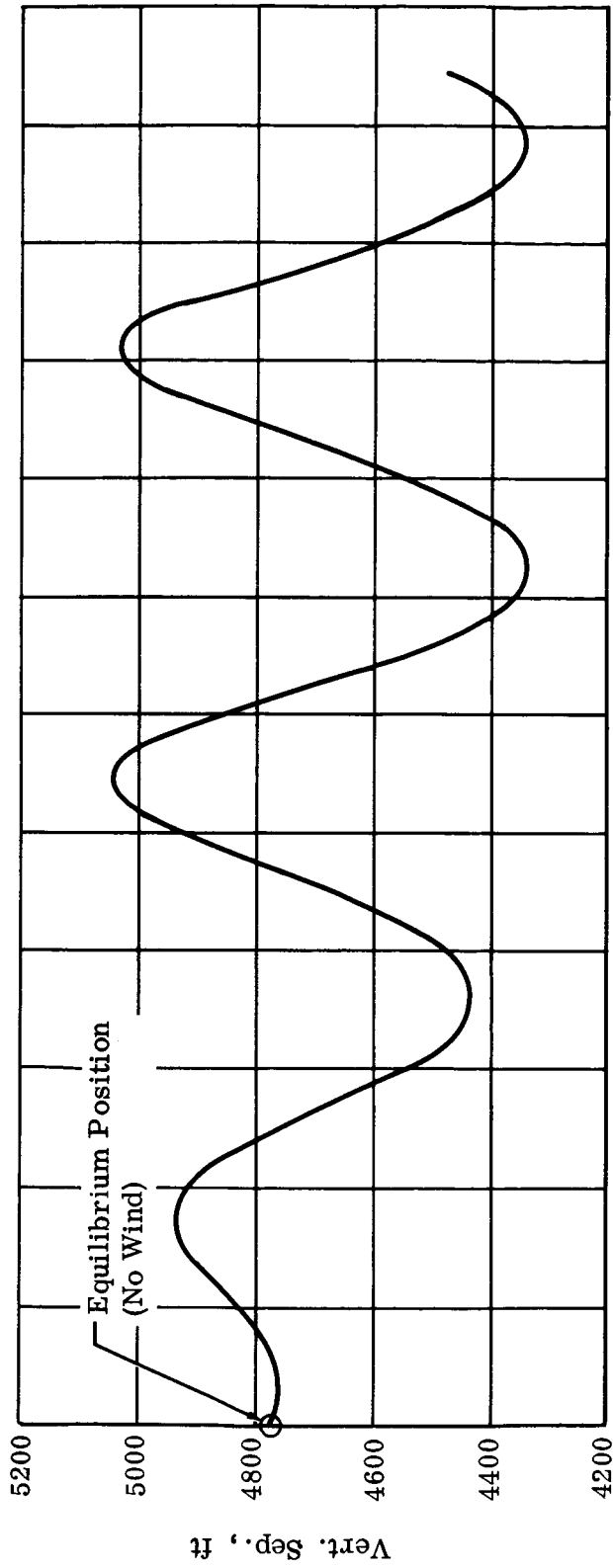


Fig. 20 Circling Line - Apollo Configuration
Effect of 5 Knot/2500 ft. Wind Shear
(Time History)



The analysis can predict the magnitude of the payload circle size to within certain limits. To increase the accuracy of these predictions and to predict vertical payload motion, wind data must be included in the calculations. It is recommended that for any further tests, wind profile data be taken so that it may be used as input for the analytical calculations.

D. Experimental Results and Comparison with Theory - Snatch Type Pickup

1) Introduction:

Three snatch type pick-up tests were conducted. Except for the length of line between the balloon and payload, all conditions were approximately the same. Test #1 was primarily conducted to acquaint the pilot and the ground crew with the behavior of the system and no data was taken. A malfunction in the Fairchild analyzer prior to test #2 prevented recording of the payload trajectory, however tension data was obtained. Both payload trajectory and tension data was obtained for test #3.

2) Test Results:

The following table summarizes the test conditions and results:

Table 3 - Snatch Type Pickup - Summary of Test Results

Test	Aircraft Cond.		Length of Line	Max Height of Traj.	Horizontal Distance Traveled to Max. Hgt.	Max. Tension
	Airspeed	Alt.				
#2	65 mph	215'	190'	-	-	365#
#3	65 mph*	158'	147'	126'	245'	365#

Figures 21 and 22 show the time histories of the line tensions measured at the airplane for tests #2 and #3. In both cases, there is a sharp increase in the tension initially. After approximately $\frac{1}{2}$ second the tensions increased to a maximum value which is maintained for 1 to 2 seconds. The tensions then maintain a relatively low value for about 3 seconds and again increases to the fairly steady value.

Figure 23 is a plot of the payload trajectory for test #3 as recorded by the Fairchild analyzer. The payload motion is initially more vertical than horizontal, rising 35 ft. while moving horizontally 20 ft. The trajectory then begins to flatten out and reaches a maximum value of 126 ft.

These plots indicate that the payload motion is highly dependent upon the initial configuration of the system since a large portion of the work done on the payload is done shortly after lift off.

* Using data obtained from motion pictures of the test, the aircraft ground speed was calculated to be 56.7 mph (avg.)

Fig. 21 Snatch Type Pickup - Ag Cat Model (Experimental Results)
 Time History of Cable Tension Measured at Airplane During
 Snatch Pickup No. 2

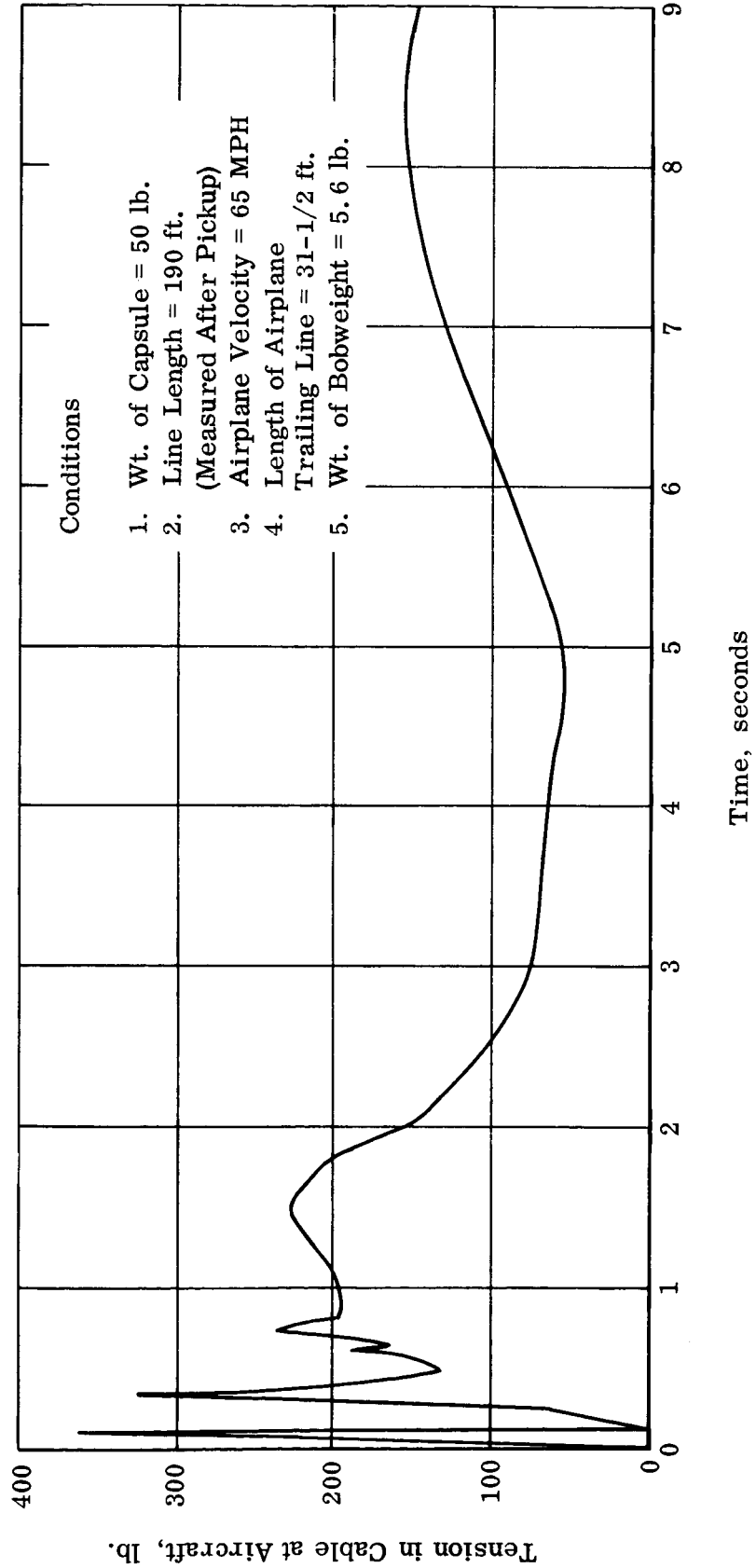


Fig. 22 Snatch Type Pickup - Ag Cat Model (Experimental Results)

Time History of Cable Tension Measured at Airplane
During Snatch Pickup No. 3

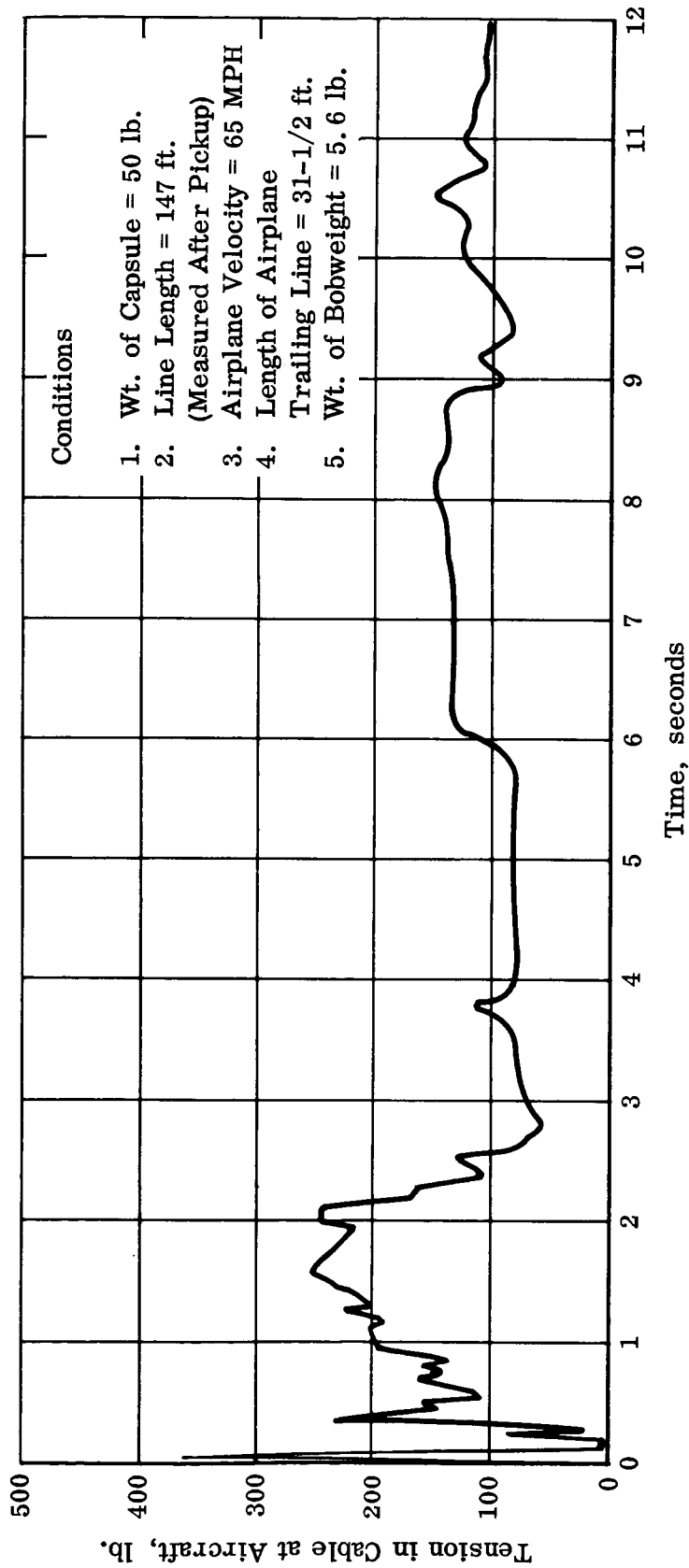
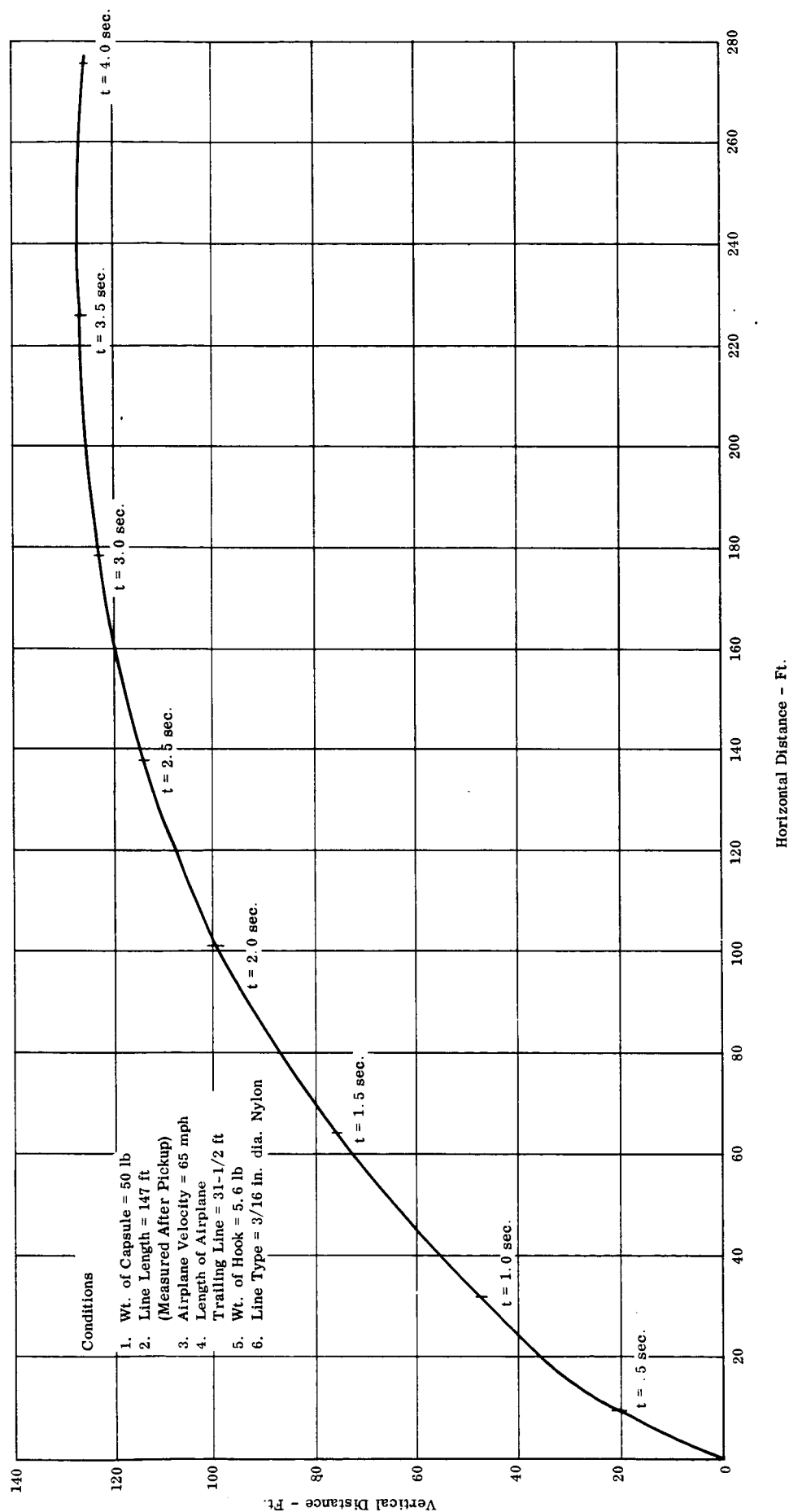


Fig. 23 Snatch Type Pickup (Experimental Results)
Trajectory of Payload for Snatch Pickup No. 3



3) Theoretical Calculations:

Because of the highly transient nature of the motion involved in the snatch type pickup and the resulting importance of the cable elastic properties, the extensible cable analysis, as developed in Section I-B, was used to calculate payload trajectory and cable loads.

4) Comparison of Experimental and Theoretical Results:

When a comparison between experimental and theoretical results was attempted, it was found that the lack of data concerning certain experimental conditions made a direct analytical simulation of the test extremely difficult. For example, no measured information was available describing the inertial and drag properties of the large supporting balloon as a function of time or the forces acting on the hook and the balloon due to impact. Therefore, a study was made to determine the relative importance of various controlling conditions using the quantitative data available along with qualitative information obtained by observing motion pictures of the pickup.

a. Effects of Balloon Drag

In order to approximate the conditions of hook and balloon impact and the complicated drag behavior of the large supporting balloon which remained attached to cable, although punctured on impact, various balloon drags were assumed in the calculations. The balloon drag was lumped at the trailing hook and was initially given its velocity. Since this drag force decreases the hook velocity, which in turn decreases the drag force, this condition gives an approximation to the forces on the hook when hitting and tearing through the balloon. As the balloon accelerates from rest the hook forces decrease while the actual balloon drag forces increase. Various balloon drag coefficients were tried in an attempt to find some average coefficient which would adequately describe the sum of these two complicated phenomena.

Figure 24 shows the large variation in initial trajectory by assuming various balloon drag coefficients. The initial geometrical configuration for these calculations was that observed experimentally (i.e. the aircraft cable in its trail configuration, and the capsule cable heeled over with the wind approximately 10 degrees). If the balloon drag is assumed to be large, say that of the unpunctured balloon (1), the resulting trajectory is extremely steep. If on the other hand the balloon drag is assumed negligible (2) the trajectory becomes extremely flat. If an average value is assumed (3) the trajectory approaches the initial experimental trajectory but is much higher later in time. If, however, this balloon drag is assumed to disappear after a half second (4) the trajectory begins to flatten out. This last case also gives a tension time history which has an early peak value, a phenomenon which is also displayed in the experimental data.

Figure 25 shows a comparison between experimental and theoretical payload trajectories for assumed balloon drags of 5% and 35% of the large balloon drag. The higher drag trajectory more closely matches the experimental trajectory just after lift off, but is lower later in time.

Fig. 24 Snatch-Type Pick-Up
Effect of Balloon Drag
(Calculated Results)

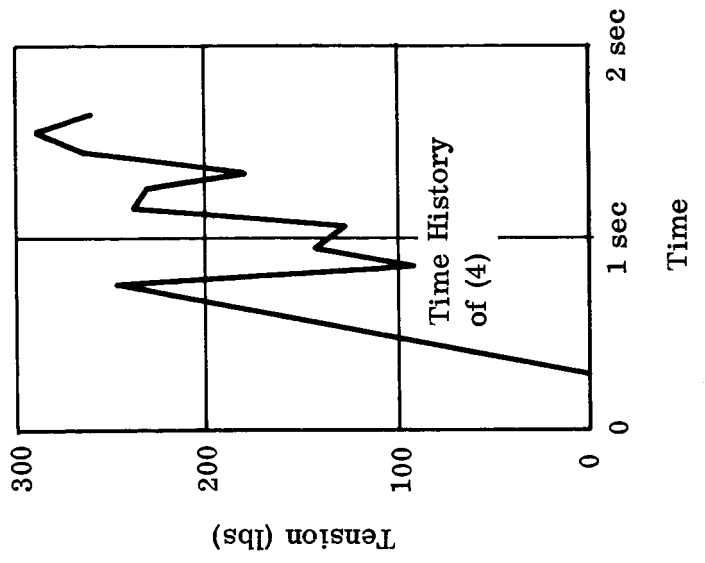
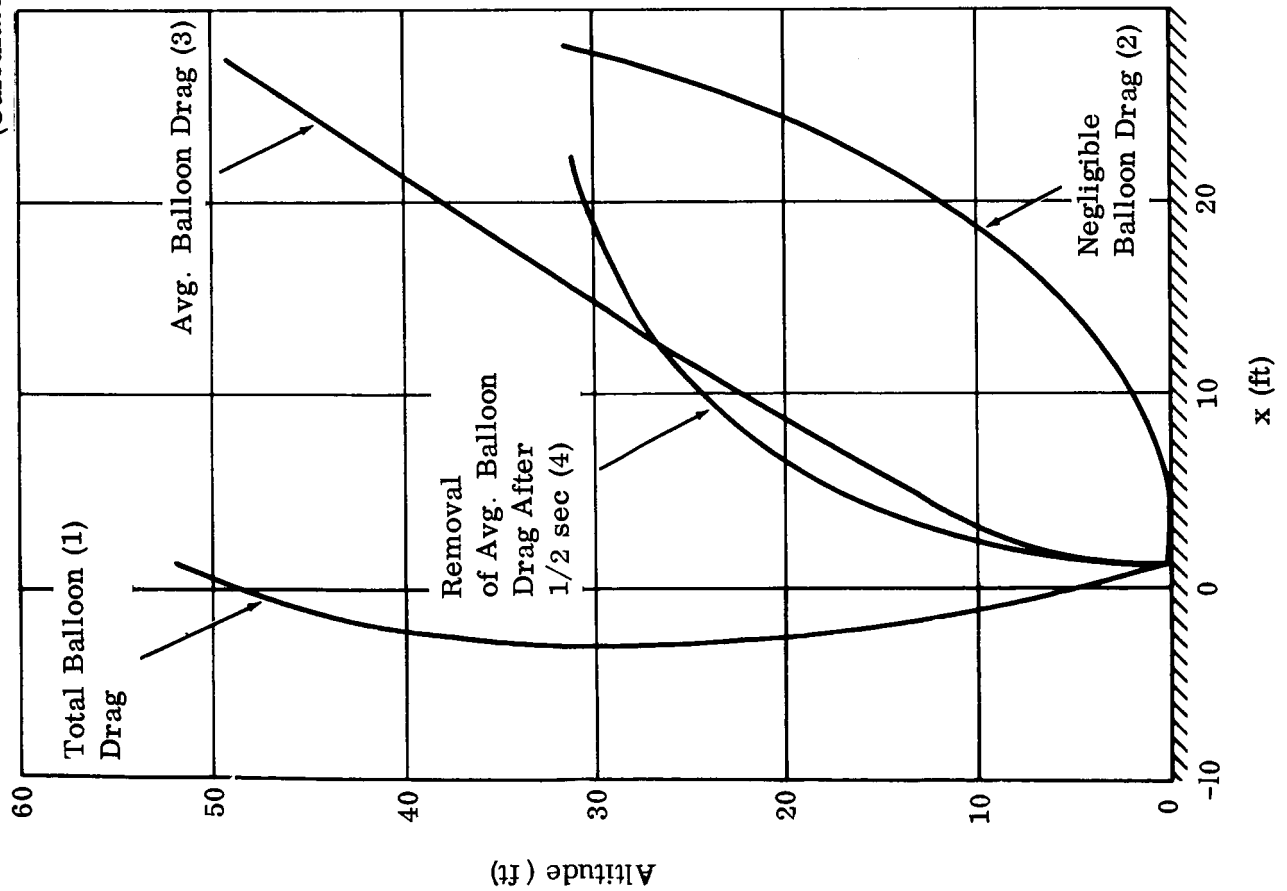


Fig. 25 Snatch Type Pickup - Ag Cat Model
Comparison of Experimental and Theoretical Results
- Payload Trajectories

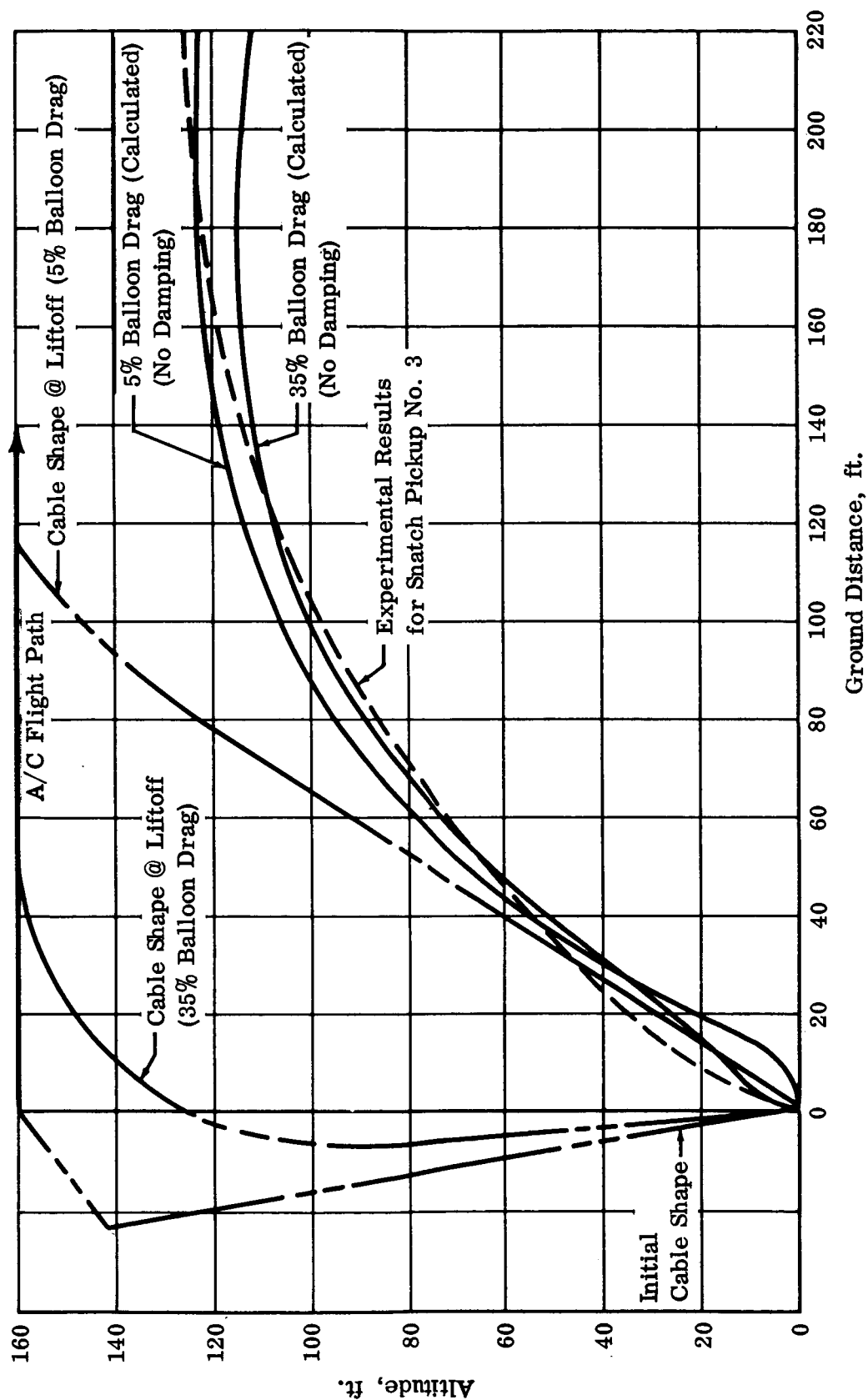


Fig. 26 Snatch Type Pickup - Ag Cat Model
Comparison of Experimental and Theoretical Results
- Tension Time History

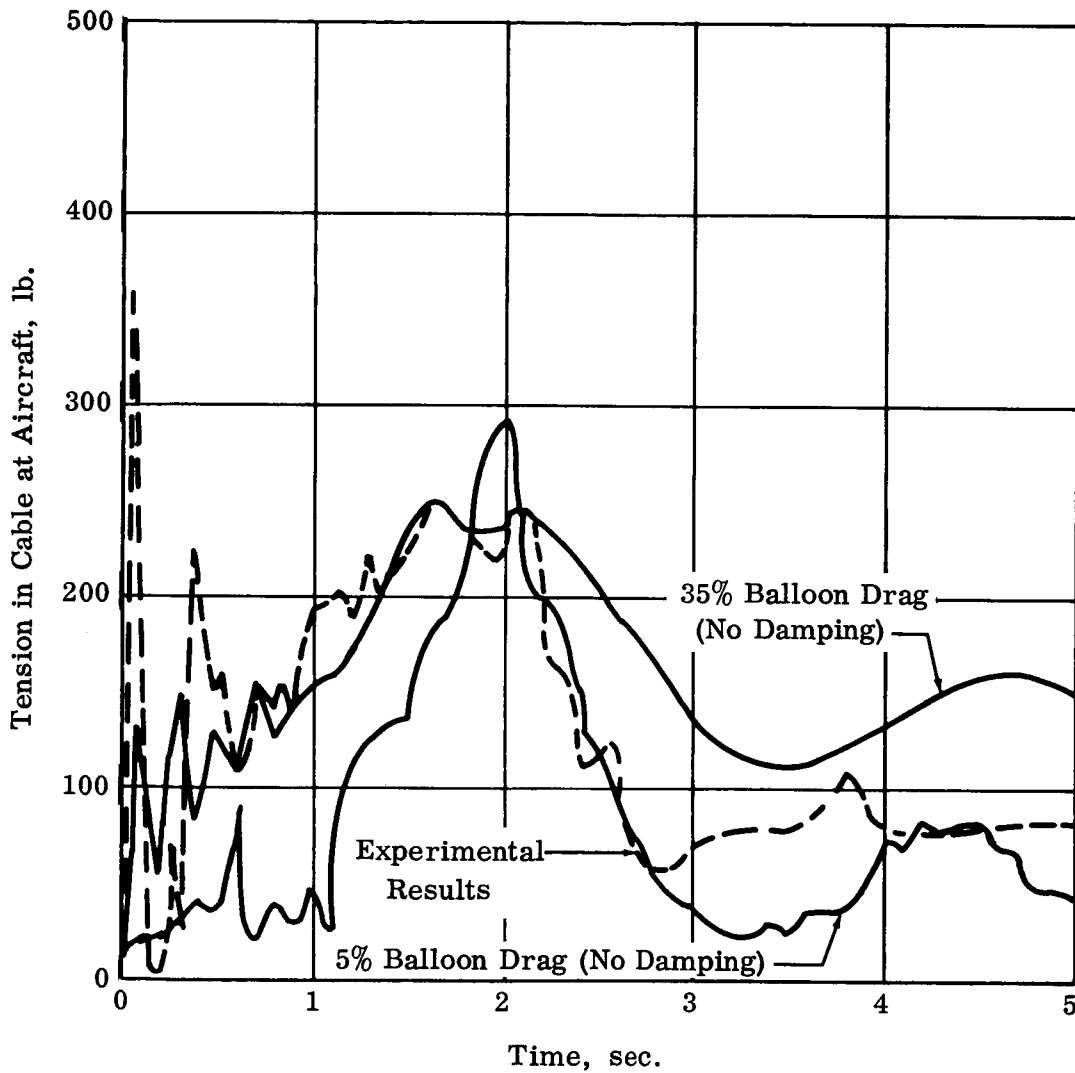


Figure 26 shows the tension time histories for these cases. The peaks calculated initially for the 35% drag case are lower in magnitude than those measured experimentally, whereas after approximately 2 seconds the predicted tensions are generally higher. The 5% drag case gives lower tensions initially and lower tensions after 2 seconds.

These results indicate that by starting with a relatively high drag coefficient and decreasing it rapidly to some lower value, a more precise match could be obtained between experimental and theoretical results. Because of time limitations, this was not done. However, a constant coefficient can be used to obtain a first approximation to trajectories and tension time histories.

b. Cable Elastic Properties

Figures 27 and 28 show the experimentally obtained cable elastic properties for the payload and airplane cables respectively. Values from these figures were included in the calculations using the technique outlined in Part I. Since no static tension tests were performed (Reference Volume I) the dynamically obtained results (loading rates of the order of 1 ft/sec.) were used as the base curves in the analyses. Figure 29 shows a comparison between the experimental base curve (re-plotted to show % deflection) and curves analytically generated. The approximation used allows prediction of an unloading curve based on a known unloading curve, although maximum loads are not necessarily the same.

Figures 30 and 31 show the effects of damping on payload trajectory and tension time history. Although theoretically the damping should be added to a statically obtained base curve, these results do indicate a certain sensitivity to variations in this parameter. Since loading rates calculated for this pickup were of the same order as those used for testing the cable, it would be expected that the payload motion would more closely correspond to that experimentally observed when no additional damping is used. For this reason, comparison between experimental and theoretical results was made for the curves calculated with no additional damping.

5) Conclusions and Recommendations:

The type of flight tests conducted made straightforward comparison between experimental and theoretical results difficult. However, the complicated behavior of hook impact and subsequent balloon behavior can be approximated by average drag coefficients to give a fairly good first approximation to payload motion and cable loads. It is recommended that an analytical investigation of these conditions be performed so that they may be adequately predicted beforehand, in order to eliminate the need for extensive flight testing to obtain average working values. Snatch type pickups from the circling line maneuver (Ref. Section III) and using a scheme such as Fulton's "Skyhook" (Ref. Volume I) should also be made in order to study other phenomena of this pickup uncomplicated by the effects of a large supporting balloon.

Fig. 27 Short-Time Load-Deflection Tests

3/16 Diameter, 3 Strand Nylon Rope

Catalogue Ultimate = 1000 Lb.

Original Length = 26"

Average Cycle Time = 1.5 Secs.

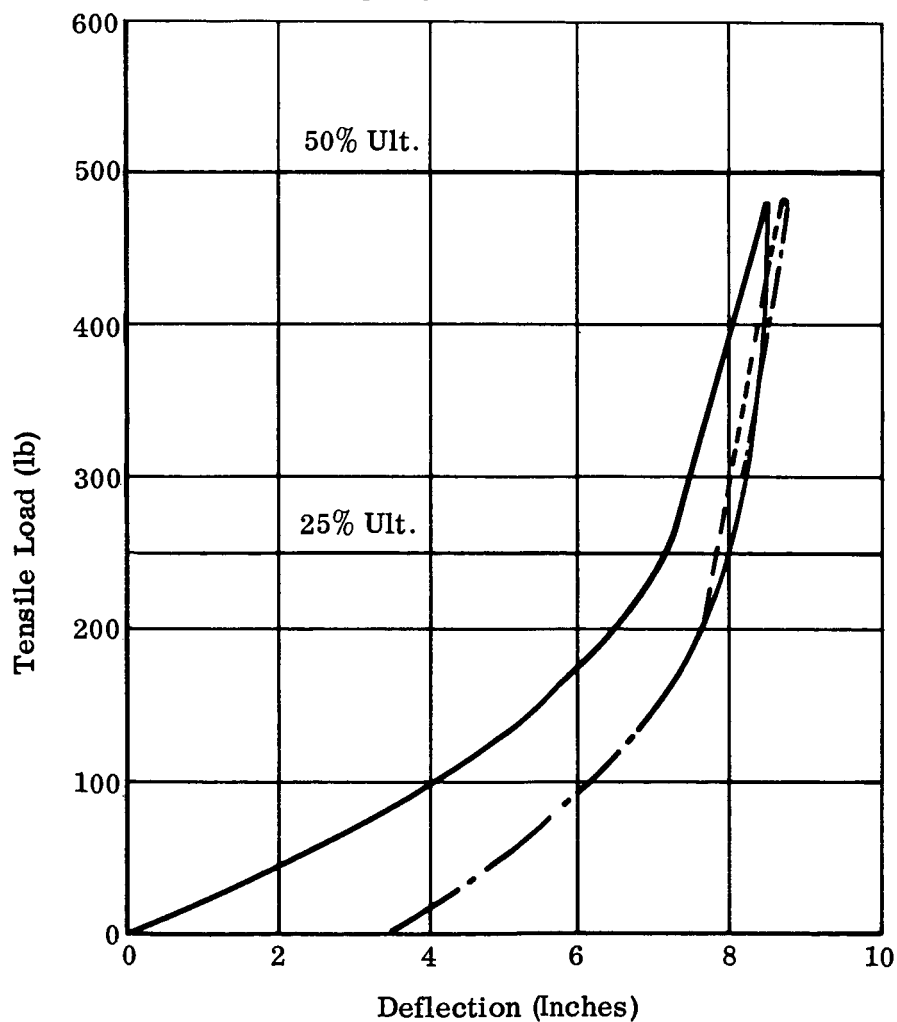


Fig. 28 Short-Time Load-Deflection Curve

Fulton Hollow Braid

Catalogue Ult. = 5000 (lb)

Average Cycle Time = 1.2 secs

Original Length 25.75 In.

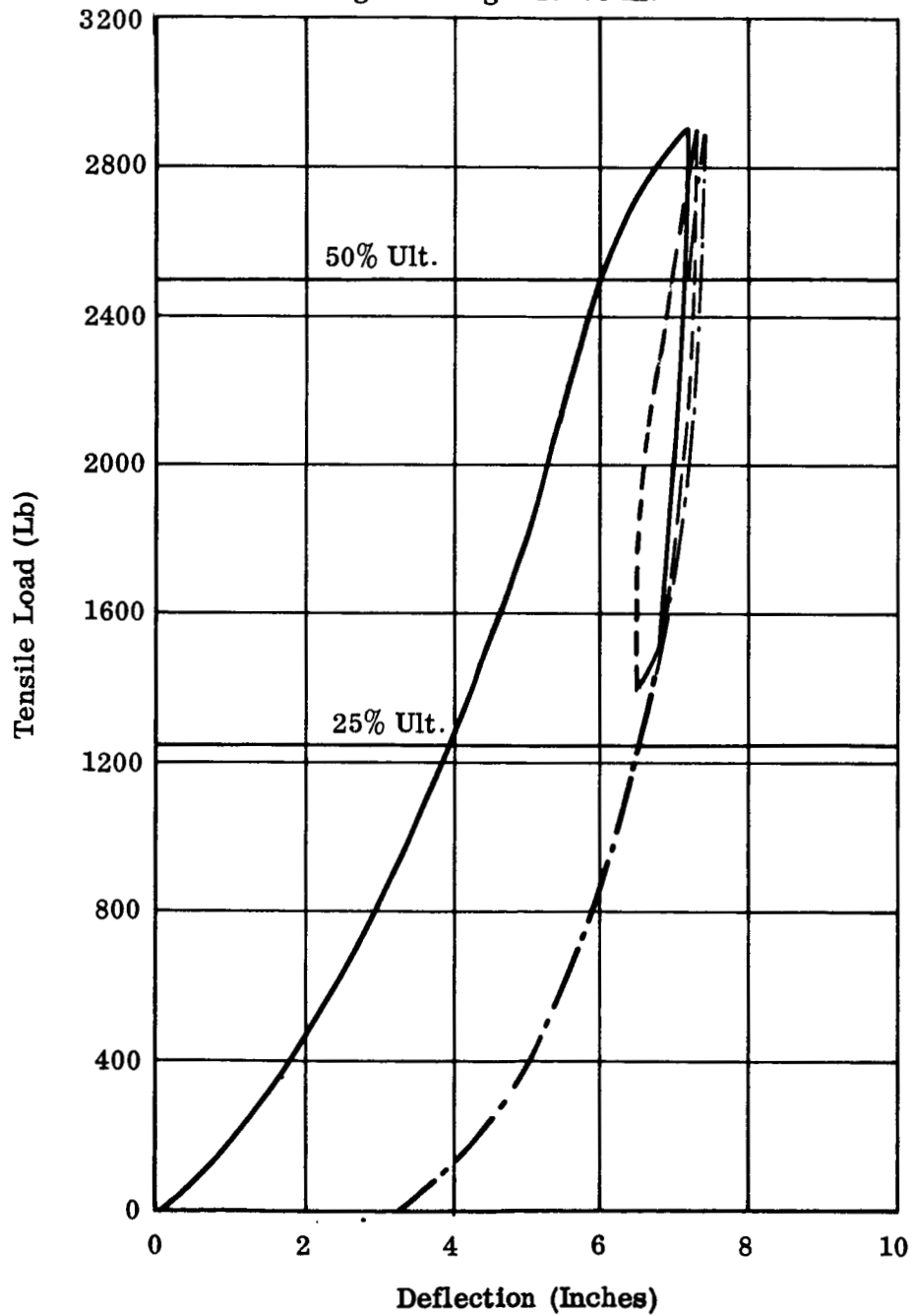


Fig. 29 Snatch Type Pickup - Ag Cat Model
Analytical Approximation to Experimental Elasticity Curve

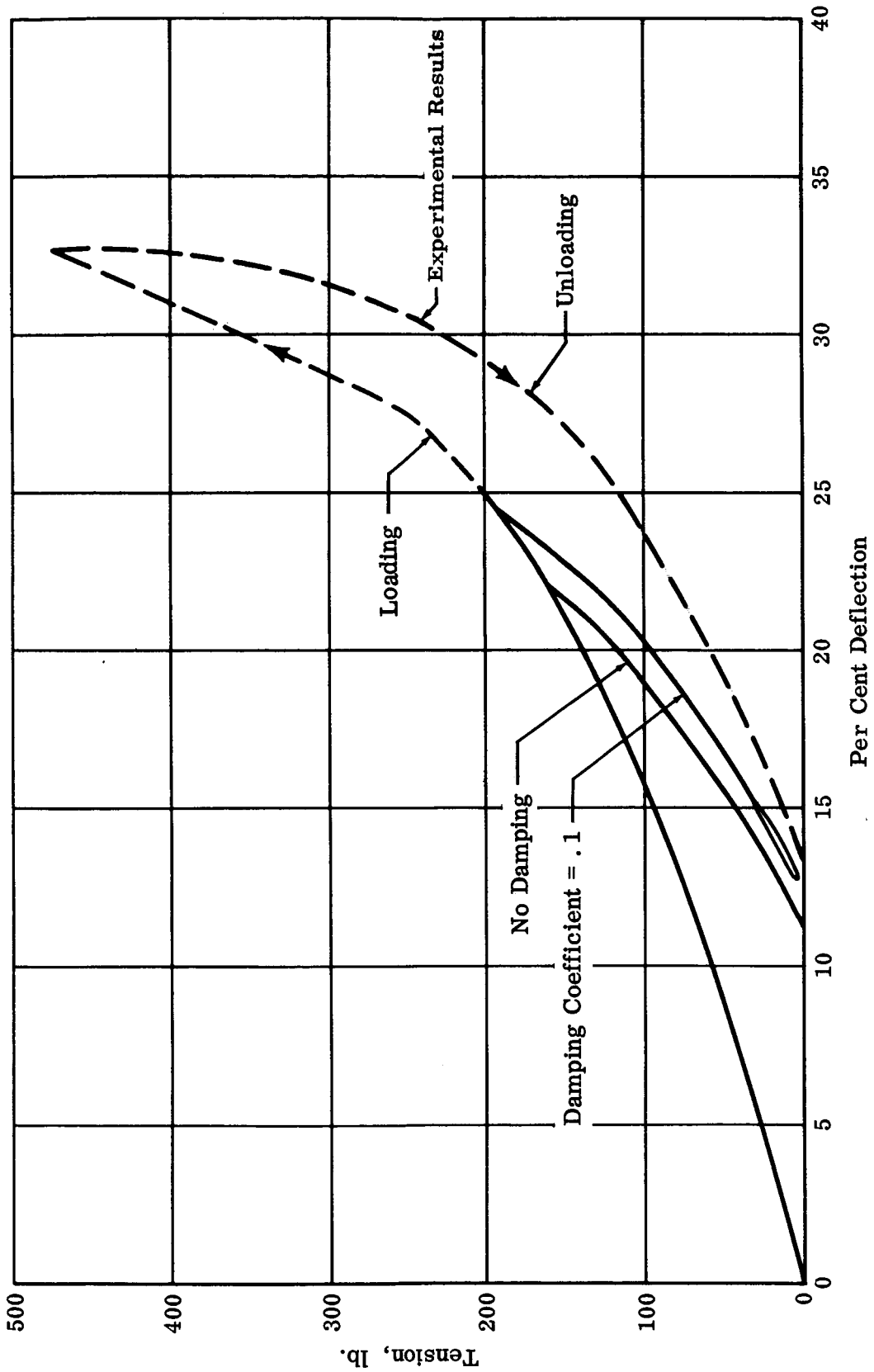


Fig. 30 Snatch Type Pickup - Ag Cat Model
Effects of Damping on Payload Trajectory
(Calculated Results)

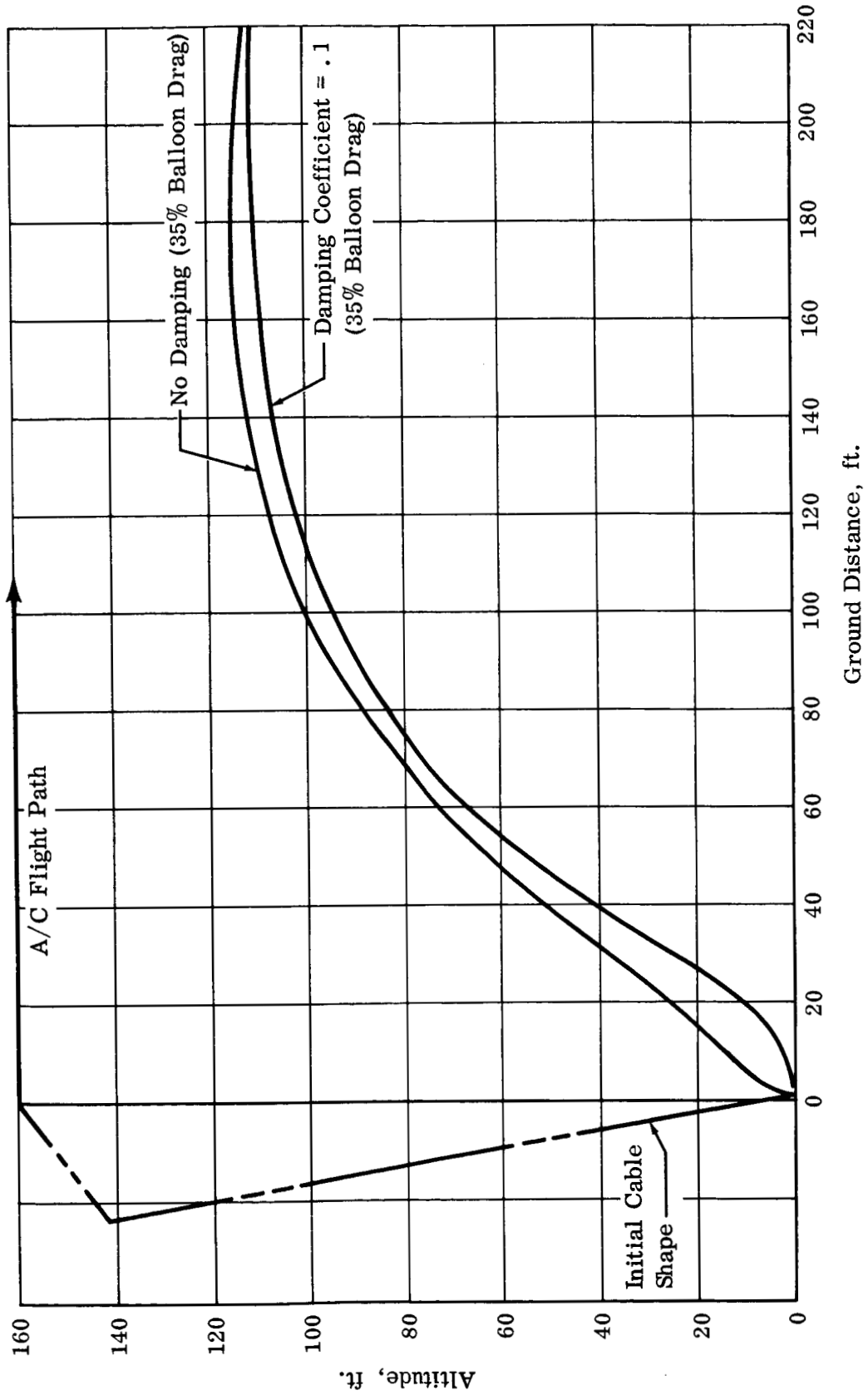
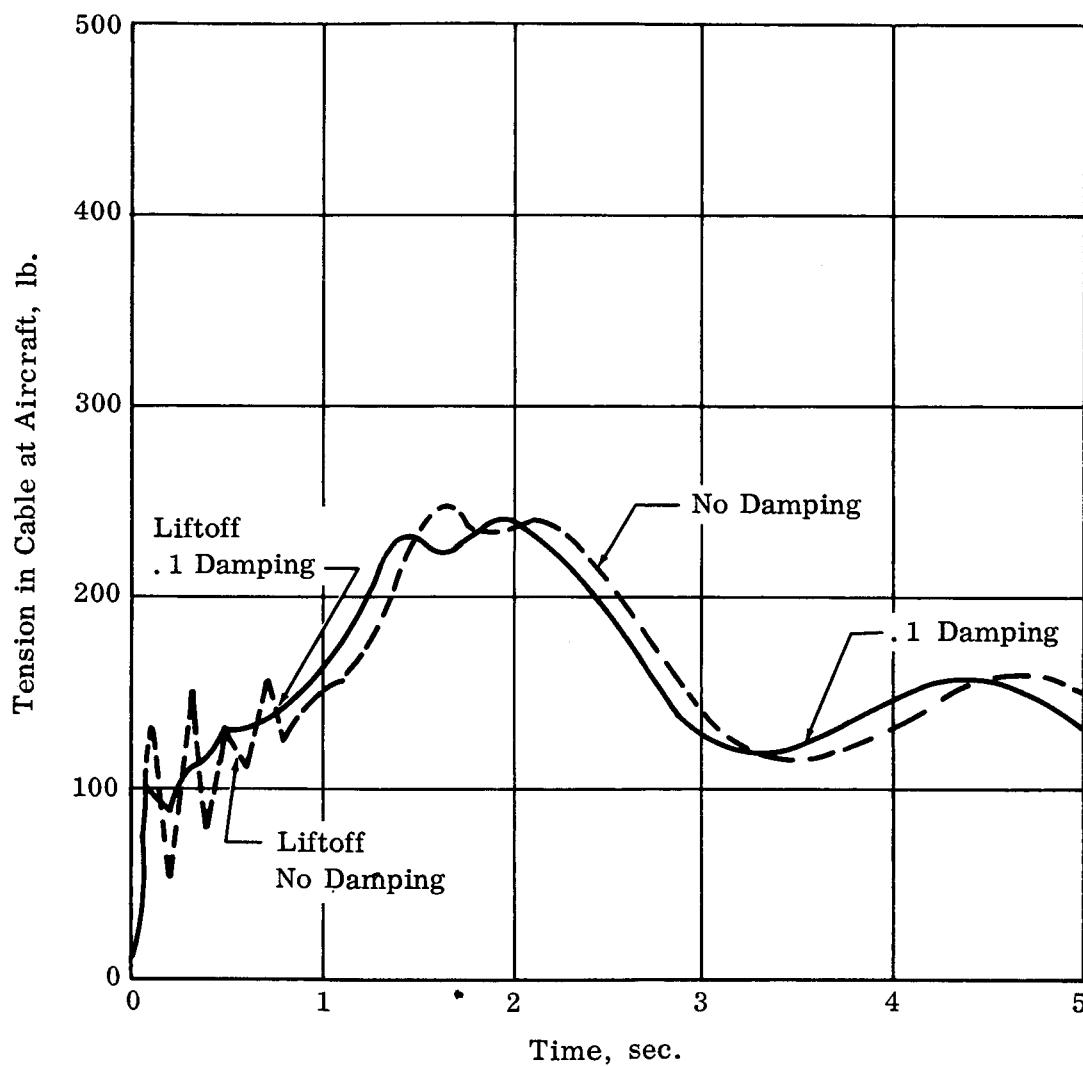


Fig. 31 Snatch Type Pickup - Ag Cat Model
Effect of Damping on Tension Time History
(Calculated Results)



SECTION III - CALCULATIONS

A. Introduction

Using the analysis as developed in Section I, a further study of the circling line maneuver was made. The behavior of the line in air as a function of certain controlling conditions (i.e. airplane circle size, line drag/weight ratio, and payload weight) was studied experimentally and analytically in the previous section. This study was continued to determine the effects of variation in other conditions such as line length and airplane velocity. In addition, ground constraints and airplane maneuvers from the circling line configuration necessary to effect capsule pickup were investigated.

In order to obtain further information about ground-to-air payload motion and to evaluate features peculiar to itself the snatch-type pickup was also investigated.

The purpose of these investigations was to determine the applicability of these two techniques to fixed winged aircraft retrieval of large space capsules, and the calculations were performed keeping this objective in mind.

B. Circling Line in Air

1) Quiescent Atmosphere:

a. Description

As was done in Part II, the equations of motion for an inextensible cable were used to study a line circling in air under zero atmospheric wind conditions. Under these conditions, the lower or free end of the cable describes a circular path concentric with and parallel to the enforced circular path of the upper end (See Figure 16). Calculations were made to determine the effect on the size of the payload or end point circle and vertical separation (i.e. vertical distance between the upper and lower ends of the cable) of variations in airplane flight conditions, cable characteristics, and payload characteristics. For the sake of completeness some of the results obtained from Part II are again presented here.

The calculations were made for two line configurations, one which might be used to effect retrieval of an Apollo spacecraft, and the other, the small scale Ag-Cat model of this configuration. Using the laws of dynamic similitude (Ref.: Volume I) results obtained for the Ag-Cat model can be scaled up to the Apollo configuration. The bulk of the calculations were made for the model since this information was necessary to set up the experimental test program. The following table gives a description of these configurations:

Table 4 - Line Configurations Used for Calculations

		Ag-Cat Models	Apollo
Airplane Flight Conditions	Apl. Velocity	55 to 75 mph	125 knots
	Apl. Circle Rad.	315 to 650 ft.	2400 ft.
Cable Characteristics	Cable Length	1800 to 2700 ft.	6667 ft.
	Cable Dia.	1/4" to 1/2"	1 1/8"
	Cable Density	.015 - .09 lbs/ft.	.3 lbs/ft.
Payload Characteristics	Payload Weight	0 - 300 lbs.	50 or 10000 lbs.

b. Effects of Airplane Flight Conditions

Airplane Velocity - Figure 32 shows the results of variations in airplane velocity. As the velocity is increased both the end point circle and the vertical separation decrease. It is important to notice that these results are for no payload, since for a heavy payload completely different results might be obtained. Of interest in this case is the fact that end point velocity remains fairly constant as the aircraft velocity is varied. Therefore, a rough estimate of the end point circle for a given velocity could have been obtained once one value was determined.

$$(\text{e.g. End point circle} = \frac{\text{End point velocity} \times \text{Airplane Circle}}{\text{Airplane Velocity}}).$$

In practice, varying airplane velocity to control end point circle or vertical separation is a limited technique, since in order to maintain a constant airplane circle size the airplane bank angle, which has operational limits, must be varied.

Airplane Circle Size - A decrease in airplane circle size produces a decrease in end point circle size and an increase in vertical separation (See Figure 33). This result was verified experimentally in the previous section. Control of the end point behavior by this technique is again limited by the operational values of airplane bank angle and airplane velocity.

c. Effects of Cable Characteristics

Cable Length - Figure 34 shows that end point circle decreases and vertical separation increases as cable length is increased. This control is limited only by the volume and weight of cable that the aircraft can handle, though large values of vertical separation might prove undesirable if visual contact with the payload is required.

Cable Diameter - The cable diameter was varied keeping a constant linear density. This variation corresponds to drag/weight variation investigated experimentally in Part II. Figure 35 shows that as cable

diameter is increased end point circle size and vertical separation decrease. It should be noticed that these results are for no payload, since the calculations performed for the experimental variation of drag/weight ratio with payload show a decrease, then an increase in end point circle size with increase in drag/weight ratio. The cable drag or the cable weight can be varied, therefore, to control the end point trajectory.

d. Effects of Payload Characteristics

Payload Weight - Figure 36 shows end point circle size and vertical separation both increase with increasing payload weight. Control of the end point trajectory can be attained by varying payload weight only in the first stage of a retrieval operation (ie. before attachment to the capsule is made) since after attachment the payload weight is largely determined by the capsule.

Payload Drag - The drag characteristics of the capsule would probably have been predetermined. However, a parachute could be added to the end of the cable to increase the drag coefficient if desired. Figure 37 shows that adding a parachute to the end of a cable decreases the end point circle size while having relatively little effect on the vertical separation.






e. Effect of Parachutes Placed Along the Line

In general, addition of a parachute (concentrated drag) decreases the end point circle as is shown in Fig. 36. However, when the parachute is placed near the top of the line the end point circle increases. A parachute in this location decreases the "effective" line length (notice sharp decrease in vertical separation) by crimping or pulling out the upper portion of the line.

f. Effects of Line Taper

The results of the study of various types of line taper are shown in Table 5. Two types of cable were studied, one where the linear density was held constant and the shape was varied and the other where the line density varied with shape (i.e. constant volume density). For a constant linear density, increasing the area near the lower end of the cable gives the smallest end point circle for the different types of tapered line. These results are consistent with those obtained in the parachute placement study, where increased drag near the bottom of the line decreases the end point circle size. However, a line of constant diameter equal to largest diameter of the tapered line produces the smallest end point circle. For the constant volume density cables, which have a lower total drag/weight ratio, the end point circle sizes are much larger than those obtained for the other type cable. Notice for this cable the sharp decrease in vertical separation when the cable is heaviest near the top. For the cases studied, line taper presents no distinct advantage over a simple drag/weight variation as a method of end point control. Future calculations, however, in which special "tapers" are introduced over shorter portions of the line, may show some advantages. The examples calculated do not cover all possible combinations, and when special operational requirements such as flotation or abrasion resistance are introduced for certain portions of the line, attention should again be given to possible changes in section.

Table 5 - Effects of Line Taper on End Point Circle & Vertical Separation for Full Scale Apollo

		End Pt. Circle Rad. (ft.)		Vertical Sep. (ft.)	
Description		Const. Linear* Density	Const. Volume** Density	Const. Linear Density	Const. Volume Density
1 1/8" dia. cable (no taper)		337	337	4775	4775
3 3/8" dia. top to 1 1/8" dia. bottom		287	670	4280	3538
3 3/8" dia. bottom to 1 1/8" dia. top		149	619	4689	5538
1 1/8" dia. at ends to 3 3/8" dia. at center		249	442	4616	5038
3 3/8" dia. cable (no taper)		141	751	4203	5055

* Constant linear density = .3#/ft.

** Constant volume density = .026#/in.³

2) Wind Effects:

In order to obtain a first approximation of the payload motion under wind action, simplified wind profiles were applied to the Apollo line configuration. Figure 38 shows a typical payload trajectory. The payload path is displaced from the center of the airplane circle and shows a cyclical variation in vertical separation. The vertical separation varies from a minimum with the aircraft flying approximately downwind (pt. 13) to a maximum with the aircraft flying approximately upwind (pt. 6). Notice, however, that when the aircraft is moving downwind the payload and a large portion of the cable is moving upwind and vice versa.

Figure 39 shows the effect of wind intensity on the payload trajectory. As the magnitude of the wind is increased the end point trajectory moves further away from the center line of the airplane circle and its projection in the horizontal plane becomes less circular. Results similar to these were calculated for the Ag-Cat model (see Section II). The magnitude of the yo-yo calculated for the Apollo configuration is considerable, reaching almost 1900 ft. under the action of a 30 knot direct wind.

:

Fig. 32 Circling Line - Ag Cat Model
 Vert. Sep. End Pt. Rad. & Vel.
 Vs. A/C Vel.

1800 ft Nylon Cable - .015 Lb/Ft Cable Dens.
 A/C Turn Rad. - 650 ft No Payload

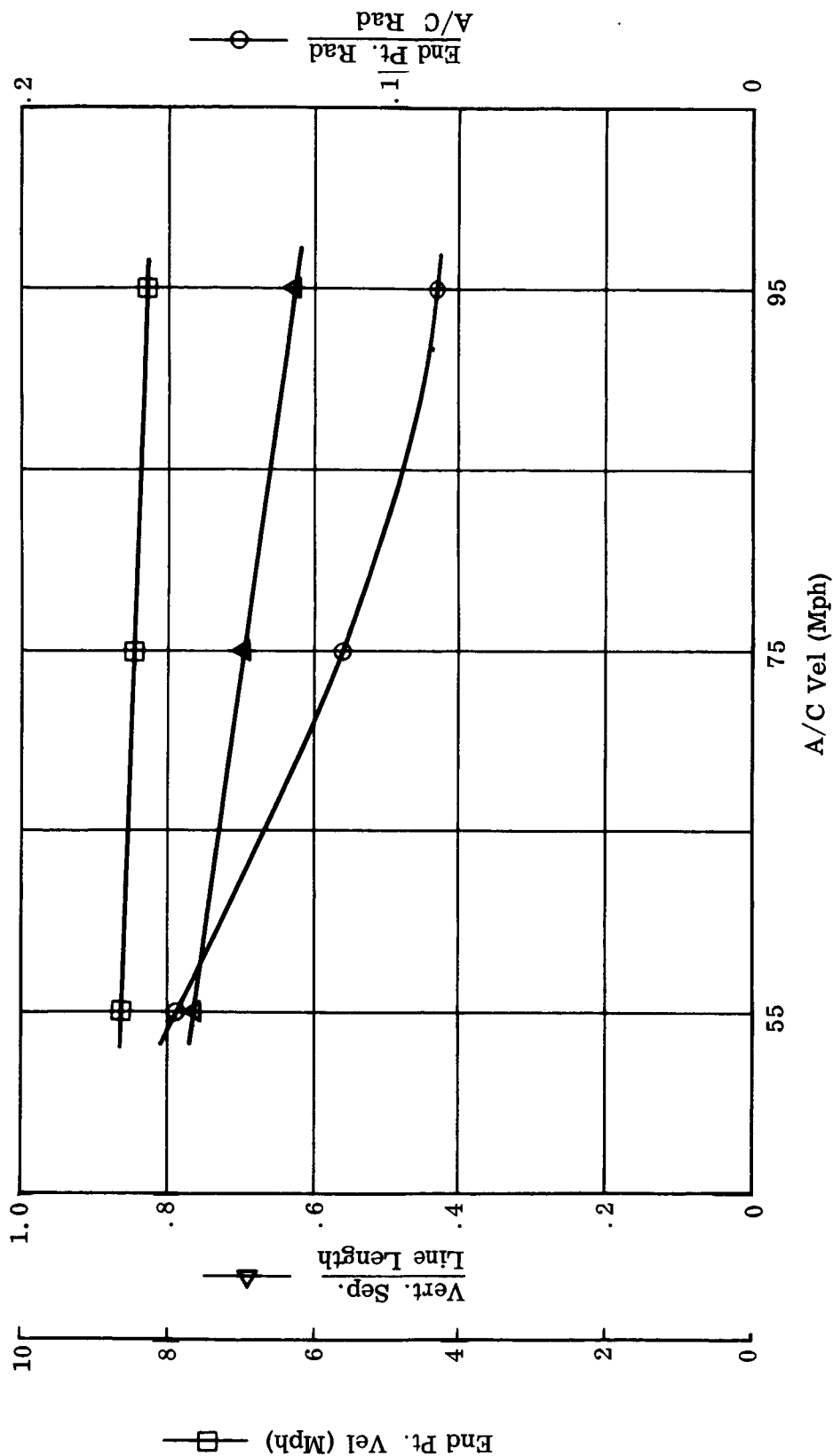


Fig. 33 Circling Line - Ag Cat Model
 Vert. Sep. & End. Pt. Rad.
 Vs. A/C Rad.

1835 ft. Cable Length - 1/2" Dia. Polypro. Cable
 A/C Vel. 75 Mph - Payload 46-1/2(lb)

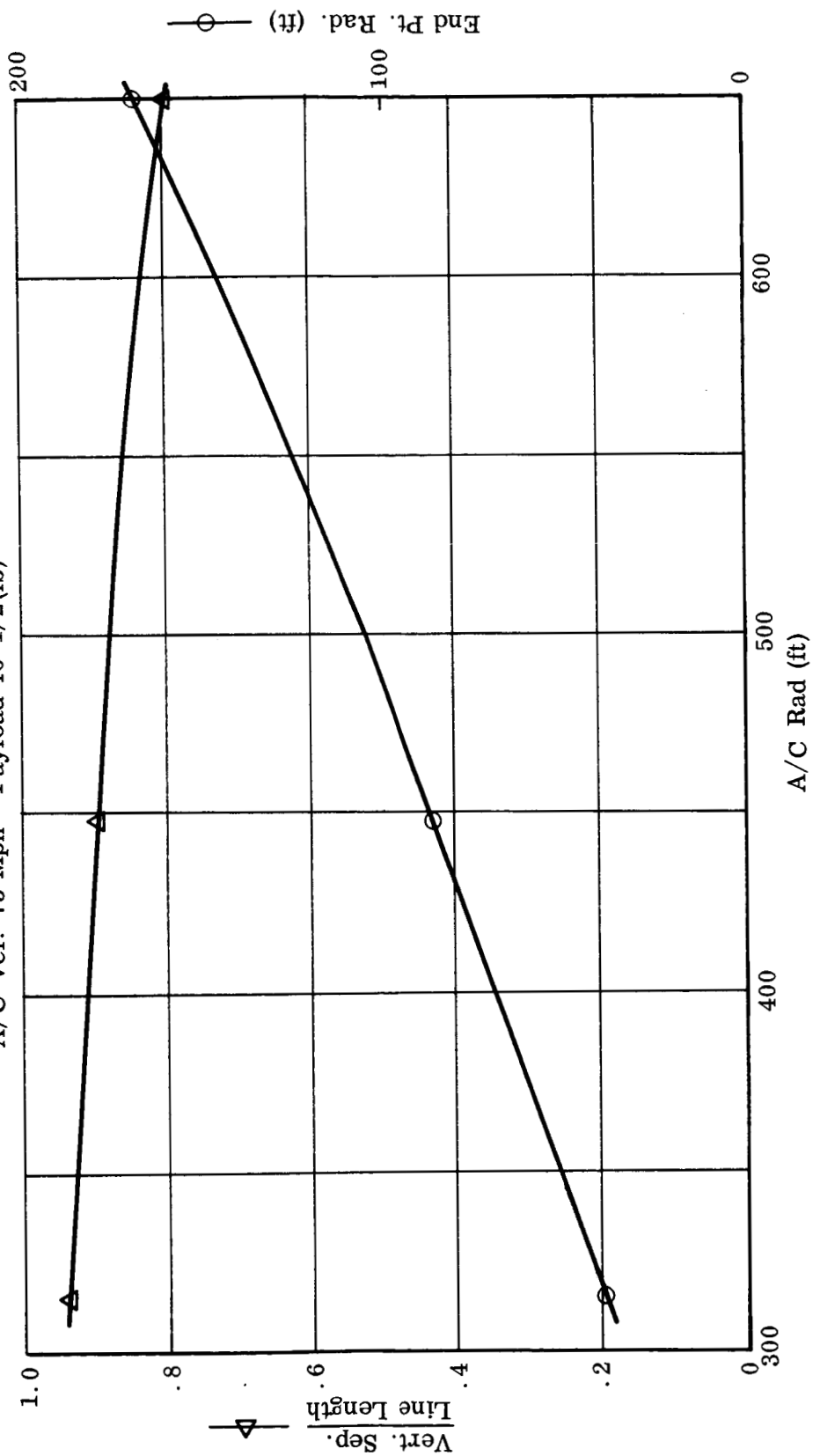


Fig. 34 Circling Line - Ag Cat Model
Vert. Sep. & End Pt. Rad.
Vs. Line Length

1/4" Nylon Cable - A/C Vel. 75 Mph
A/C Rad. 650 ft - No Payload

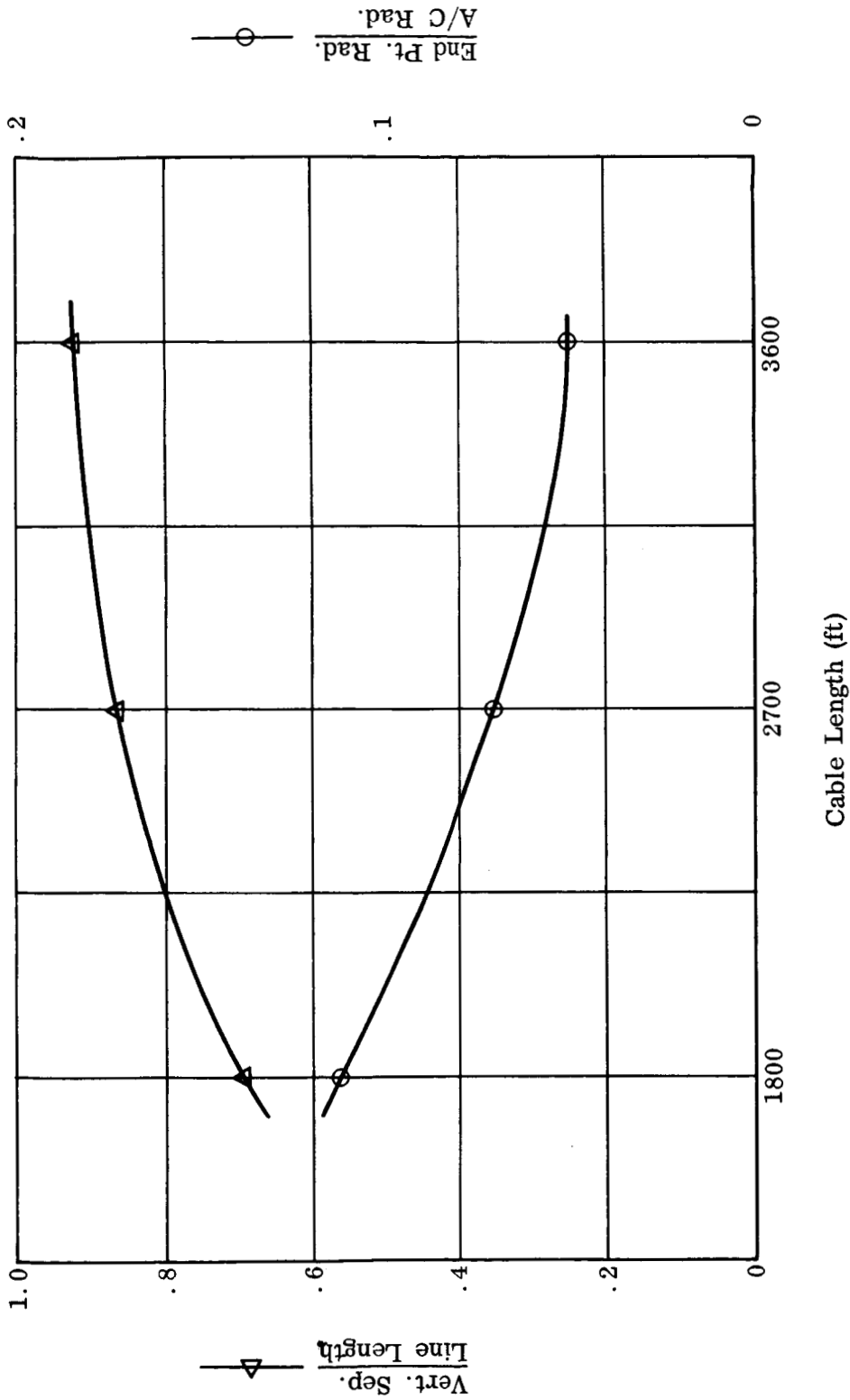


Fig. 35 Circling Line - Ag Cat Model Vert. Sep.
& End Pt. Rad. Vs. Cable Dia.

1800 ft Cable Length - .015 Lb/Ft Cable Dens.
A/C Vel. - 75 Mph - A/C Rad - 650 ft
No Payload

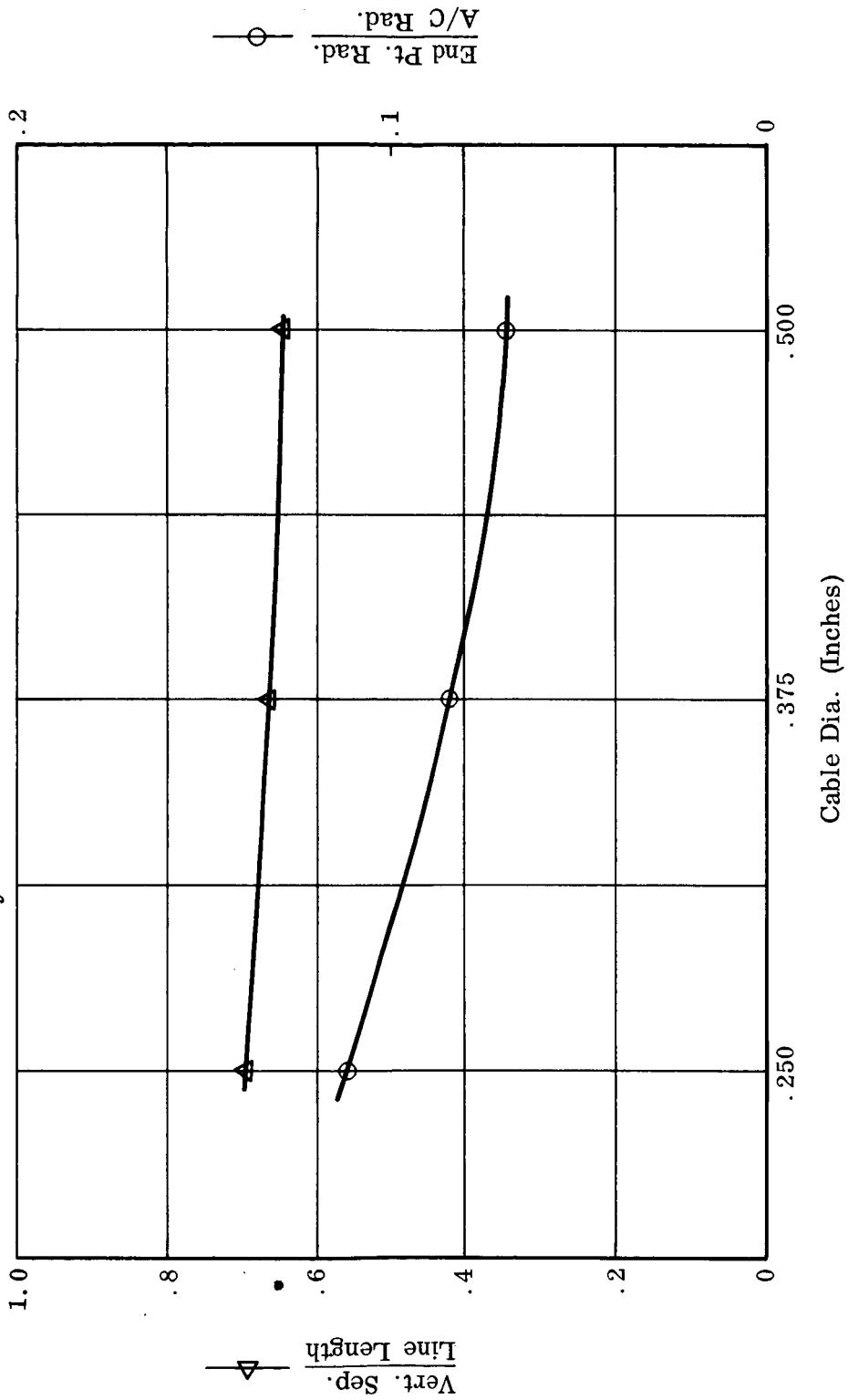


Fig. 36 Circling Line - Ag Cat Model
Vert. Sep. & End Pt. Rad.
Vs. Payload Wgt.

1800 ft Cable Length - 1/4" Dia Nylon Cable
A/C Vel. - 75 Mph - A/C Rad. - 650 ft.

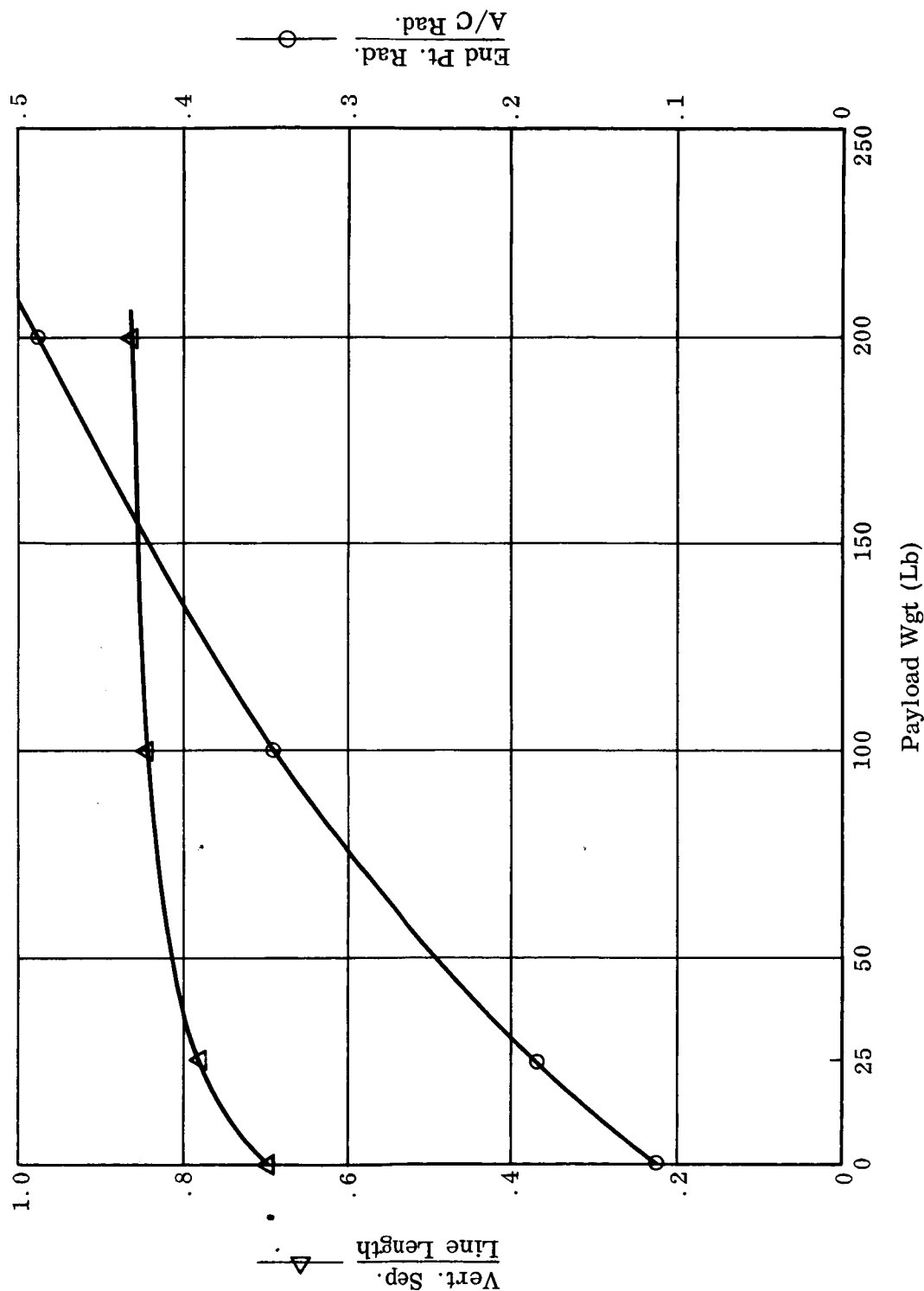


Fig. 37 Circling Line - Apollo Configuration
Effect of 12 ft. Dia. Parachute On
Vert. Sep. & End Pt. Rad

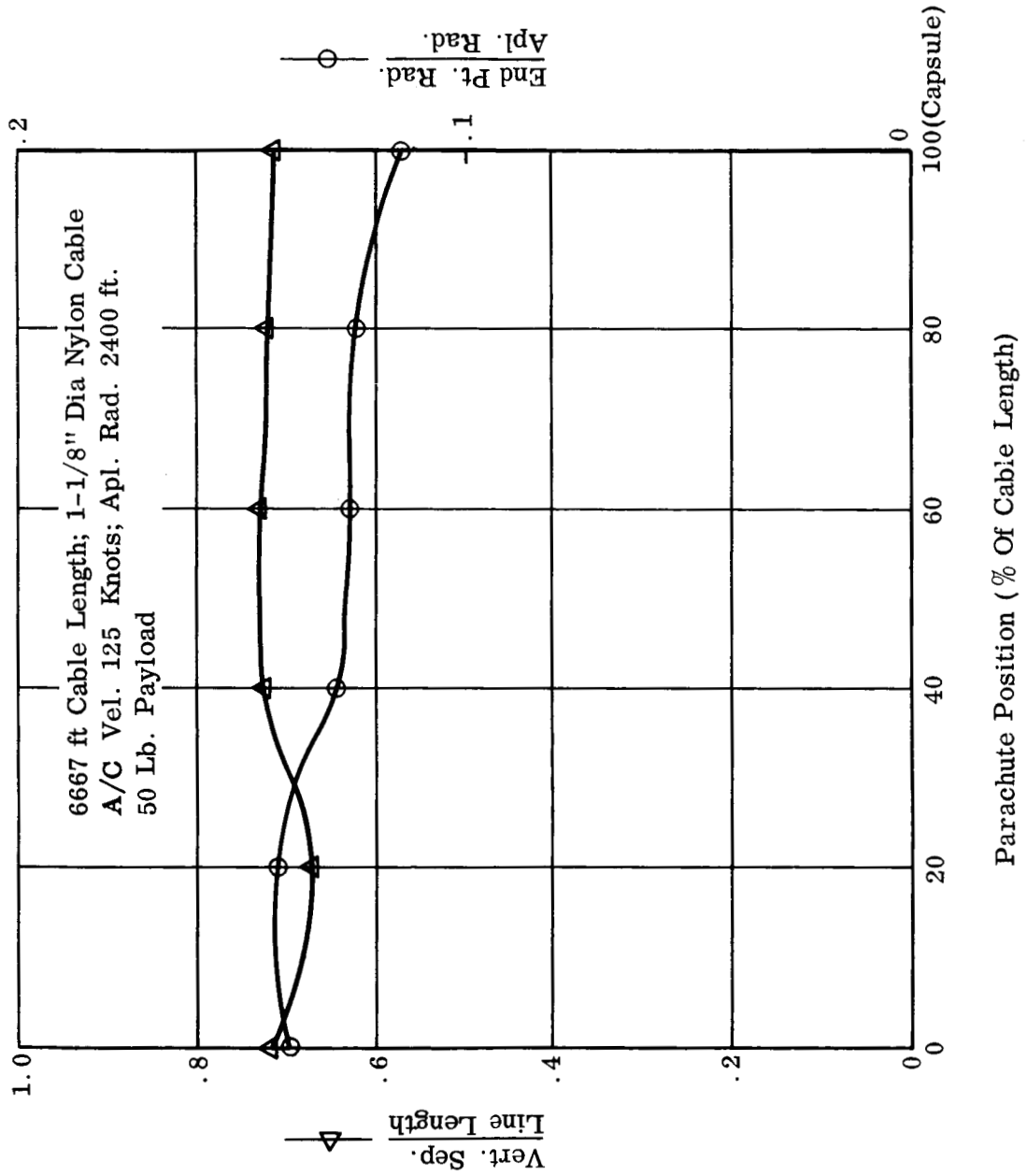


Fig. 38 Circling Line - Apollo Configuration
Effect of 5 knot/2500 ft Wind Shear
Payload Weight = 50 lbs.

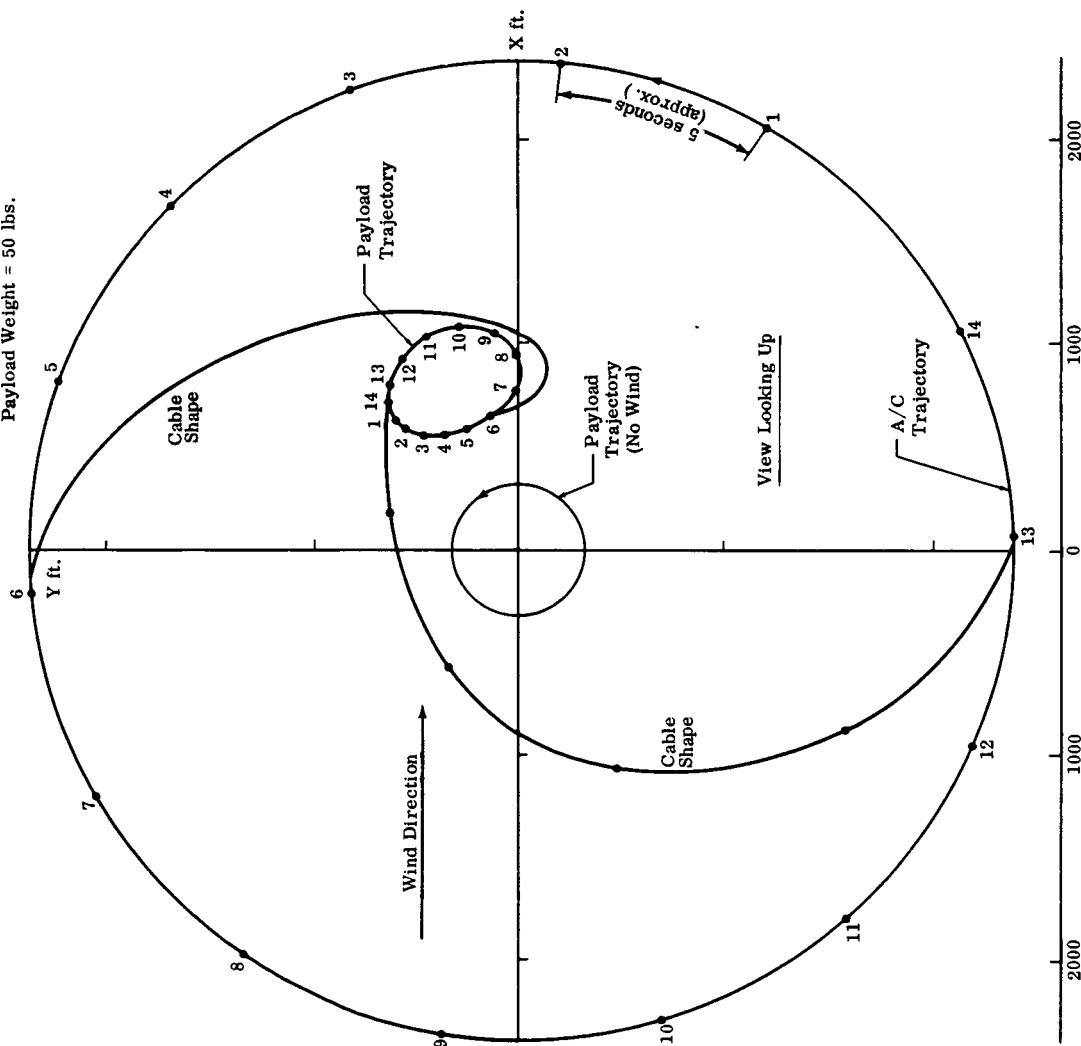
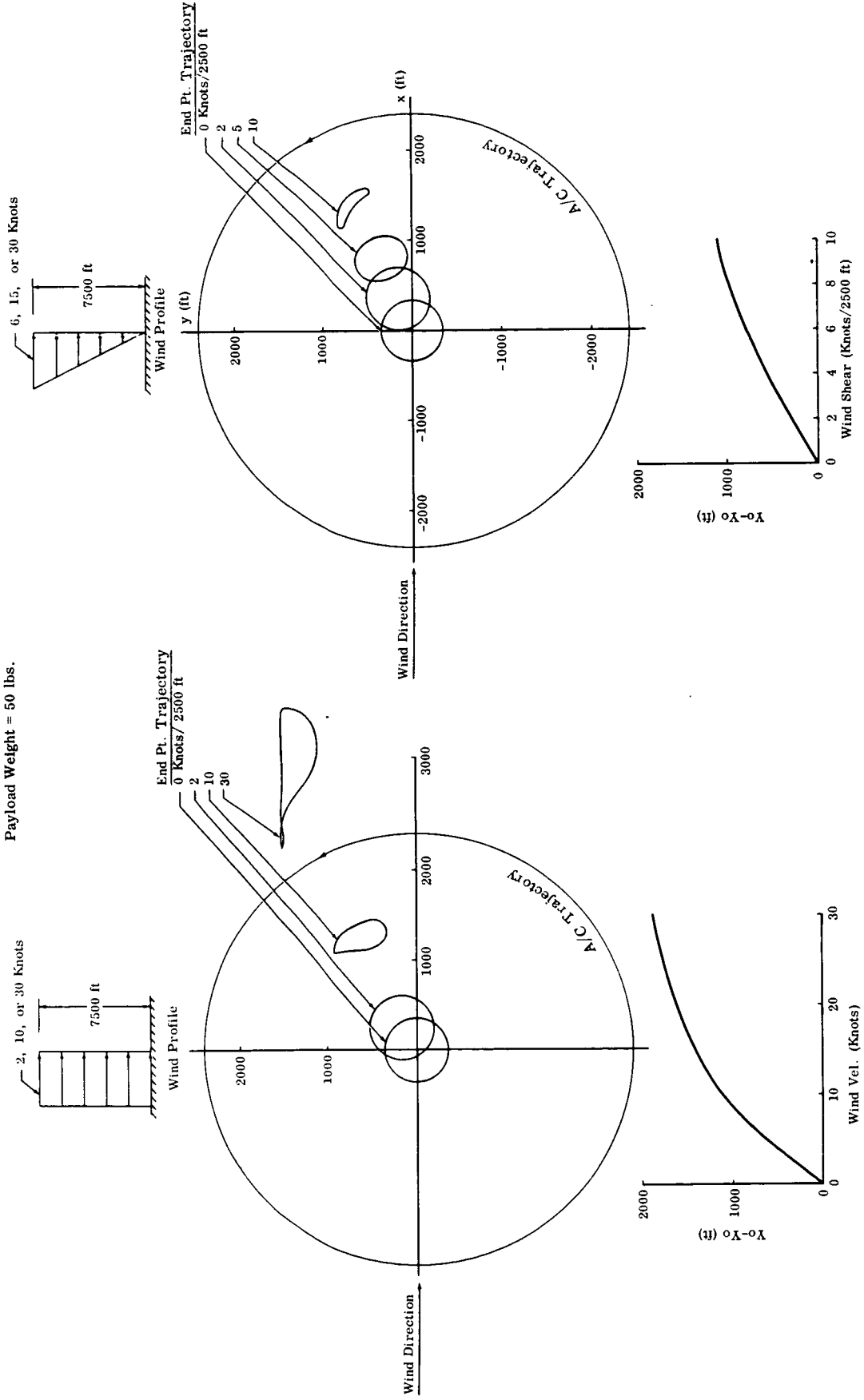


Fig. 39. Circling Line - Apollo Configuration
Effects of Wind and Wind Shear
Payload Weight = 50 lbs.



C. Capsule Pickups

1) Snatch Type:

Calculations were performed for snatch-type pickups of a heavy capsule (10,000 lbs), using various lengths of cable. For this type pickup, the aircraft must make connection with a cable which extends upward from the capsule. This capsule cable is usually balloon supported.

It was found that by increasing the length of the cable the maximum tensions during the pickup could be reduced and fairly good capsule trajectory could be obtained (See Figure 40). For example, for cables of 1000 ft. and 3000 ft. calculations predict satisfactory trajectories and maximum tensions of 50,000 lbs. and 25,000 lbs. respectively.

This technique has the drawback of having to deliver to the payload an extremely heavy drop kit which contains the cable, a balloon to support the cable, and a device to inflate the balloon. Therefore, calculations were performed for pickups which have cable extending from the aircraft as well as cable extending from the capsule in order to reduce the length of the latter. It was found, however, that the capsule tended to dip lower in its trajectory after an initial peak, to the extent that in some cases the capsule hits the ground again. This is due to the fact that the airplane cable trails relatively high, requiring the aircraft to fly too low relative to the total length of cable between airplane and capsule.

2) Circling Line:

a. Hook Attachment

Having obtained equilibrium shapes in Part B of this section for the Apollo configuration, the next problem considered was that of transporting the attachment package from its equilibrium position in the air to the retrievable capsule, which was assumed to be on the ground at the center of the airplane circle.

To accomplish this, the airplane was made to lose altitude slowly enough so that no transients were introduced in the cable motion. With the hook package at ground level, a run was made to move it from the point at which it landed to the capsule, along a prescribed path. This was a semi-circle, shown in Figure 41, along which the hook moved such that its velocity decreased from that of the free end circle to zero at the capsule. This trajectory was chosen to introduce least transients, and it can be seen that the effect on cable shape is minor.


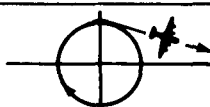
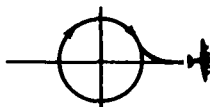
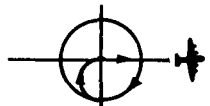
Figure 41 also shows the time history of horizontal force required to effect this end-point motion. It is noteworthy that the maximum force is less than 200 pounds, and this could very likely be reduced by decreasing the airplane altitude.

b. Lift-off

Delivery and attachment of the hook to the payload having been accomplished, the retrieval aircraft was assumed to circle over the capsule at an altitude equivalent to the vertical separation corresponding to the weight of the hook (50 lbs.).

Several maneuvers were tried by means of which lift-off of the capsule (weighing 10,000 lbs.) was effected. These are described in the following table.

Table 6 - Lift-off Maneuvers Originating from the Circling Line Configuration

Maneuver #	Description	
1	Airplane climbs while circling over the capsule	
2	Airplane flies out of the circle in a tangent straight line at constant altitude	
3	Airplane makes the transition from circle to straight radial line via an outside tangent arc	
4	Airplane makes the transition from circle to straight radial line via an inside tangent semicircle	

Maneuver #1 was tried at a climb rate of 20 feet per second, with the capsule simply resting on the ground. (See Figure 42.) The coefficients of break-away and sliding friction used were .5 and .2 respectively. Two effects were experienced as the airplane climbed and weight was transferred from the ground to the cable. First, reducing the weight on the ground decreased the friction force holding the capsule in place, and second, increasing the load on the cable, which tends to increase the end point circle size, put an outward radial force on the capsule. The result was that the capsule dragged along the ground a considerable distance (about 700 feet) before the vertical tension component was sufficient to lift it off.

The same maneuver, at the same climb rate, was tried again with the capsule assumed tied down such that a vertical tension component of 20,000 lbs. was required to make it break loose. This is shown in Figure 43. The resulting lift-off was quite steep, but the relatively high initial acceleration caused cable tension to exceed reasonable limits.

The generally satisfactory payload trajectories resulting from long-line snatch type pickups, discussed above, led to consideration of the modified circling line pickups exemplified by Maneuvers 2, 3 and 4.

Fig. 40 Snatch Type Pickup Apollo Config: Variations in Airplane and Capsule Cable Lengths
 Airplane Vel. = 125 Knots; Cable Dia. = .51 lb/ft - Payload = 10,000 lb

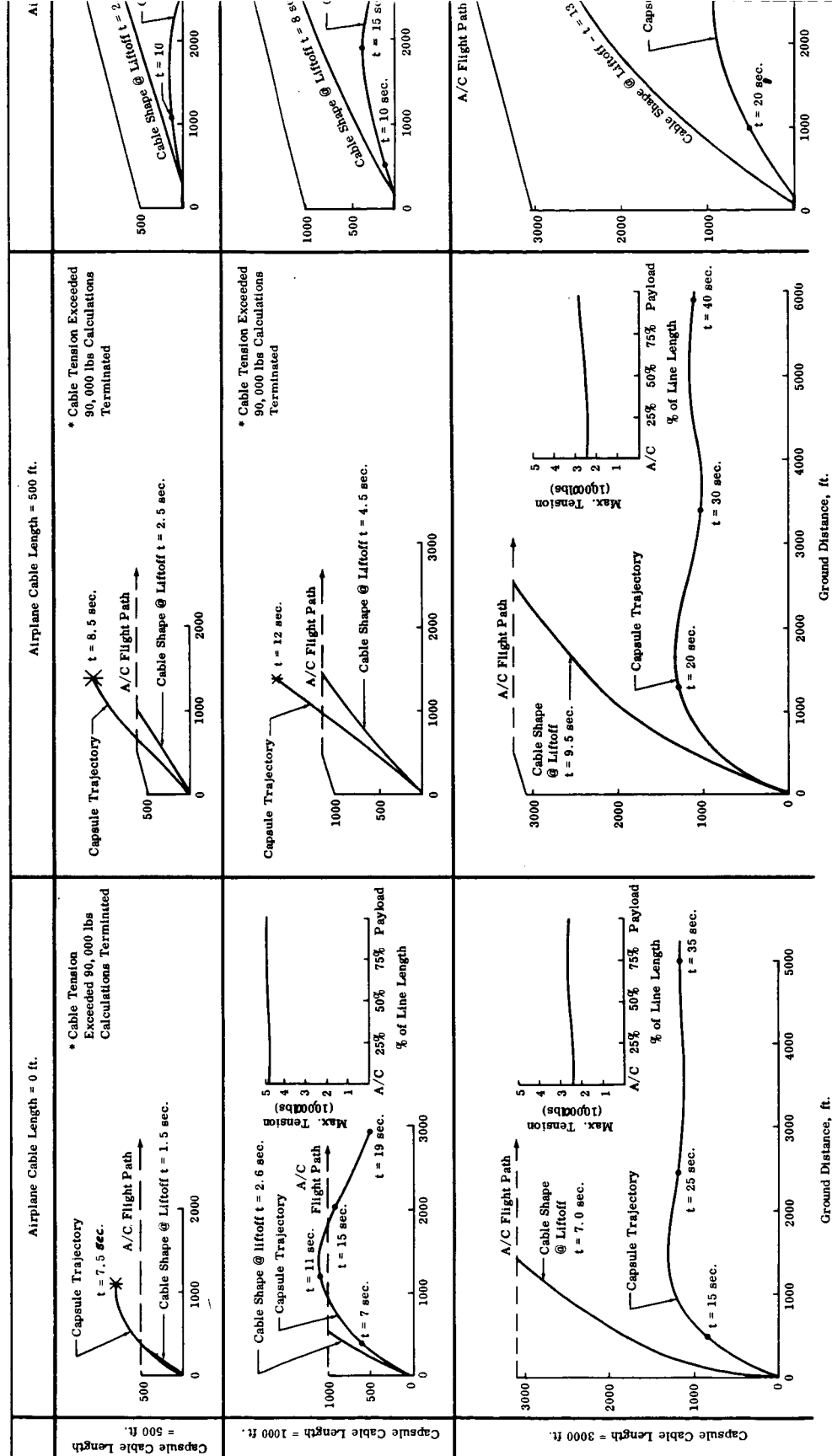


Fig. 40 Snatch Type Pickup Apollo Config: Variations in Airplane and Capsule Cable Lengths
 Airplane Vel. = 125 Knots; Cable Dia. = 1.4" Cable Dens. = .51 lb/ft - Payload = 10,000 lb

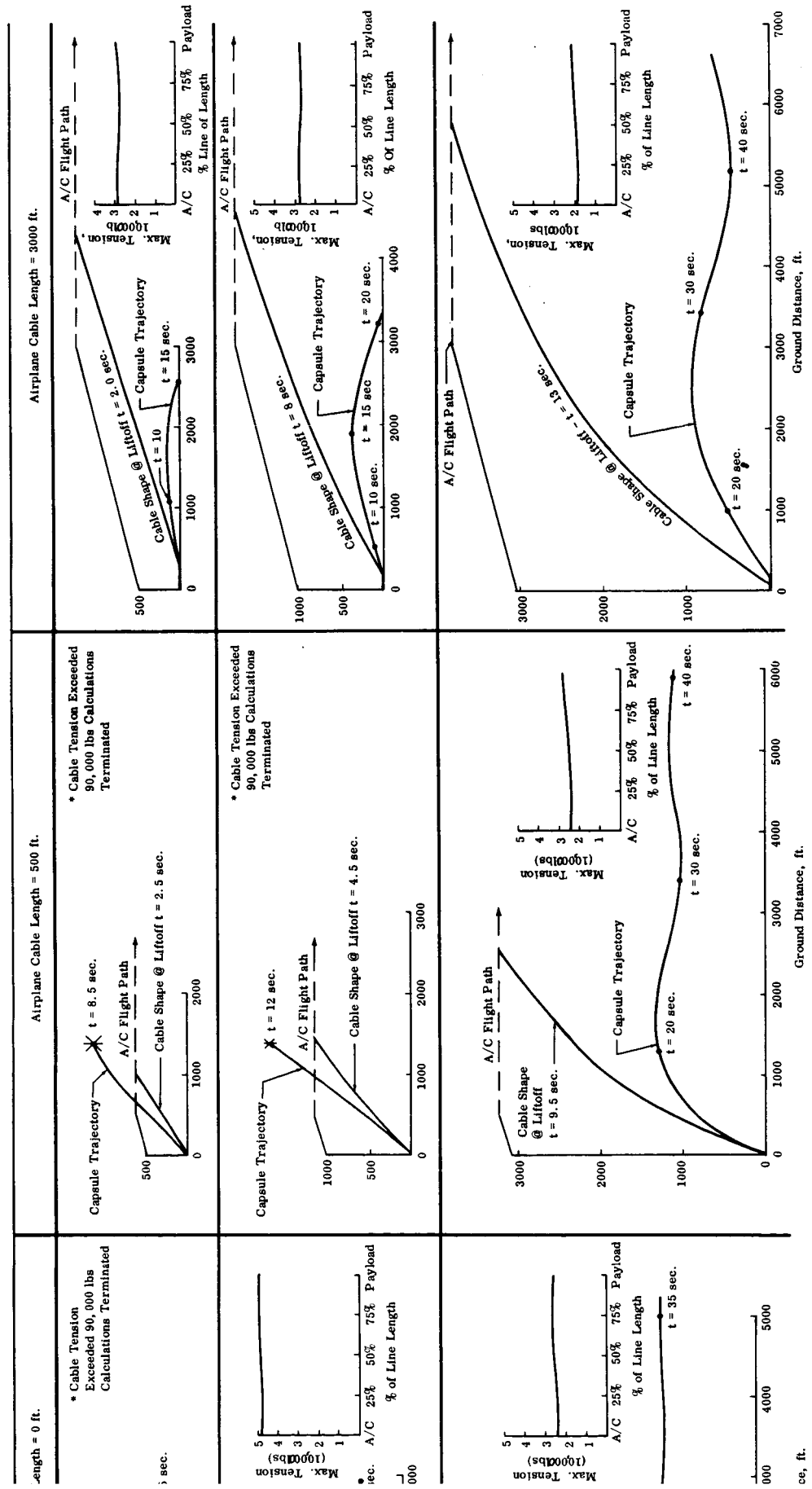


Fig. 41 Circling Line - Apollo Configuration
Horizontal Force Required to Move
Bottom of Cable in a Specified Path on the Ground
Payload Weight = 50 pounds
Airplane Altitude = 4845 feet

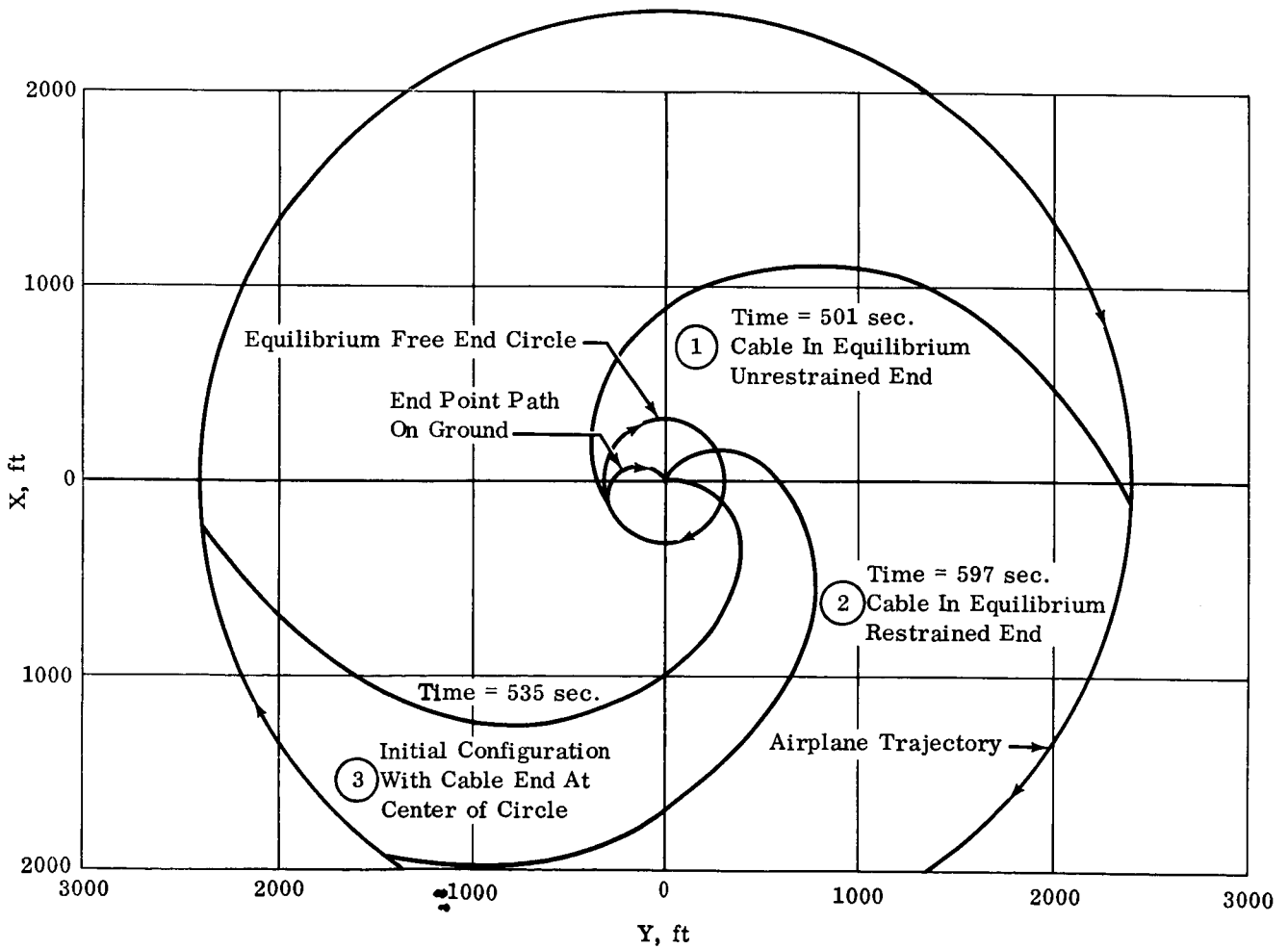
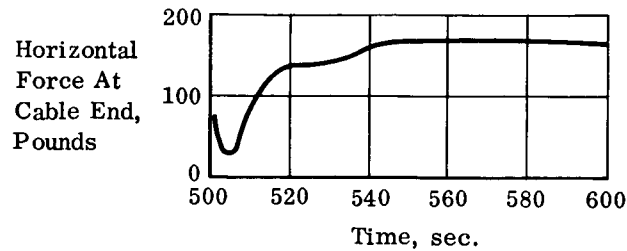


Fig. 42 Circling Line - Apollo Configuration

Pickup Using Maneuver No. 1
 Payload Weight = 10,000 lbs
 Airplane Climb Rate = 20 fps
 Max. Tension = 17853 lbs
 Ground Forces on Capsule:
 .5 Breakaway Friction Coef.
 .2 Sliding Friction Coef.

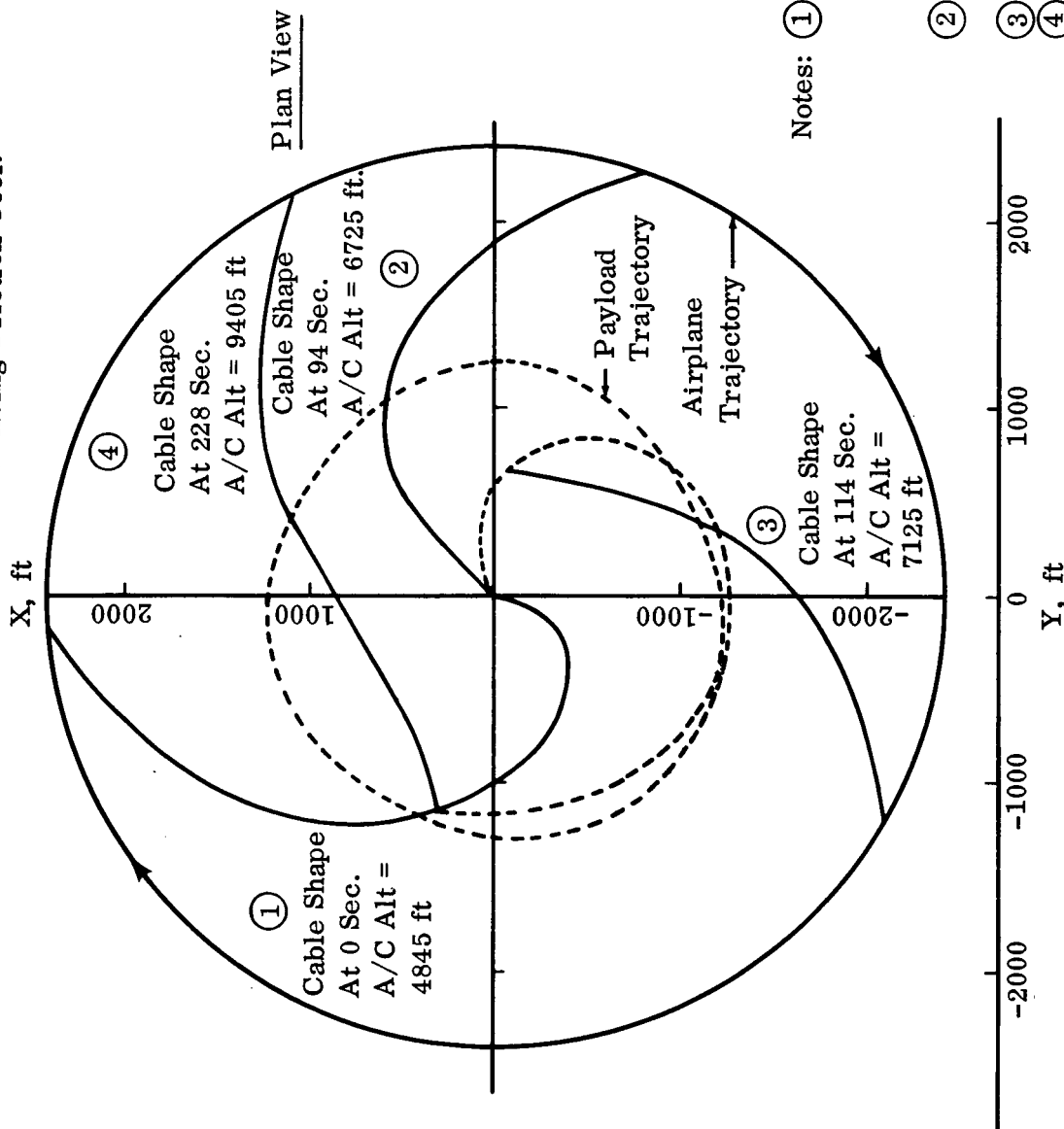
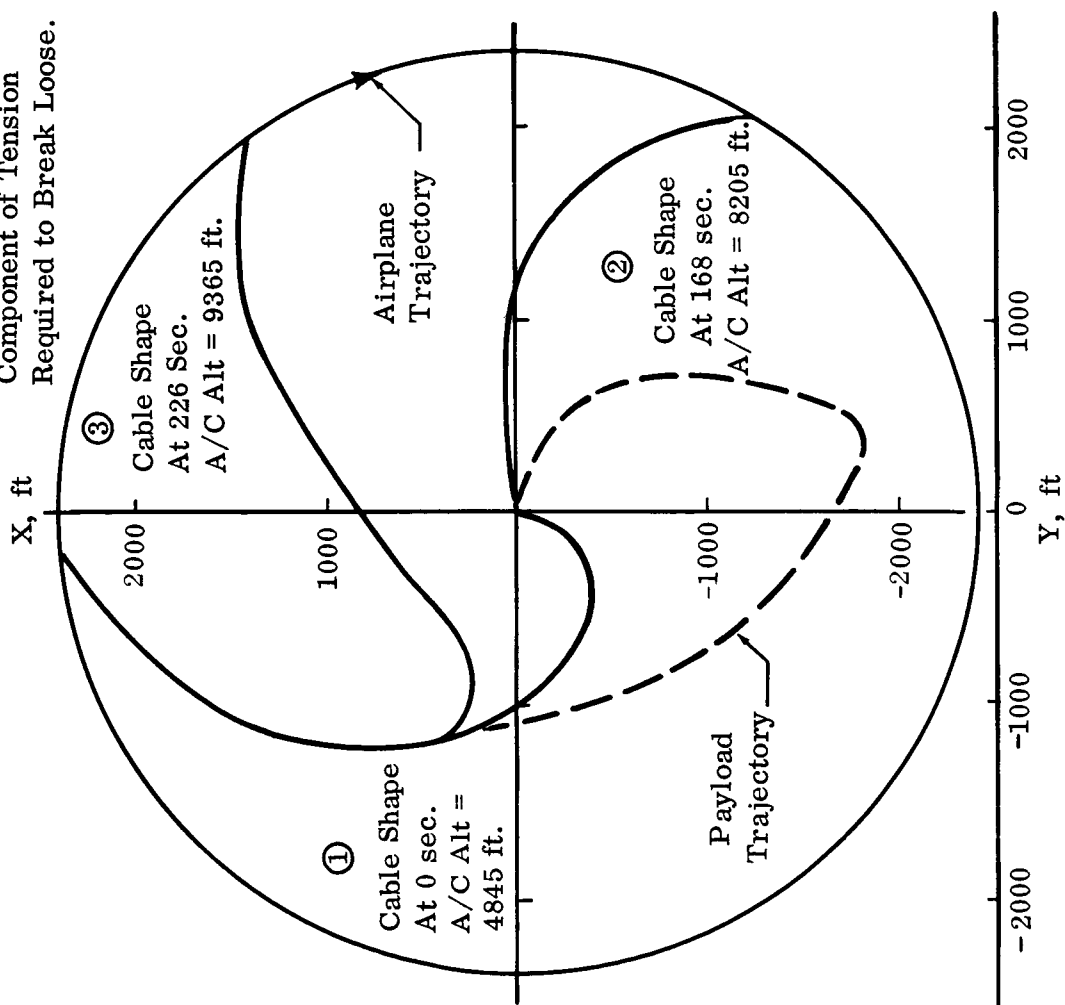


Fig. 43 Circling Line - Apollo Configuration

Pickup Using Maneuver No. 1
 Payload Weight = 10,000 lb
 Airplane Climb Rate = 20 fps
 Ground Forces On Capsule:
 Capsule Tied Down, With
 20,000 lb. Vertical
 Component of Tension
 Required to Break Loose.



Notes: ① Start of Run;
 Cable In Equilibrium
 With End Held At
 Center
 ② Incipient Lift-Off
 ③ End of Run
 * Tension Exceeded
 30000 lb

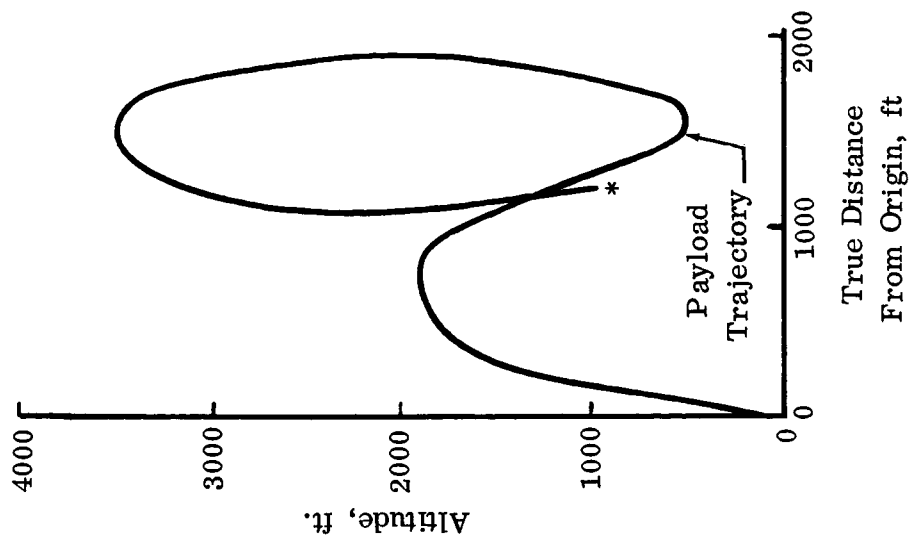


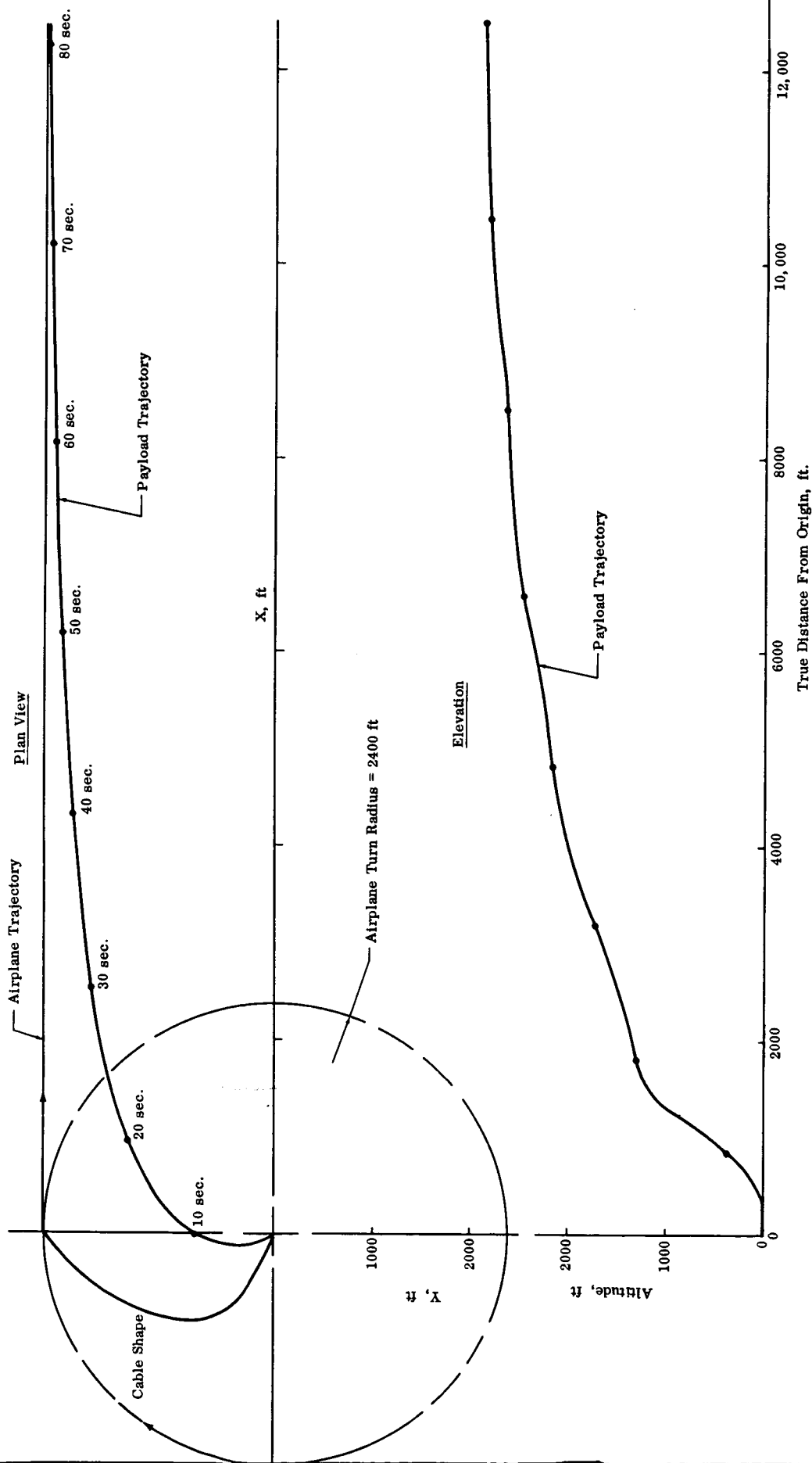
Fig. 44 Circling Line - Apollo Configuration

Pickup Using Maneuver No. 2

Payload Weight = 10,000 lb

Airplane Alt. = 5243 ft

Max. Tension = 16032 lb



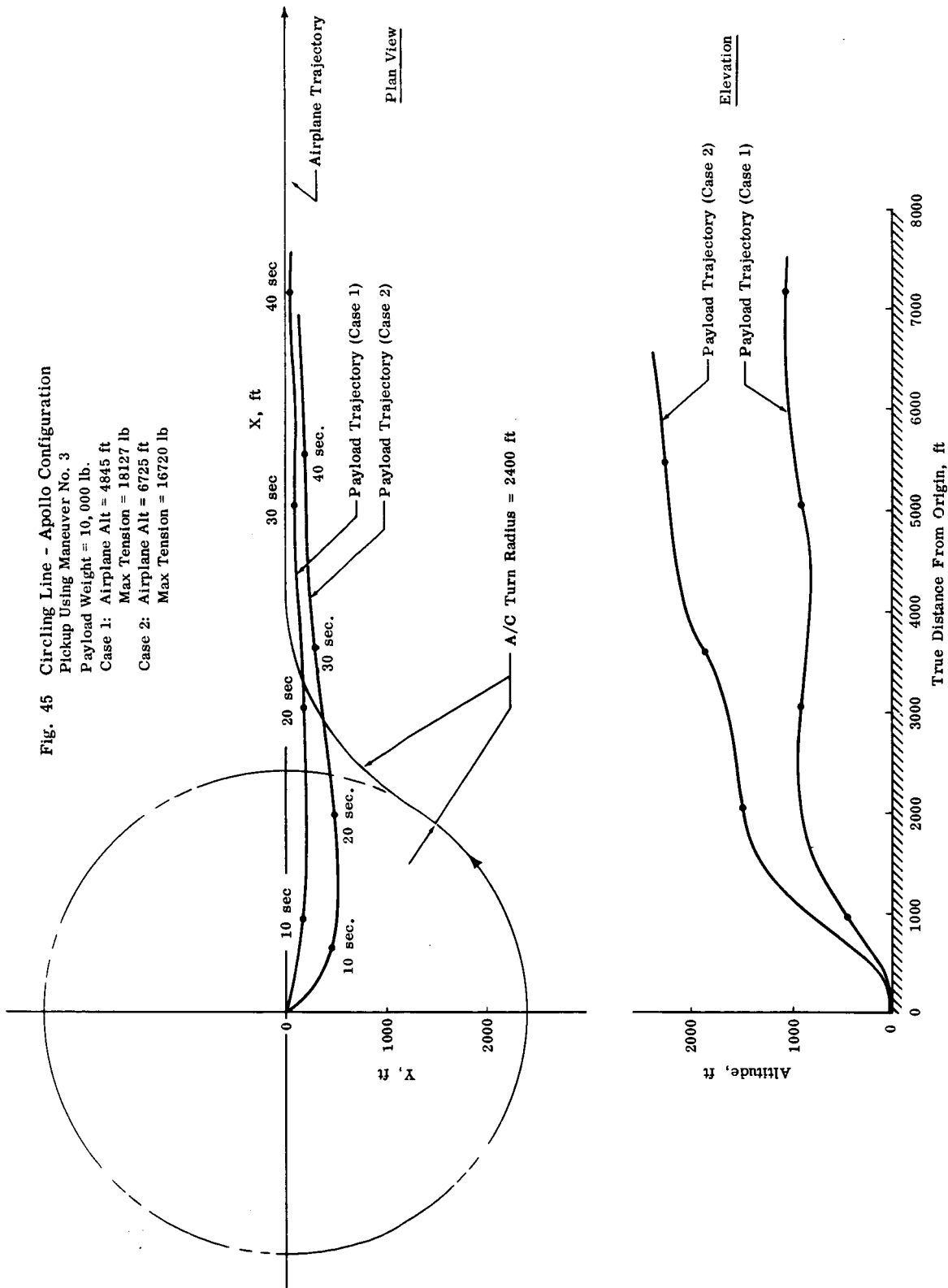


Fig. 46 Circling Line - Apollo Configuration

Pickup Using Maneuver No. 4

Payload Weight = 10,000 lb.

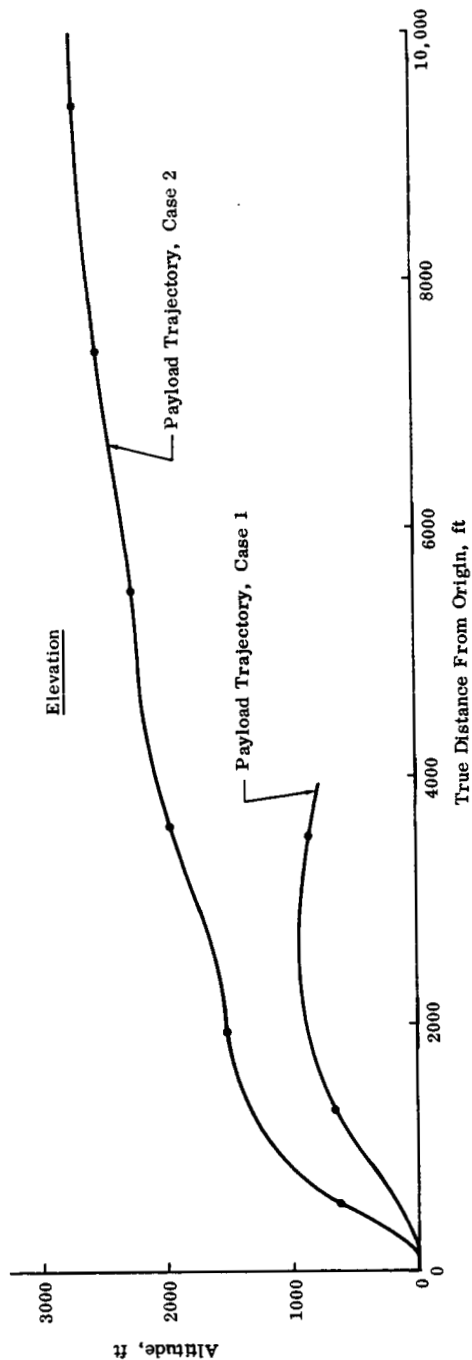
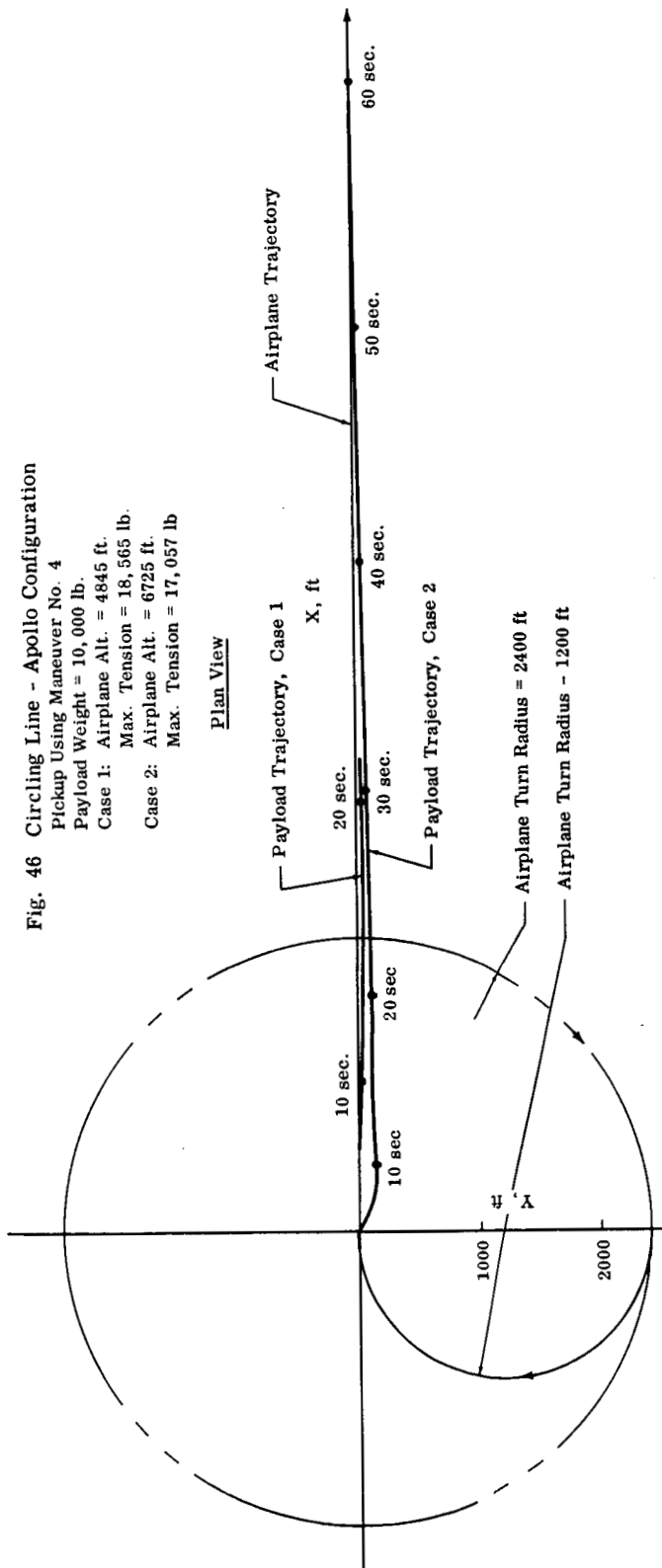
Case 1: Airplane Alt. = 4845 ft.

Max. Tension = 18,565 lb.

Case 2: Airplane Alt. = 6725 ft.

Max. Tension = 17,057 lb

Plan View



Pickups were made from two different aircraft altitudes, with the capsule resting on the ground subject to the friction forces used in Maneuver #1. Figures 44 through 46 show the resulting lift-off trajectories. These all appeared better, to various degrees, than those obtained with Maneuver #1, in that the capsule left the ground much sooner, at a steeper rate of ascent.

D. Conclusions and Recommendations

The calculations described in Part B show that certain controls on end-point motion are available which can be used to facilitate delivery of the end of a towed cable to the object being retrieved. These are summarized in the following table.

Table 7 - Variations in Circling Line Configuration Necessary to Reduce End Point Circle and Vertical Separation

		To Decrease End Point Circle	To Decrease Vertical Separation
Airplane Flight Conditions	Apl. Velocity	increase	increase
	Apl. Circle Rad.	decrease	increase
Cable Characteristics	Cable Length	increase	decrease
	Cable Dia.	increase	increase
	Cable Linear Density	decrease	*
Payload Characteristics	Payload Weight	decrease	decrease
	Payload Drag	increase	*

In general, it was found that increasing drag forces decreases end point circle size while increasing mass increases the circle size. Hard and fast rules are difficult to make, however, since position of mass and drag forces along the cable is of considerable importance, and since interaction of all these effects is extremely complex.

Atmospheric wind is a factor which must be taken into consideration in the overall design of circling line retrieval systems because of the vertical end point motion it produces. It is felt that further study should be undertaken to alleviate this effect, since it appears to be a difficulty which must be overcome, particularly when trying to land the retrieved capsule. One possibility is to investigate aircraft maneuvers which might reduce the yo-yo. Another might be to attach devices to damp this motion out, such as parachutes or balloons.

It should be noted that Table 7 indicates that the heavy capsule attached to the cable will result in large end point circles. In returning the capsule to the ground, this leads to the problems of a) placement, and b) impact loads due to high velocity. Because of these phenomena, alternative schemes for landing the capsule are discussed in Volume I of this report.

* These parameters have a negligible effect on vertical separation for the cases studied.

A variety of promising techniques for effecting lift-off of the capsule are discussed in Part C. Snatch type pickups of heavy capsules can be used, with relatively low accelerations, if long cables are used. This has the disadvantage, however, of excessive drop-kit weights. Part of the line could be initially attached to the airplane, but this leads to less satisfactory end point trajectories.

Pickup techniques based on the circling line maneuver show considerable potential. Landing and attachment of the hook from this maneuver appears straightforward, and it is felt that satisfactory lift-off trajectories could be obtained by means of slight variations on the maneuvers studied. This type of pickup does not involve the difficulties of dropping large equipment packages or of making high-speed contact with a balloon-supported line.

Due to the press of time only relatively simple examples of pickup maneuvers were tried. Much could be gained by an optimization study of these techniques, in which the effects of accelerating the airplane, climbing, reeling in line, using different maneuvers and different kinds of cable, to mention a few possibilities, would be studied.

BIBLIOGRAPHY

- a. PDR 306-A-1, "Feasibility Study of Techniques for Surface-to-Air Retrieval by Fixed Wing Aircraft" - Proposal 10 November 1961.
- b. NASA Contract NAS9-195, 8 January 1962, "Feasibility Study of Surface-to-Air Retrieval Techniques by Fixed Wing Aircraft".
- c. Grumman Project 226A, "Preliminary Study of Capsule Recovery for the First Series of Project Mercury Orbital Flights", Contract NAS 5-71, Report dated July 1959.
- d. Grumman Project 258 - "Study of Retrieval Concepts under ARDC Study Requirement No. 49759", April 1961.
- e. North American Instruments, Inc., "Feasibility Study of Aerial Pickup Systems - Morphological Investigation of Aerial Pickup Systems Involving Fixed Wing Aircraft", P.S. Chase, 30 September 1953, AD29255.
- f. North American Instruments, Inc., "Feasibility Study of Aerial Pickup Systems - Bibliography of Literature Pertaining to Aerial Pickup Systems", P.S. Chase, November 1953, AD 29254.
- g. GWIT 152 "Subsonic Wind Tunnel Investigation of 1/10 Scale Exit, Reentry, and Abort Apollo Configurations", November 1961.
- h. GWIT 105, "Report of Wind Tunnel Tests of the 1/7 Scale 'MIS' Capsule Model", January 1959.
- i. "Fluid-Dynamic Drag", Hoerner 1958.
- j. NACA TN 3038 "Low-Speed Drag of Cylinders of Various Shapes", Delaney and Sorensen, November 1953.
- k. AFFTC-TR-60-10 "C-130B Category II Performance Tests", April 1960, ASTIA No. AD 237105.
- l. Lockheed Report No. ER-4599, "C-130E Substantiating Data Report", 15 August 1961, Proprietary.
- m. T.O. 1-C-97(k)G-1, "USAF Series KC-97G Aircraft Flight Handbook", 15 December 1956, revised 15 November 1957.
- n. T.O. 1C-1308-1, "Flight Manual, USAF Series C-130B Aircraft and USCG SC-130B Aircraft", 30 September 1961.
- o. FHB-45-1 "Partial Flight Manual, USAF Series JC-130B Aircraft", 1 September 1961.
- p. AER 227 "C-130 Loading and Terminal Operations Planning Handbook", Lockheed Aircraft Corp., Georgia Division, April 1961.

- q. Booz-Allen Applied Research Inc., "The Domain of the Ground Effect Machine", Vol. I and II, Office of Naval Research Contract Nonr 3375(00), August 1961.
- r. "U.S. Navy, Marine Climatic Atlas of the World", Vol. I and II, "North Atlantic and North Pacific Oceans", Navaer 50-1C-528 and Navaer 50-1C-529, 1956.
- s. U.S. Weather Bureau, Washington, D.C., "Summary of Hourly Observations" (for various cities of the U.S.).
- t. U.S. Air Force Air Weather Service, "Summary of Hourly Observations", (for various locations), D Summary.
- u. "The Stability of a Body Towed by a Light Wire", H. Glauert, February 1930.
- v. AFCRC TN 60-198, "Aerodynamic Characteristics of Trailing-Wire Antennas at Supersonic Speeds", F. B. Harris, Jr., March 1960.
- w. Sandia SC-4219(1TR), "A Method for Determining the Positions of a Towed Vehicle with Respect to the Towing Aircraft", M.T. Kane and F.G. Blattner, August 1958.
- x. DTMB Rep. 713 "An Experimental Investigation of the Hydrodynamic Forces on Stranded Cables", L. Pote, May 1950.
- y. ATT 4 6126 "Initial Circular Flying Pickup Test", F. M. Johnson, December 1948.
- z. DTMB Rep. 687, "Tables for Computing the Equilibrium Configuration of a Flexible Cable in a Uniform Stream", L. Pote.
- aa. British ARC R&M 2303 "Collected Researches on the Stability of Kites and Towed Gliders", L. W. Bryant, W.S. Brown, and N.E. Sweeting, February 1942.
- bb. R&M 2334 "Extension of Glider Tow Cable Theory to Elastic Cables Subjected to Air Forces of a Generalized Form", F. O'Hara, M.A., 2 November 1954.
- cc. Kaman Report G-61 "An Analysis of the Forces in a Flexible Cable Subject to Wind and Gravity", Contributing Engineer Quentin Wald, 5 April 1954, Confidential.
- dd. Systems Engineering Division, Pneumodynamics Corp., Bethesda, Md., "Preliminary Design of a Cable Towed Oceanographic Instrumentation System" by W.M. Ellsworth and S.M. Gay, February 1961, AD 252872.
- ee. Systems Engineering Division, Pneumodynamics Corp., Bethesda, Md. "General Design Criteria for Cable-Towed Body Systems Using Faired and Unfaired Cable", W.M. Ellsworth, October 1960, AD 252870.

- ff. Reports and Memoranda, No. 554, Advisory Committee for Aeronautics, London, "On the Action of Wind on Flexible Cables, with Application to Cables Towed Below Aeroplanes, and Balloon Cables", A.R. McLeon, M.A., October 1918.
- gg. NACA TN No. 1796 "Theoretical Analysis of Oscillations of a Towed Cable", William H. Phillips, January 1949.
- hh. NADC-ED-5919, "The Long Line Investigation", J.G. Dahms, N.E. D'Apuzzo.
- ii. Film Nos. 6047B and 6058B from Naval Missile Center, Pt. Mugu, Calif.
- jj. Vickers Inc., Bulletin No. A-5237, "Studies on Self-Sufficient Aircraft Starting Systems".
- kk. ASD TR 61-623, "Analytical Formulation of Damped Stress-Strain Relations Based on Experimental Data with Applications to Vibrating Structures, T. J. Mentel, C.C. Fu, Univ. of Minnesota.
- ll. NASA TN D-976, "The Smoke Trail Method for Obtaining Detailed Measurement of the Vertical Wind Profile for Application to Missile Dynamic Response Problems", Henry, Brandon, Tolefson, London.